

**Targeting the BCL9/B9L Binding Interaction with β -catenin as a Potential
Anticancer Strategy**

by

Steven Akira Kawamoto

**A dissertation submitted in partial fulfillment
of the requirements for the degree of
Doctor of Philosophy
(Medicinal Chemistry)
in The University of Michigan
2010**

Doctoral Committee:

**Professor Shaomeng Wang, Chair
Professor Ronald W. Woodard
Professor Henry I. Mosberg
Associate Professor Anna K. Mapp
Assistant Professor Jason Edward Gestwicki**

Dedication

This work is dedicated to my loving and supportive family.

Acknowledgements

I would like to thank my mentor Dr. Shaomeng Wang for his guidance and support throughout this project. I would also like to thank Dr. Zaneta Nikolovska-Coleska for her invaluable training and discussions regarding the development of our FP and SPR assays. I would also like to thank Adriana Coleska, Andrea Thompson and Powell Perng for their help with synthesizing mutant and stapled BC9 peptides, and Dr. Chao-Yie Yang for his help with the computational modeling of triazole-stapled peptides. I would like to thank Han Yi for her work in purifying recombinant β -catenin and Dr. Eric Fearon for the TOP flash reporter construct and for his discussions regarding our project. I would also like to thank Steve vander Roest, Martha Larson and Paul Kirchhoff for their help with high throughput screening and data triage.

Table of Contents

Dedication	ii
Acknowledgements	iii
List of Figures	vi
List of Tables	vii
List of Schemes	viii
List of Appendices	ix
List of Abbreviations	x
Abstract	xii
Chapter	
1. Introduction	1
Wnt Signaling	1
Inhibitors of Wnt Signaling	10
Studies on the Mechanism of Action of BCL9 and B9L	14
2. Development and optimization of two BCL9-competitive binding assays and analysis of the BCL9 binding interaction with β -catenin	17
Background	17
Results	19
Discussion	28
Summary	30
Experimental Methods	30
3. HTS for inhibitors of the BCL9/B9L binding interaction with β -catenin	35
Background	35
Results	36
Discussion	39
Summary	41
Experimental Methods	41
4. siRNA and stabilized BCL9 peptides for validating BCL9 and	

B9L as targets for inhibiting Wnt signaling	43
Background	43
Results	46
Discussion	69
Summary	75
Experimental Methods	76
5. Conclusions and Future Directions	82
Importance of Wnt signaling and the role of BCL9/B9L	82
Summary and conclusions of our work	84
Future Directions	88
Appendices	93
References	124

List of Figures

Figure

1.1	Canonical Wnt signaling	5
1.2	Common mechanisms of dysregulation of Wnt signaling	9
1.3	Examples of different classes of Wnt signaling inhibitors	12
2.1	Development and validation of a BCL9/ β -catenin FP binding assay.....	19
2.2	Mutational analysis of four BCL9 binding residues	21
2.3	Mapping of the minimal β -catenin-binding region of BCL9	23
2.4	K_d and dynamic range for shortened BCL9-derived peptide tracers	24
2.5	Stability of BCL9 FP assay	25
2.6	Calculated Z'-factors for competitive FP-based assays	26
2.7	SPR-based BCL9 binding assays	27
3.1	Effects of BSA and Triton X-100 on the signal and binding affinity of 8-R	37
3.2	Calculated Z'-factor for competitive FP-based assay using 8-R	38
3.3	Dose-response assays for HTS active compounds	39
4.1	Comparison of selected techniques for stabilizing peptide helices	45
4.2	Effects of siRNA knockdown of BCL9 and B9L	48
4.3	<i>In vitro</i> characterization of CPP-tagged BCL9 peptides	50
4.4	Solvent-exposed residues in BCL9	55
4.5	Computational modeling of possible triazole-stapled BCL9 peptides	58
4.6	Triazole-stapled BCL9 peptides and their β -catenin binding affinities	59
4.7	CD spectra of triazole-stapled BCL9 peptides	60
4.8	Aqueous solubility of BCL9 and B9L peptides	63
4.9	Binding affinities and aqueous solubility of mutated BCL9 peptides	64
4.10	Binding affinities and aqueous solubility of BCL9 M372 mutant peptides	65
4.11	Binding affinities and aqueous solubility of arginine mutated BCL9 peptides.....	66
4.12	Binding affinities and aqueous solubility of triazole-stapled BCL9 peptides	67
4.13	Trypsin cleavage of triazole-stapled BCL9 peptides	69
5.1	BCL9 binding residues	90

List of Tables

Table

1.1	Known inhibitors of Wnt signaling	14
4.1	Binding affinities of HBS-stabilized BCL9 peptides	52
4.2	Binding affinities of triazole-stapled BCL9 peptides with different linkers	62

List of Schemes

Scheme

1. Synthesis of Fmoc-disubstituted olefin amino acid54
2. Synthesis of Fmoc-L-Nle(ϵ N₃)-OH56
3. Synthesis of Fmoc-propargylalanine (Paa)61

List of Appendices

Appendix

1.	Table of BCL9 and B9L peptides	93
2.	Table of HBS, stapled and mutant BCL9 and B9L peptides	96
3.	Circular dichroism experiments with BCL9 peptides	99
4.	Synthesis scheme for Fmoc-glutaminy-N-allyl-leucine	100
5.	Spectral data for synthesized amino acids	101
6.	Evaluation of the Smac binding site of Survivin for the design of potential inhibitors of Survivin	105
7.	Peptide library for SVV	122

List of Abbreviations

AML	acute myeloid leukemia
APC	Adenomatous polyposis coli
Arm	Armadillo
APC	adenomatous polyposis coli
β -TrCP	b-transducin repeat-containing protein
BCL9	B-cell lymphoma 9
B9L	BCL9-like
CBP	cAMP response element-binding protein-binding protein
CD	circular dichroism
CK1 α	casein kinase-1 α
CIW	chlorotryptophan
CPP	cell-penetrating peptide
DKK	Dickkopf
Dvl	Dishevelled
EDC	N-(3-Dimethylaminopropyl)-N'-ethylcarbodiimide
5-FAM	5-carboxyfluorescein
FP	fluorescence polarization
Fz	Frizzled
GSK-3 β	glycogen synthase kinase-3 β
HBS	hydrogen bond surrogate
HD	homology domain
Hfe	homophenylalanine
Hle	homoleucine
HTS	high-throughput screening
Int-1	integration-1
LEF	lymphoid enhancer factor
Lgs	Legless
LRP	low-density lipoprotein-related protein

MDR1	multidrug resistance 1
MMTV	mouse mammary tumor virus
mP	millipolarization
Mtt	4-methyltrityl
Nal	naphthylalanine
NHS	N-hydroxysuccinimide
Nle	norleucine
Nva	norvaline
Paa	propargylalanine
PDB	Protein Data Bank
Porcn	porcupine
Pra	propargylglycine
Pygo	Pygopus
sFRP	secreted Frizzled-related protein
siRNA	short interfering RNA
SPR	surface plasmon resonance
5-TAMRA	5-carboxytetramethyl rhodamine
TCF	T-cell factor
Tle	t-butyl-leucine
TLE	transducin-like enhancer-of-split
Wg	wingless
WIF	Wnt inhibitory factor
Wnt	combination of Wg and Int-1
WTX	Wilm's tumor X-protein

Abstract

Wnt signaling plays a critical role in numerous cellular processes including embryonic development, cell proliferation and tissue homeostasis. The multifunctional protein β -catenin is the primary mediator of canonical Wnt signaling and acts as a transcriptional activator in this context. Dysregulated Wnt signaling is a hallmark of many human cancers and results in the stabilization and accumulation of β -catenin, leading to the increased transcription and expression of Wnt target genes. The transcriptional activation function of β -catenin requires the formation of a nuclear super-complex with protein cofactors including BCL9/B9L, TCF and CBP. It has been demonstrated that binding to these cofactors is essential for transcriptional. Of these critical cofactors, BCL9 and its homolog B9L are the most recently identified and their exact roles are not fully understood. To explore the consequences of the BCL9/B9L- β -catenin binding interaction we developed and optimized a quantitative, reliable and high throughput fluorescence polarization (FP) binding assay along with a surface plasmon resonance (SPR)-based secondary assay. Using our FP assay, we performed extensive mutational analysis of four key hydrophobic residues in BCL9 and determined their contribution to the interaction with β -catenin. We also mapped the precise region of BCL9 required for high affinity binding to β -catenin. With our optimized FP assay, we performed high throughput screening (HTS) for small molecule inhibitors and identified one molecule that warrants further characterization in cell-based assays. We also synthesized BCL9 peptides tagged with cell penetrating peptides (CPPs), but found that their usefulness was limited by their poor solubility. We then tried synthesizing cell-permeable stabilized α -helical BCL9 peptides by three different methods and determined that triazole-stapling, mediated by the Huisgen 1,3-dipolar cycloaddition reaction, was the most robust and highest yielding method in our hands. Our detailed study of this stapling technique defined the optimal azido and alkynyl linker combinations required for stabilizing one turn of the BCL9 α -helix. In summary, we confirmed the requirement for BCL9/B9L in β -catenin transcriptional activation, identified a potentially druggable site around the BCL9 F374 binding pocket and demonstrated that triazole stapling can increase helicity and binding affinity of our BCL9 peptides. Our work has laid the foundation for the design

and discovery of both peptide and non-peptide small molecule inhibitors of the BCL9/B9L interaction with β -catenin. Such inhibitors can serve as both pharmacological tools for further investigation of the role of this interaction in the Wnt signaling pathway and as lead compounds for the development of a new class of potential anticancer drugs.

Chapter 1

Introduction

1.1 Wnt Signaling

1.1.1 Wnt Background

The Wnt signaling pathways have been extensively studied for over thirty years. The first gene, identified in *Drosophila melanogaster*, was named *wingless* (Wg) due to the absence of wings in mutant embryos¹. Fourteen years later, Rijsewijk *et al.* realized that the oncogene *integration-1* (int-1), which was the frequent site of mouse mammary tumor virus (MMTV) gene integration in mouse mammary gland tumors², was homologous to the Wg gene³. Thus, the Wnt family name was coined as a chimera of the Wg and Int-1 genes. Since its discovery, the Wnt signaling pathways have been implicated in numerous cellular processes including embryonic development, cell proliferation and differentiation, cell polarity, cell motility, tissue homeostasis, stem cell renewal and more⁴⁻⁸.

Multiple pathways have been identified in Wnt signaling and are now divided into two classes: β -catenin-dependent (canonical) Wnt signaling and β -catenin-independent (non-canonical) Wnt signaling. Canonical Wnt signaling is the most well studied of the pathways and is responsible for transmitting extracellular signals to the nuclear transcriptional machinery to effect the expression of Wnt target genes involved in such diverse processes as cell embryonic development, tissue homeostasis, stem cell maintenance, tumor suppression and oncogenesis^{6,9}. The non-canonical Wnt signaling pathway is further divided into arguably two or three subclasses. The planar cell polarity (PCP) pathway has been well characterized in *Drosophila* and is known to control gastrulation and convergent extension movements of developing embryos, the distribution and orientation of prehair in fly wing cells, spindle formation during mitosis, and inner ear development in vertebrates^{10,11}. The second subclass is referred to as the

Wnt/Ca²⁺ pathway, which controls the intracellular release of calcium and the activation of protein kinase C (PKC) and calcium/calmodulin-dependent kinase II (CamKII)^{11,12}. It is still debated whether Wnt/Ca²⁺ signaling represents a distinct pathway or whether it is actually a vertebrate extension of the PCP pathway, especially in light of the fact that certain signaling molecules such as Dishevelled (Dvl) are used in both¹¹. Non-canonical Wnt signaling has also been reported to activate the Rho family of G proteins and also the JNK pathway¹¹. Whether the involvement of these signaling pathways constitutes another distinct subclass of non-canonical Wnt signaling remains under debate as well.

1.1.2 Wnt Ligands

In general, the initiators of the Wnt signaling pathways are the Wnt proteins themselves. To date, nineteen Wnt ligands have been identified in mammals. For an up to date listing of Wnt ligands and pathway members readers are referred to the review by Chien *et al.*⁹ and the Wnt Homepage (www.stanford.edu/~rnusse/wntwindow.html). Wnt ligands are 350-400 amino acid cysteine-rich, secreted glycoproteins that are glycosylated on their N-termini¹³. They also have multiple sites that are modified through lipidation including a conserved cysteine residue (C77 in Wnt3A) required for receptor binding¹⁴ and a serine residue (S209 in Wnt3A) required for secretion^{15,16}. The lipidation of Wnt proteins is performed, at least in part, by the membrane-bound O-acyltransferase protein Porcupine (porcn)^{16,17}. Due to the highly hydrophobic nature of these proteins, it has been difficult for investigators to isolate and purify Wnt proteins for detailed characterization and analysis. Most of the information about Wnt ligands functions is the result of genetic knockout experiments. Nevertheless, researchers have been able to roughly classify the Wnts into those that activate the canonical pathway (e.g. Wnt-1, Wnt3, Wnt10), those that activate the non-canonical pathway (e.g. Wnt7, Wnt11) and those that can activate both pathways (e.g. Wnt5a)⁹. These classifications, however, are not stringent since it appears that the cellular context can have a significant impact on determining which pathways are most activated by particular Wnt ligands.

In addition to the Wnt family of ligands, other non-Wnt molecules have been identified that are capable of activating Wnt signaling. Norrie diseases protein (NDP), alternatively named Norrin, has been shown to activate the canonical Wnt pathway through binding to the same cell surface receptors as Wnts and is involved in proper vasculature formation in the retina and cochlea¹⁸. Also, the R-Spondins (Rspo) family of secreted proteins is

capable of activating the canonical Wnt signaling pathway and has been implicated in skin differentiation, sex determination and muscle formation¹⁹⁻²².

1.1.3 Wnt Receptors

Signals originating with the various Wnt and non-Wnt ligands are transmitted to the cell by Wnt receptors. The primary Wnt receptors are the seven-pass transmembrane family of Frizzled (Fz) receptors and their co-receptors the single-span transmembrane low-density lipoprotein-related proteins 5 and 6 (LRP5/6)^{6,23,24}. In mammals, there are currently ten identified Fz receptors that each have varying capacities for activating Wnt signaling²⁵. Fz receptors possess a cysteine-rich domain (CRD) in their extracellular N-termini that is responsible for binding Wnt ligands^{23,26}. The expression of the different Fz receptors is tissue and context dependent and in the presence of a Wnt ligand, Fzs can form complexes with LRP5/6 or homo- or hetero-oligomers^{27,28}. In addition, the transmembrane tyrosine kinases Ryk and Ror2 have also been shown to bind Wnts¹⁸. Combine these numerous receptor combinations with the plethora of Wnt ligands and it is easy to see how the Wnt signaling pathways can influence a multitude of cellular processes.

1.1.4 Endogenous Regulation of Wnt Signaling

At the extracellular and membrane level of Wnt signaling there exist numerous regulatory molecules that help modulate Wnt signaling (Table 1.1). The Dickkopf (DKK) family of secreted ligands has been shown to bind to LRP receptors and to crosslink them to another family of single-span transmembrane proteins, the Kremens²⁹⁻³². The binding of DKK to LRP and Kremens leads to the internalization and inactivation of LRP receptors through endocytosis³³. The antagonistic role of DKK is still unclear, however, since recent reports have shown that in certain cases of hepatoblastomas, Wilm's tumors and hepatocellular carcinomas DKK1 is actually upregulated and correlated with poor prognosis³⁴. Thus, in different cellular contexts, DKK may be either a Wnt signaling inhibitor or a potential oncogene.

The family of secreted Fz-related proteins (sFRPs) represents another class of Wnt inhibitors. Among the five known sFRP members in humans, the N-terminal regions are 50% homologous to Fz receptors, contain a CRD similar to Fzs, but lack the transmembrane portion of Fzs³⁵. The sFRPs inhibit Wnt signaling by binding to Wnts and

forming self-dimers with themselves or heterodimers with Fz receptors thereby creating inactivating complexes³⁶.

Another endogenous Wnt signaling antagonist is Wnt-inhibitory factor-1 (WIF-1), which was also shown to bind and form inhibitory complexes with Wnt ligands³⁷. Unlike the sFRPs, WIF-1 does not show homology to Fz, but instead possesses a unique WIF domain that resembles part of the extracellular portion of the Wnt receptor RYK.

Other Wnt modulators are the Wise and sclerostin (SOST) proteins. The Wise protein was recently identified as both a potential agonist and antagonist of Wnt signaling depending on the cellular context³⁸. This secreted protein was shown to bind to LRP6 and block the binding of Wnt8. The secreted SOST protein was shown to bind to LRPs preventing their complexation with Fzs and, thus, antagonizing Wnt signaling^{39,40}.

1.1.5 β -catenin and Canonical Wnt Signaling

Once a Wnt ligand has bound and activated a Wnt receptor complex, the signal can be transduced through either canonical or non-canonical pathways. The canonical pathway is the most highly studied of the pathways and is the focus of the work herein.

The multifunctional protein β -catenin is the primary intracellular effector molecule of the canonical Wnt signaling pathway. β -Catenin was first identified as an intracellular binding partner of the cell adhesion molecule E-cadherin and was named for the latin word "catena," meaning chain since it was postulated to connect adherin junctions to the cytoskeleton⁴¹⁻⁴⁴. In humans, β -catenin encodes a 88 kDa protein that contains 12 copies of the armadillo (arm) motif, which pack to form a superhelix of helices⁴⁵. The protein also contains an unstructured N-terminal region that contains several conserved serine/threonine residues that are involved in regulating β -catenin stability. The C-terminus of β -catenin is also unstructured and has been shown to bind numerous cytoplasmic and nuclear proteins⁴⁶.

1.1.6 β -catenin Destruction Complex

In the absence of a Wnt signal, the cytoplasmic and nuclear levels of free β -catenin are stringently controlled by a β -catenin destruction complex (Figure 1.1A)^{47,48}. In this complex, Axin acts as a scaffold protein and binds β -catenin, adenomatous polyposis coli (APC), glycogen synthase kinase-3 β (GSK-3 β), casein kinase 1a (CK1 α) and Wilm's

tumor X-protein (WTX)^{48,49}. Although the exact order of binding remains unclear, it is known that CK1 α phosphorylates S45 of β -catenin, which primes the protein for the subsequent phosphorylation of S33, S37 and T41 by GSK3 β ^{50,51}. Phospho- β -catenin is then recognized by the F-box/WD40 repeat protein β -transducin repeat-containing protein (β -TrCP), which is a member of the E3 ubiquitin ligase complex⁵². Polyubiquitination of β -catenin then leads to the rapid degradation of β -catenin by the 26S proteasome⁵³.

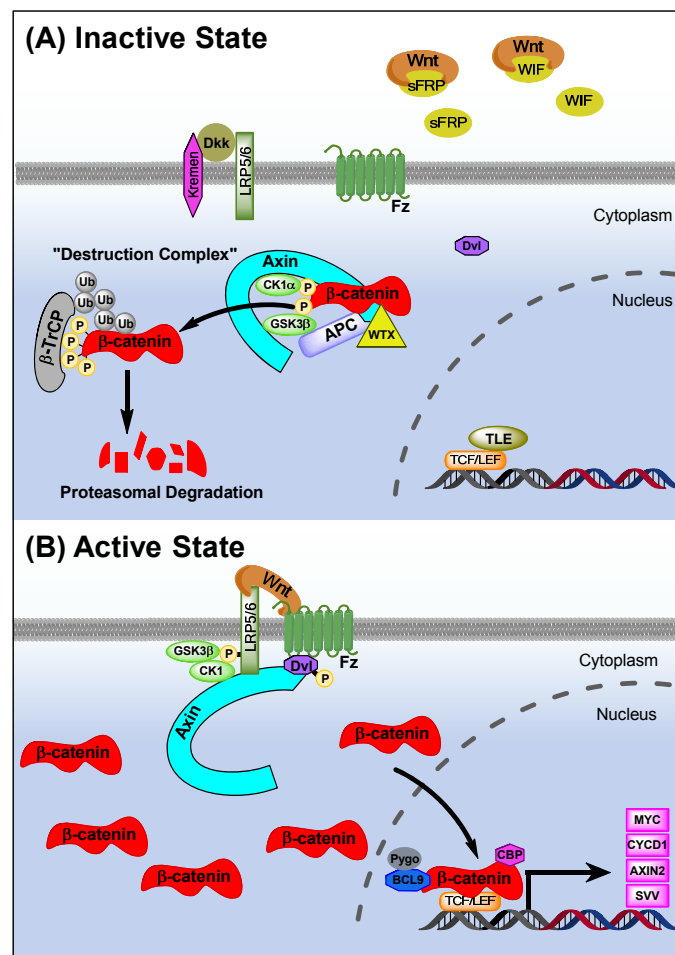


Figure 1.1. Canonical Wnt signaling. (A) The Inactive State. Lack of Wnt signaling either through the absence of Wnt production or the presence of endogenous Wnt inhibitors (e.g. sFRP, WIF) results in β -catenin being bound and phosphorylated by the destruction complex. Recognition by the β -TrCP E3 ubiquitin ligase complex causes polyubiquitination and proteasomal degradation of β -catenin. (B) The Active State. In the presence of a Wnt signal, LRP5/6 is phosphorylated by GSK3 β and the CK1 family of kinases. Dvl and Axin are then recruited to the membrane resulting in the dissolution of the destruction complex, and the accumulation and translocation of β -catenin to the nucleus. Inside the nucleus, β -catenin forms a transcriptional activation super-complex with TCF/LEF, BCL9/B9L, CBP and other cofactors and causes the activation of Wnt target genes.

1.1.7 Active Canonical Wnt Signaling

In the presence of a Wnt signal, the Fz-LRP5/6-Wnt ternary complex causes the phosphorylation of the C-terminal cytoplasmic tail of LRP5/6 by GSK-3 β and various members of the CK1 family of kinases^{54,55}. Then, by mechanisms that are not completely understood, Axin and Dvl are recruited to the membrane leading to the breakdown of the β -catenin destruction complex (Figure 1.1B)^{55,56}. Although the exact role of Dvl in canonical Wnt signaling is not well understood, it is known that Wnt signaling causes the phosphorylation of Dvl and that the interaction of Dvl with the Wnt receptor complex is required for signal transduction⁵⁶. Studies have suggested that the PDZ domain of Dvl binds to the intracellular portion of Fz and that through its DIX (Dvl-Axin) domain either recruits Axin to the membrane or stabilizes the interaction of Axin with LRP^{57,58}.

The dissolution of the β -catenin destruction complex results in the stabilization and accumulation of β -catenin in the cytoplasm. Then by passive diffusion, β -catenin translocates to the nucleus where it accumulates due to interactions with its nuclear binding partners such as T-cell factor/lymphoid enhancer factor (TCF/LEF), B-cell lymphoma-9 (BCL9) and others⁵⁹. Once in the nucleus, β -catenin binds TCF/LEF and additional cofactors including BCL9, BCL9-like (B9L) and the histone acyltransferase (HAT) cyclic response element binding protein-binding protein (CREB binding protein; CBP) to form a transcriptional activation complex^{60,61}. These cofactors help recruit additional members of the transcriptional machinery such as RNA polymerase II and together, this β -catenin-containing nuclear super-complex causes the transcriptional activation of Wnt target genes⁶².

To date, well over a hundred genes have been identified as targets of Wnt signaling (Wnt Homepage). Wnt target genes such as c-myc, cyclin D1 and survivin are involved in cell proliferation, cell cycle regulation, oncogenesis and inhibition of apoptosis⁶³⁻⁶⁵. Another gene axin2 is believed to have similar functions as its homolog axin1 and represents a negative feedback loop for Wnt signaling⁶⁶. The multidrug resistance 1 (MDR1) gene encodes for the P-glycoprotein, which is responsible for drug efflux and resistance to small molecule therapeutics⁶⁷. Furthermore, Wnt target genes such as vascular endothelial growth factor (VEGF) and matrix metalloproteases (MMPs) are involved in wound repair, tumor vascularization, and metastasis^{68,69}. Thus, the effects of Wnt target gene expression are both diverse in function and critical to normal and disease state cellular processes.

1.1.8 Nuclear β -catenin Transcriptional Activation Complex

The transcriptional activation of Wnt target genes requires the formation of a nuclear protein complex in which β -catenin acts as the central scaffold (Figure 1.1B). The primary DNA-binding protein in the complex is TCF/LEF, of which there are four family members in vertebrates; however, numerous alternative splice variants also exist^{7,70}. TCFs are members of the high-mobility group (HMG) box proteins that cause strong DNA bending ($\sim 130^\circ$) upon binding to Wnt response elements (WREs), which is speculated to help expose DNA making it accessible to the transcriptional machinery^{71,72}. In the absence of β -catenin, TCF/LEF binds transducin-like enhancer-of-split (TLE) to form a transcriptional repressor complex⁷³⁻⁷⁷. TLE recruits histone deacetylases (HDACs) causing chromatin condensation and gene silencing⁷⁸. However, in the presence of β -catenin, TCF/LEF binds along the major groove of β -catenin causing the displacement of TLE and the conversion to a transcriptional activation complex⁷⁹.

Binding of β -catenin to TCF/LEF alone is not sufficient to activate transcription. Through a groove formed in the first arm repeat, β -catenin also binds to the homology domain 2 (HD2) region of BCL9/B9L^{61,80}. BCL9/B9L appear to have dual roles such that they act as linkers to recruit an another cofactor Pygopus (Pygo)^{61,81,82} and also use their C-termini for an extra transcriptional activation function⁸³⁻⁸⁵. Additionally, β -catenin uses its C-terminus to bind the HAT proteins CBP and p300 to effect chromatin unpacking and recruit RNA Pol II⁶⁰. Thus, this multiprotein super-complex, likely with additional other proteins, forms the functionally active transcriptional activation complex that leads to the expression of Wnt target genes.

1.1.9 Dysregulation of Wnt Signaling

Due to the involvement of Wnt signaling in critical processes such as cell growth, proliferation, differentiation and motility, it is reasonable to expect that the dysregulation of Wnt signaling can lead to developmental abnormalities and disease. In fact, aberrant Wnt signaling has been implicated in numerous pathological conditions such as cancer, pulmonary fibrosis, osteopetrosis, osteoporosis, tetra-amelia and schizophrenia^{5,15,86}. Gain- or loss-of-function abnormalities have been identified at nearly every level of the Wnt signaling pathway. Interestingly, certain genetic abnormalities appear to have tissue-specific effects and often predispose organisms to pathological conditions in specific organs^{6,87}.

At the head of the Wnt signaling pathway, increased expression of Wnt1 has been associated with aggressive prostate and lung cancer⁸⁸. Similarly, mutation of the secreted inhibitor SOST causes activation of Wnt signaling and is implicated in sclerosteosis (overgrowth of bone tissue)^{89,90}. In contrast, the rare genetic disorder tetra-amelia (absence of all four limbs) is characterized by loss of Wnt3A⁹¹. At the receptor level, a single amino acid substitution (G171V) in LRP has been shown to inhibit the binding of DKK. This subtle mutation prevents Wnt regulation by DKK and is believed to lead to elevated osteoblast counts and osteopetrosis (high bone density)^{92,93}. Furthermore, truncation of LRP5 due to aberrant mRNA splicing leads to constitutive activation of β -catenin and is believed to be involved in the development of hyperparathyroid tumors⁹⁴. Also at the receptor level, overexpression of Dvl-3 leading to β -catenin activation has been found in non-small cell lung cancer (NSCLC) as well as malignant pleural mesothelioma^{95,96}.

At the level of the β -catenin destruction complex, there are a multitude of examples of genetic abnormalities that result in constitutively activated β -catenin. The most well characterized class of mutations are those that occur in APC, which have been identified in 85% of both inherited and sporadic forms of colorectal neoplasias (Figure 1.2)^{97,98}. Nearly twenty years ago, patients with familial adenomatous polyposis (FAP) were recognized to have truncating mutations in one of their APC alleles^{97,99}. Upon mutation or loss of the second allele, this dominant negative form of APC, which is unable to bind Axin or β -catenin causes the breakdown of the destruction complex and the constitutive activation of β -catenin. As a result, FAP patients were found to have to hundreds to thousands of colonic adenomatous polyps, some of which would eventually progress to carcinomas if not surgically removed¹⁰⁰. At the same time, similar mutations were identified in cases of sporadic colorectal cancer and gastric cancer^{97,99,101,102}.

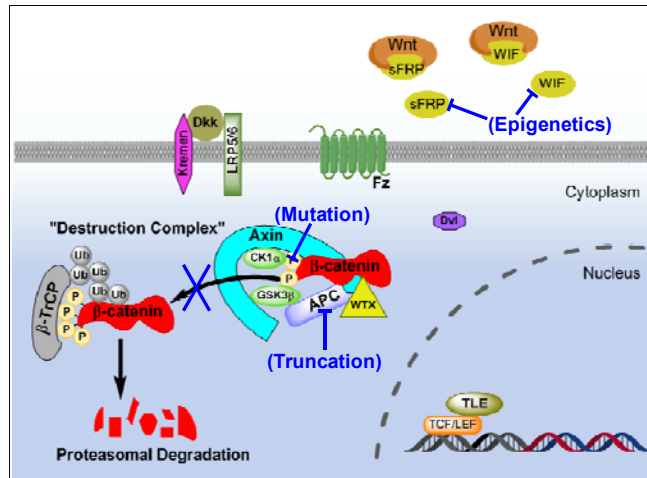


Figure 1.2. Common mechanisms of dysregulation of Wnt signaling. Truncating mutations in APC prevent the formation of the destruction complex. Activating mutations in β -catenin can prevent its phosphorylation and inhibit its degradation. Epigenetic silencing (e.g. hypermethylation) of endogenous inhibitors can result in activation of Wnt signaling by Wnt proteins.

In the remaining 15% of colon cancer patients that possessed wild type APC, it was found that mutations in β -catenin were the cause of constitutively activated Wnt signaling (Figure 1.2)^{100,103}. The most common alterations were either mutation or deletion of one of the N-terminal conserved serine/threonine residues required for phosphorylation and proteasomal degradation of β -catenin. To date, numerous examples of β -catenin mutations in the N-terminal phosphorylation region have been identified in cancers of the colon, liver, pancreas, thyroid, ovary and more¹⁰³.

Further underscoring the important regulatory role of the β -catenin destruction complex has been the recent identification of Axin mutations. In 25% of cases of colorectal cancer with defective DNA mismatch repair (MMR) genes, Liu *et al.* found truncating mutations in Axin that eliminated the DIX domain believed to be involved in binding to β -catenin and presumably for formation of the destruction complex¹⁰⁴. Patients with hereditary mutations in Axin were found to have tooth agenesis (lack of mature tooth development) and predisposition to colon cancer¹⁰⁵. In hepatocellular carcinomas, Axin mutations have been identified in many of the cases in which β -catenin and APC mutations are not detected¹⁰⁶. Furthermore, the recent discovery WTX as a member of the destruction complex has provided another possible mechanism for β -catenin dysregulation. Indeed, deletion or truncation of WTX has been reported in as many as 30% of Wilm's tumors (pediatric kidney cancers)^{49,107}.

In addition to genetic mutations, the recent surge in epigenetic research has revealed a host of Wnt regulatory genes that are silenced through promoter methylation or deacetylation¹⁰⁸. In breast cancer, mutations in APC or β -catenin are extremely rare. However, extensive promoter hypermethylation of Wnt antagonists was recently reported in over 60% of primary breast tumors and breast cancer cell lines analyzed (Figure 1.2)^{109,110}. DKK1 promoter methylation has also been noted in both breast and gastrointestinal cancers¹¹⁰⁻¹¹³. Likewise, WIF1 has been found to be silenced through promoter methylation in kidney, breast, bladder cancers and others¹¹⁴⁻¹¹⁶.

Thus, the dysregulation of the Wnt signaling pathway is a common occurrence in numerous pathological disorders and is likely a major driving factor in the progression of many diseases such as cancer. The design of Wnt signaling inhibitors is an attractive approach to treating such diseases and extensive research has been performed in this field.

1.2 Inhibitors of Wnt Signaling

1.2.1 Biomolecular Wnt Inhibitors

Some of the first targeted Wnt pathway inhibitors were monoclonal antibodies (mAbs) directed against Wnt ligands (Figure 1.3; Table 1.1). In metastatic lung sarcomas a Wnt1 mAb was shown to decrease the levels of Dvl3 and cytoplasmic β -catenin, inhibit the expression of Survivin and induce apoptosis¹¹⁷. Similarly, a Wnt2 mAb was shown to downregulate β -catenin-mediated transcriptional activity, inhibit the expression of Survivin and induce apoptosis in NSCLC¹¹⁸. The use of short interfering RNAs (siRNAs) to target both Wnts and downstream signaling members including Dvl and β -catenin has also proven effective at inhibiting β -catenin activity^{95,96,117-119}. As further proof-of-principle, a dominant-negative form of TCF4 lacking the β -catenin binding site was shown to reduce piled-up foci and restore the formation of a simple monolayer of polarized columnar cells (indicated by microvilli on the apical surface and restoration of tight junctions) in the DLD-1 colon cancer cell line¹²⁰.

Kwong *et al.* used a TCF-responsive promoter to drive the expression of the herpes simplex virus thymidine kinase (HSV-TK) in cancer cell with constitutively activated β -catenin¹²¹. When treated with ganciclovir (GCV) cells expressing HSV-TK selectively phosphorylate and activate GCV which then acts as a DNA chain terminator. This

approach was shown to be selective for colon cancer cells with constitutively activated β -catenin but not in hepatoma cells lacking active Wnt signaling.

1.2.2 Peptide and Small Molecule Inhibitors of Wnt Signaling

Even before Wnt signaling was linked to FAP and colon cancer, investigators noted that regular low-dose use of non-steroidal anti-inflammatory drugs (NSAIDs) reduced the risk of colon cancer (Table 1.1)^{122,123}. These observations have triggered extensive research to determine the efficacy and mechanisms of action of various NSAIDs^{124,125}. To date, the mechanism of action appears to differ between the different NSAIDs and multiple roles may actually exist. Studies performed with sulindac have demonstrated the ability to inhibit the formation of piled up foci and to reduce the number and severity of adenomatous polyps^{120,123}. Subsequent studies with exisulind (AptosynTM), a metabolite of sulindac, demonstrated the prevention of polyps in FAP patients and additive/synergistic antineoplastic effects with various other chemotherapy agents¹²⁶. Exisulind does not inhibit cyclooxygenase-2 (COX2) and its chemopreventative effects were attributed to its inhibition of cyclic GMP phosphodiesterases (PDEs) and increased expression and activity of protein kinase G (PKG), which phosphorylated β -catenin on its C-terminal tail leading to proteasomal degradation¹²⁷.

Other NSAIDs including aspirin, indomethacin and celecoxib have all shown promise in inhibiting Wnt signaling^{125,128}. Aspirin's mechanism of action has been proposed to be the inhibitory phosphorylation of protein phosphatase 2A (PP2A), which is believed to be involved in the dephosphorylation of β -catenin or other members of the β -catenin destruction complex¹²⁹. Currently, celecoxib is the only NSAID that is approved by the FDA for use in preventing and treating polyp formation in FAP patients¹²⁵.

In addition to the use of NSAIDs, researchers are actively pursuing direct inhibitors of the Wnt signaling pathway. Recently, direct inhibitors of the β -catenin binding interaction with TCF have been identified using virtual and biochemical high throughput screening (Table 1.1)^{130,131}. Several compounds were demonstrated to inhibit β -catenin activity, expression of known Wnt target genes and cell growth in colon and prostate cancers^{130,132}. In addition, acute myeloid leukemia (AML) cells were over 100-fold more sensitive to TCF inhibitors than normal peripheral blood mononuclear cells¹³³. Nevertheless, TCF inhibitors are also potential inhibitors of APC, Axin and E-cadherin

due to their shared binding sites on β -catenin¹³⁴. Indeed, the most well characterized small molecule TCF inhibitors, to date, are also inhibitors of APC binding to β -catenin¹³⁰.

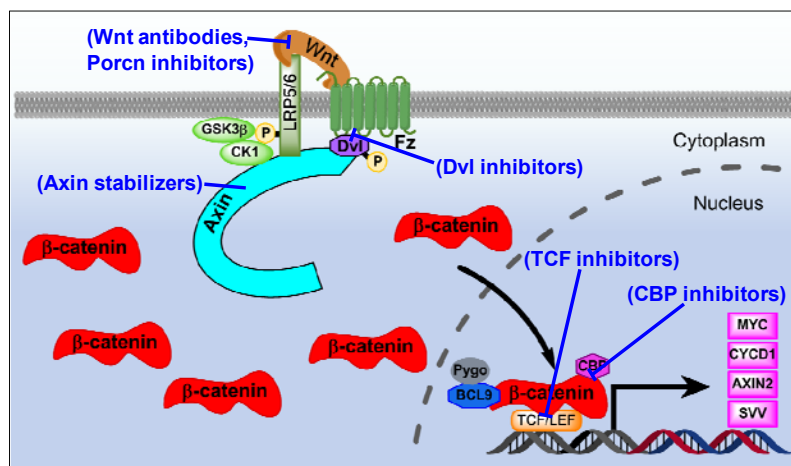


Figure 1.3. Examples of different classes of Wnt signaling inhibitors.

To avoid potential undesired toxicities associated with TCF inhibitors, research has also focused on inhibitors of the histone acyltransferase CBP (Figure 1.3), which binds to the C-terminal tail of β -catenin. The small molecule ICG-001 was identified as a specific CBP inhibitor that binds to CBP, but not p300, preventing its interaction with β -catenin and inhibiting β -catenin-mediated transcriptional activation (Table 1.1)¹³⁵. ICG-001 was also demonstrated to selectively induce apoptosis in transformed colorectal cancer cells, inhibit tumor growth in mouse xenograft models, and was efficacious in inhibiting polyp formation in the Min mouse, which contains constitutively activated β -catenin.

Dvl inhibitors have also been identified and shown to inhibit the interaction of Dvl with the Fz receptors (Figure 1.3)¹³⁶⁻¹⁴⁰. Consequently, Dvl inhibitors prevent β -catenin-mediated transcriptional activation, induce apoptosis in lung cancer and melanoma cell lines and inhibit tumor growth in mouse xenograft models. The main drawback to Dvl inhibitors is the fact that they only inhibit autocrine-induced Wnt signaling¹³⁷. Thus, diseases that arise from activating mutations in pathway members downstream of Dvl such as at the level of the β -catenin destruction complex or in β -catenin itself are likely to be resistant to Dvl inhibitors^{137,138}.

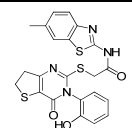
Two additional classes of Wnt signaling inhibitors, Porcupine inhibitors and Axin2 stabilizers, were recently identified from a cell-based high throughput screen (Figure 1.3; Table 1.1)¹⁴¹. Porcupine inhibitors were shown to inhibit the palmitoylation and

maturation of Wnt3A and Wnt5 thereby preventing autocrine-induced Wnt signaling. Compounds that stabilized Axin2 caused an overall increase in Axin2 protein levels, which resulted in enhanced degradation of β -catenin in colon and prostate cancer cell lines. These results were consistent with recent evidence proposing Axin to be the limiting factor in the formation of the β -catenin destruction complex¹⁴². Thus, increasing Axin protein levels was expected to also increase the formation of the destruction complex. Interestingly, Axin2 stabilizing agents caused degradation of β -catenin even in cell lines with mutant APC indicating that elevated levels of Axin2 can compensate for loss of APC.

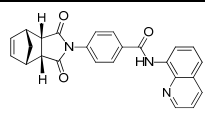
Although Dvl inhibitors, Porcupine inhibitors and Axin stabilizers show promise as potential anticancer agents, they target steps early in the Wnt signaling cascade. Dysregulation downstream of these checkpoints, such as the presence of activating mutations in β -catenin¹⁰³ would be predicted to circumvent these inhibitors. An ideal point to disrupt β -catenin transcriptional activation would be at the utmost downstream component, the transcriptional activation complex itself. However, inhibiting the interaction with TCF/LEF is potentially a risky strategy due to the shared binding sites of TCF/LEF and other important β -catenin binding partners such as E-cadherin, APC and Axin. Targeting CBP avoids the possibility of inhibiting other desired β -catenin binding interactions; however, CBP binds numerous other proteins and participates in transcriptional activation of genes unrelated to Wnt signaling¹⁴³. Thus, CBP inhibitors may also have undesired side effects. In contrast, the β -catenin cofactors BCL9/B9L bind to a unique binding site on the first arm repeat of β -catenin and inhibitors of this interaction would likely have fewer toxic side effects. Currently, no inhibitors of the BCL9/B9L binding interaction with β -catenin have been reported.

Table 1.1. Known inhibitors of Wnt signaling.

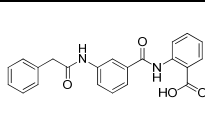
Class	Examples	Mechanism of Action	References
Endogenous Inhibitors	sFRPs, WIF-1	Bind Wnts	35, 36, 37
	DKK-1, WISE, SOST	Bind LRPs	29, 30, 31, 38, 39, 40
Biomolecular Inhibitors	Wnt-1 mAb, Wnt-2 mAb	Bind Wnts	117; 118
	Dominant negative TCF	Missing β -catenin binding site	120
	Dvl siRNA, β -catenin antisense	Depletion of Dvl or β -catenin	95, 119
	TOP-TK + GCV	DNA chain terminator	121
Peptide Inhibitors	EIVLWSDIP	Binds Dvl PDZ inhibiting binding to Fz	138
Small Molecule Inhibitors	NSAIDs (sulindac, indomethacin, celecoxib, aspirin)	Mechanism unclear; possible inhibition of cGMP phosphodiesterases, PP2A causing degradation of β -catenin	120, 125, 127, 128, 129
	IWP-2 (porcupine inhibitor)	Binds porcupine and inhibits Wnt palmitoylation	141
	IWR-1 (axin2 stabilizer)	Stabilizes Axin2 promoting β -catenin degradation	141
	FJ9, 3289-8625	Bind Dvl PDZ inhibiting binding to Fz	136, 139, 140
	CPG049090, PKF115-584, PNU-74654	Bind β -catenin inhibiting interaction with TCF	130, 131, 133,
	ICG-001	Binds CBP inhibiting binding to β -catenin	135



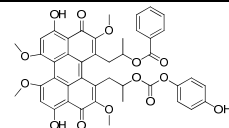
(IWP-2)



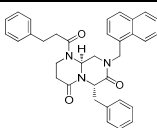
(IWR-1)



(3289-8625)



(PKF115-584)



(ICG-001)

1.3 Studies on the Mechanism of Action of BCL9 and B9L

1.3.1 Role of BCL9/B9L

The 1400 amino acid protein BCL9 was first identified in B-cell malignancies as a gene commonly upregulated due to chromosomal translocation^{144,145}. Around the same time, the *Drosophila* homolog of BCL9, called legless (lgs), was identified as a binding partner of arm (the *Drosophila* homolog of β -catenin) and was proposed to act as an adapter molecule to recruit another cofactor Pygo^{61,81,146,147}. A homolog of BCL9 (B9L) was also identified in vertebrates and was shown to have 35% sequence identity and 46% sequence similarity to BCL9^{83,148}. In addition, B9L also contained a putative nuclear localization signal that distinguished it from BCL9 and lgs. Sequence alignments of BCL9, B9L and lgs reveal six homology domains (HDs). The HD2 region of BCL9 was shown to mediate its binding with arm/ β -catenin while the HD1 region was shown to be critical for the interaction with Pygo^{80,81,83,147-149}. While Pygo has been shown to be

essential for Wg signaling in *Drosophila*, its necessity in vertebrate Wnt signaling is still unclear^{83,85,148}. Besides recruiting Pygo to the nuclear β -catenin transcriptional complex, BCL9/B9L have been shown to also possess a C-terminal transcriptional activation domain located between HD4 and HD5⁸³⁻⁸⁵.

The full involvement of BCL9/B9L in pathological disorders such as cancer is still being elucidated. Recent work has shown BCL9/B9L to be upregulated in colon cancer and breast cancer and to be correlated with tumor stage^{83,84,150,151}. BCL9 and B9L were also demonstrated to be Wnt target genes and thus, have been proposed to be part of a positive-feedback loop to further stimulate Wnt signaling activity⁸⁴. However, the universal requirement of BCL9/B9L for β -catenin transcriptional activation potential is still unclear. The controversy around the essential nature of BCL9/B9L was underscored by the recent report by Sustmann *et al.* that demonstrated a critical role for BCL9 in lymphoid cells but not fibroblasts⁸⁵. Nevertheless, increasing evidence supports the vital role of BCL9/B9L in Wnt signaling in at least a subset of human malignancies. Further investigation is clearly required to determine the true extent of BCL9/B9L involvement in Wnt signaling and human diseases.

1.3.2 Biomolecular Inhibition of BCL9/B9L

To help elucidate the functional importance of BCL9/B9L in Wnt signaling, a number of genetic mutants and siRNAs have developed in both vertebrate and invertebrate model systems. Several studies have demonstrated that the D164A mutation in β -catenin/arm, which disrupts a critical salt bridge with BCL9/Igs, abolished the binding interaction with BCL9/Igs and inhibited β -catenin-mediated transcriptional activation^{80,146}. Dominant negative constructs of BCL9/B9L that lacked the C-terminal portion of the protein were also shown to inhibit β -catenin activity⁸³⁻⁸⁵. Brembeck *et al.* also demonstrated that expression of only the B9L HD2 region was sufficient for blocking β -catenin activity¹⁴⁸.

siRNA-mediated knockdown of BCL9/B9L has also been shown to inhibit β -catenin activity in cell-based reporter assays and to block the transcription of known Wnt target genes^{83,84,147}. In transformed colon cancer cells, knockdown of B9L inhibited β -catenin transcriptional activation, cell migration, and also induced an epithelial-like phenotype¹⁴⁸. Nevertheless, the mechanism by which BCL9/B9L enhance β -catenin-mediated gene transcription is still not fully understood. In *Drosophila*, BCL9/Igs is required for recruiting Pygo to the β -catenin complex^{61,81,147}. However, in humans the evidence for

Pygo being a critical cofactor is less compelling^{84,85}. On the other hand, the C-terminus of BCL9/B9L appears to harbor an additional transactivation domain that may represent its critical contribution to the β -catenin-TCF complex^{84,85}. However, this transactivation domain was mapped to a region between the HD4 and HD5 regions. Thus, there are still three conserved HD regions in these 1400 amino acid proteins that, to date, have no known function. Clearly, additional investigation is required to elucidate the full functional roles of BCL9 and B9L.

Despite the questions that still remain regarding the complete functional significance of BCL9/B9L in different tissue and cancer types, BCL9/B9L are attractive targets for designing selective inhibitors of β -catenin-mediated Wnt signaling. Because the binding sites for BCL9 and B9L appear to be one and the same and the fact that their binding site is distinct from those of other known β -catenin binding partners, suggests that compounds can be designed that are capable of selectively inhibiting the binding of BCL9 and B9L with β -catenin and antagonizing canonical Wnt signaling. Such a class of inhibitors could have tremendous potential in treating countless hyperproliferative human diseases.

In this work, I have undertaken the initial steps toward the design and discovery of potent peptide and small molecule inhibitors of β -catenin with the BCL9 and B9L proteins. In Chapter 2, I have developed and optimized both FP and SPR-based binding assays for this interaction, and I used the FP assay to characterize the interaction of four key binding residues of BCL9 with BCL9. In Chapter 3, I describe the results of our initial HTS for potential inhibitors of the BCL9/B9L interaction with β -catenin using our FP and SPR-based assays. In Chapter 4, I explored the use of cell-penetrating peptides to design cell-permeable BCL9 peptide-based inhibitors. In addition, I examined three methods of synthesizing stabilized α -helical BCL9 peptides: the hydrogen bond surrogate (HBS) method, the hydrocarbon stapling method, and the triazole stapling method. Our extensive investigation of the triazole stapling technique allowed us to define the optimal combination of azido and alkynyl linkers for stapling one turn of an α -helix.

Chapter 2

Development and optimization of two BCL9-competitive binding assays and analysis of the BCL9 binding interaction with β -catenin

2.1 Background

2.1.1 The BCL9/B9L binding site on β -catenin

Recent reports have suggested that the interaction of β -catenin and BCL9 represents an attractive target for designing inhibitors of β -catenin-mediated Wnt signaling^{61,81,84,85,146,147}. Our work and others have shown that BCL9 and B9L siRNAs and dominant negative gene constructs inhibit β -catenin transcriptional activity, the expression of Wnt target genes and cancer cell migration^{83,84,148}. However, no small molecule or peptide-based inhibitors of the BCL9/ β -catenin interaction have been reported to date.

Analysis of the crystal structure of β -catenin (PDB code 2GL7) in complex with BCL9 and TCF shows that the interaction between β -catenin and BCL9 is distinct from that of other instances of β -catenin binding⁸⁰. This interaction is mediated by a well-defined binding groove in β -catenin and several hydrophobic and charged residues from the α -helix of BCL9. In addition, the binding is associated with a relatively high affinity whose K_d value is 0.5 μM ⁸⁰ (for comparison, p53 α -helix binds MDM2 with a K_d value of 0.2-0.4 μM ^{152,153}). Hence, the BCL9 binding site in β -catenin appears to be a very attractive site for the design of potent and specific small-molecule inhibitors to block the interaction between BCL9 and β -catenin and to inhibit β -catenin-mediated signaling.

2.1.2 Fluorescence polarization (FP) and surface plasmon resonance (SPR) assays for the BCL9/B9L interactions with β -catenin

The lack of a reliable, quantitative and high throughput binding assay for determining the potency of potential inhibitors of BCL9 binding to β -catenin led us to design and develop

a BCL9-competitive FP binding assay. For *in vitro* assessment of inhibitor binding affinities, FP-based assays are extremely useful due to their simplicity, homogenous nature and often large signal-to-noise ratio^{154,155}. The fact that the polarization readout is actually a ratiometric measurement also accounts for variability in lamp intensity. Furthermore, the cost effectiveness and safety of FP assays often make them a preferable method for high throughput screening (HTS) compared to techniques that employ expensive antibodies or radiolabeled probes.

The primary disadvantage of an FP assay arises from the fact that it is a fluorescence-based technique. Thus, compounds having absorption or emission spectra overlapping with those of the fluorophore can cause interference with the signal measurement. The development of red-shifted fluorophores that are excited at longer wavelengths has helped significantly in minimizing this problem¹⁵⁵.

To aid in the discovery and characterization of inhibitors of the BCL9/ β -catenin binding interaction, we developed a quantitative, FP-based binding assay using a fluorescently tagged BCL9 peptide and β -catenin protein. Using our initial FP-based competitive binding assay, we performed extensive mutational analysis on four critical hydrophobic residues in the BCL9 peptide and determined the precise region in BCL9 responsible for binding to β -catenin. These results led to further optimization of our FP assay, making it amenable for identification of non-peptide, small-molecule inhibitors through HTS.

Even though an FP assay has many advantages, the limitations due to autofluorescent/quenching compounds led us to develop a SPR-based secondary screening assay, which is not based upon fluorescence principles and is, thus, an excellent complementary assay. SPR-based methods are able to directly measure the binding of one molecule to another molecule due to changes in the refractive index of the surface to which one molecule is immobilized¹⁵⁶. We therefore developed and optimized a BCL9-competitive SPR-based secondary binding assay to eliminate false positive hits from high throughput screening that arise from autofluorescent/quenching compounds.

2.2 Results

2.2.1 Development of an initial fluorescence polarization assay for the β -catenin/BCL9 interaction

Prior studies have demonstrated that the conserved α -helical HD2 region of BCL9 and B9L is responsible for binding to the first four armadillo (arm) repeats of β -catenin⁶¹ with sub-micromolar affinity⁸⁰. In addition, the crystal structure of BCL9 complexed with β -catenin and TCF4 (PDB code 2GL7) reveals that only 19 residues of the BCL9 HD2 region (residues 356-374) have direct contacts with β -catenin⁸⁰. However, we hypothesized that a BCL9 peptide longer than 19 amino acids may be needed for stabilizing the α -helical secondary structure of the peptide and achieving high binding affinity. For this reason, we first synthesized fluorescein-labeled BCL9 peptide tracer (**1-F**) consisting of 35 residues (residues 347-381). Saturation experiments showed that **1-F** binds to β -catenin with a K_d value of $0.6 \pm 0.3 \mu\text{M}$ (Figure 2.1A), which is in good agreement with the value previously determined by isothermal calorimetry⁸⁰.

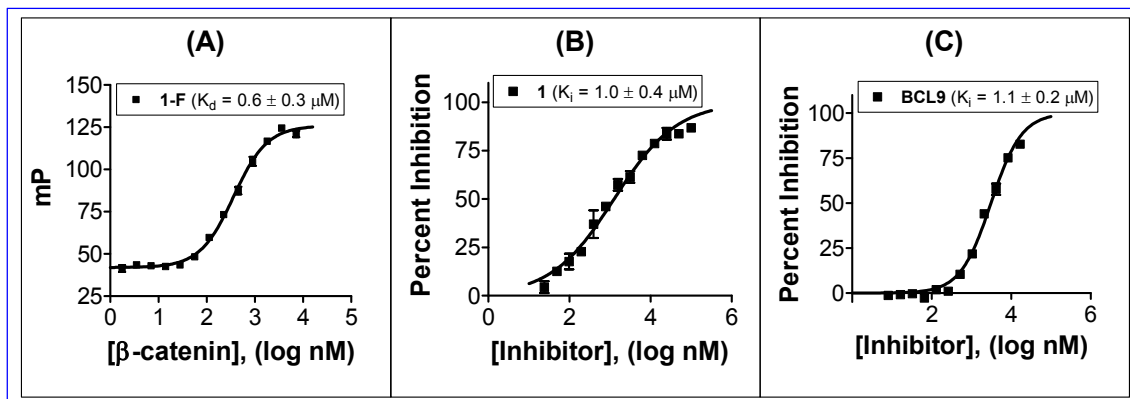


Figure 2.1 Development and validation of a BCL9/ β -catenin FP binding assay. (A) Saturation experiment to determine the K_d value of **1-F** binding to β -catenin. **1-F** (50 nM) was titrated with β -catenin (1-10,000 nM) and the FP signal read after 3 hours. (B) Competitive binding experiment to determine the ability of unlabeled BCL9 peptide **1** to displace the fluorescently-labeled **1-F** (50 nM) from β -catenin (1,000 nM). (C) Competitive binding experiment to determine the ability of recombinant BCL9 protein to displace the fluorescently-labeled **1-F** (50 nM) from β -catenin (1000 nM). K_i values were calculated from the IC_{50} , K_d and protein concentration.

Using **1-F** as a tracer we established a competitive FP-based assay. To achieve a reasonable signal-to-noise ratio, we chose to use $1 \mu\text{M}$ β -catenin and 50 nM **1-F**. To validate the competitive FP assay, we tested the ability of unlabeled BCL9 35-mer peptide **1** and recombinant BCL9 protein to displace **1-F** from β -catenin. Both **1** and BCL9 protein competitively inhibited the binding of **1-F** to β -catenin in a dose-dependent

manner, with K_i values of $1.0 \pm 0.4 \mu\text{M}$ and $1.1 \pm 0.2 \mu\text{M}$, respectively (Figure 2.1B, Figure 2.1C). Additionally, the B9L peptide **48** was also able to competitively displace **1-F** as was expected based on the high degree of sequence identity in the HD2 regions of BCL9 and B9L (Appendix 1). These data showed that the binding of **1-F** effectively mimics BCL9 protein binding and the fluorescein tag has minimal effect on the binding.

2.2.2 Mutational analysis of residues critical for BCL9 binding to β -catenin.

We next investigated the importance of several key hydrophobic residues in BCL9 for the binding interaction of BCL9 with β -catenin. The crystal structure of BCL9 complexed with β -catenin shows that both basic and hydrophobic residues in BCL9 are involved in binding to β -catenin⁸⁰. Since the hydrogen bond involving H358 and the salt bridge involving R359 of BCL9 have previously been shown to be critical for binding, and that mutations at these sites abolish binding to β -catenin^{80,84}, we did not alter these residues during our mutational studies. Instead, we focused our analysis on L366, I369, L373 and F374 residues that insert into deep hydrophobic pockets in β -catenin (Figure 2.2A). Mutations at L366, I369 and L373 have previously confirmed the involvement of these residues for binding to β -catenin, but, no studies of F374 have been reported. While L373 binds in a deep cleft similar to L366 and I369, F374 binds in a wider and slightly shallower pocket which appeared to be able to accommodate larger ring systems.

To facilitate the synthesis, we employed BCL9 peptides with 20 residues (residues 356-375) spanning those which are visible in the reported β -catenin/BCL9 co-crystal structure (Figure 2.2A) and have direct contacts with β -catenin. We predicted that, although such shorter peptides may have lower affinities to β -catenin than that of the longer BCL9 35-mer **1** due to a potential decrease in helical propensity, they nevertheless are sufficient for determination of the binding contributions of these residues to β -catenin.

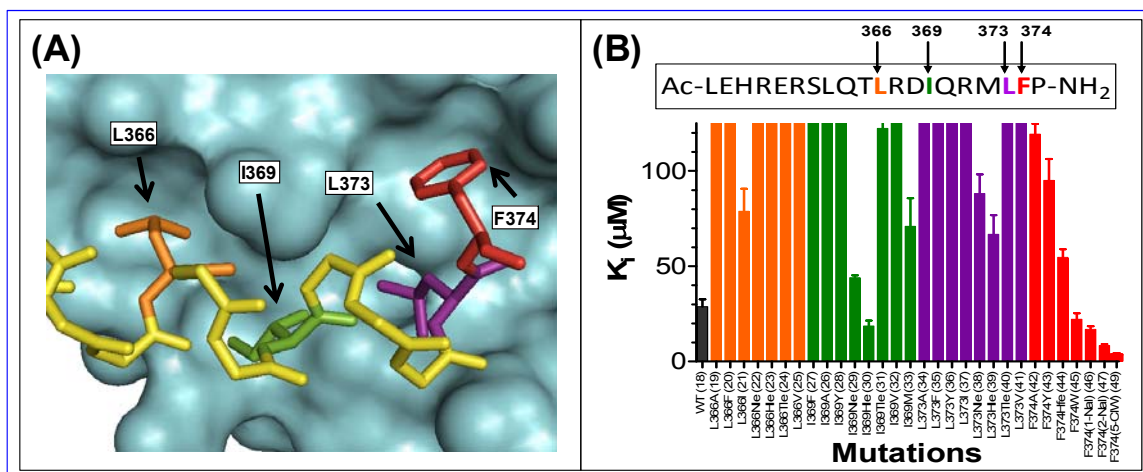


Figure 2.2. Mutational analysis of four BCL9 binding residues. (A) Crystal structure of BCL9 in complex with β -catenin (PDB code 2GL7). β -Catenin is colored cyan. For clarity, only the side chains of BCL9 residues L366 (orange), I369 (green), L373 (purple) and F374 (red) are shown. The backbones of non-mutated BCL9 residues are shown in yellow. (B) K_i values of BCL9 20-mer mutant peptides. Wild-type BCL9 (peptide **18**) is shown in black while single point mutations for the indicated BCL9 residue are color coded as in (A). K_i values were determined using the competitive FP assay with 50 nM 1-F and 1,000 nM β -catenin and exact values are listed in Appendix 1. In order to show differences in K_i values below 30 μ M, the range of illustrated K_i values was limited to 125 μ M.

The binding affinities of these mutated BCL9 peptides were then determined using our initial BCL9-competitive FP-based assay. As expected, the wild-type BCL9 20-mer **18** was 30-fold less potent (K_i = 28 μ M) than **1** (K_i = 0.964 μ M; Appendix 1). Circular dichroism experiments confirmed that the BCL9 35-mer peptide lacking the C-terminal β -Ala-Lys used for labeling (Appendix 1, peptide **1-b**) was more helical than **18** (16.9% versus 9.7%) in distilled water (Appendix 3A). Using **18** as a standard, we compared the binding affinities of BCL9-based peptides bearing single amino acid mutations at L366, I369, L373 or F374 (Figure 2.2B, Appendix 1). As shown in Figure 2.2B, L366 and L373 were intolerant of substitutions with either larger or smaller hydrophobic residues, with a drastic reduction in binding affinity for nearly all mutant peptides (Appendix 1, peptides **19-25**, **34-41**). Most mutations at I369 were also detrimental to binding affinity with the exceptions of norleucine (Nle) and homoleucine (Hle) (Appendix 1, peptides **29** and **30**), which showed approximately equal binding affinity compared to **18**. In contrast, mutation of F374 to residues possessing larger bicyclic aromatic side chains (Appendix 1, peptides **45-47**) resulted in an increase in binding affinity with 2-naphthylalanine (2-Nal) and 5-chlorotryptophan (5-CIW) showing the best improvement with 3-fold and 8-fold increases, respectively. When the F374(2-Nal) mutation was made in the longer BCL9

35-mer (Appendix 1, peptide **2**) we found a similar 3-fold improvement relative to peptide **1**. However, when the F374(5-CIW) mutation was made in longer BCL9 peptides (Appendix 1, peptide **50**), we did not see the corresponding 8-fold improvement as was seen in the BCL9 20-mer. Instead, we only found a 2-3 fold improvement. This discrepancy may be due to possible differences in binding mode or helical propensity induced by the presence of the 5-CIW moiety.

2.2.3 Determination of the minimal domain in BCL9 for wild type-like binding affinity for β -catenin

Although, the wild type BCL9 20-mer peptide **18** appeared to possess all of the β -catenin binding residues based upon the BCL9/ β -catenin co-crystal structure (PDB code 2GL7), the longer peptide **1** is 30 times more potent than **18** in its binding affinity for β -catenin. Since there is only a 2-fold difference in the helical content of **1** and **18**, we hypothesized that at least some of the additional residues in **1** were involved in additional binding interactions that are not visualized in the crystal structure. Therefore, we next determined the minimal domain in BCL9 responsible for its high affinity binding to β -catenin.

As shown in Figure 2.3, removal of the C-terminal six residues of **1** (peptide **10**) did not result in any noticeable decrease in binding affinity. In contrast, deletion of the N-terminal nine residues of **1** (peptide **9**) resulted in a 17-fold decrease in binding affinity to β -catenin.

Having identified the N-terminus of the peptide as being critical to maintaining wild-type binding affinity of BCL9 peptide to β -catenin, we proceeded to identify the precise residues which are required for enhancing the binding affinity of BCL9. Since the α -helical region of BCL9 HD2 is predicted to initiate approximately at L351, we systematically deleted 2-amino acid sections from the N-terminus of our elongated BCL9 peptide **10**. Evaluation of these increasingly shorter peptides indicated that the N-terminal four amino acids (NPDG) were extraneous but any further truncation of the peptide resulted in significant (>30-fold) decreases in BCL9 peptide binding affinity (Figure 2.3B, C, peptides **11-14**). These results were in good agreement with a recent report that demonstrated that the L351A mutation in BCL9 protein abolished binding of BCL9 to β -catenin⁸⁴.

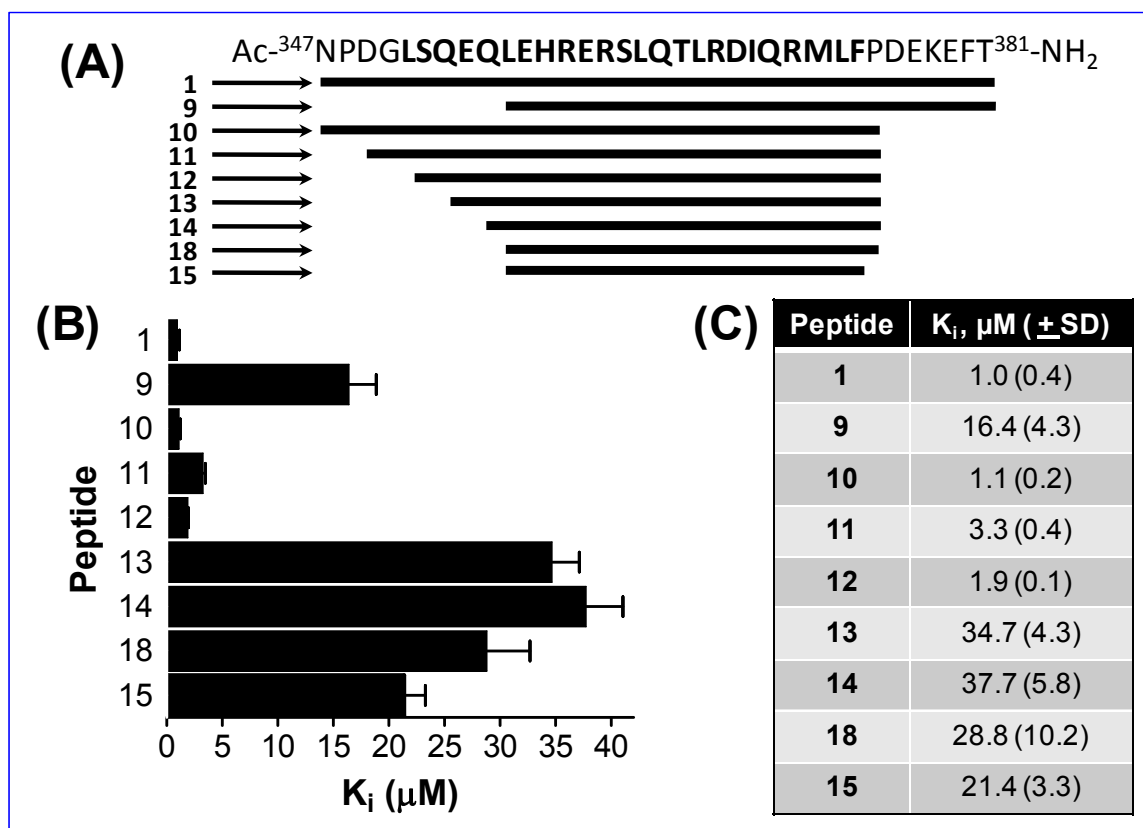


Figure 2.3 Mapping of the minimal β -catenin-binding region of BCL9. (A) BCL9 peptides of different lengths. Peptide sequences correspond to the underlined region. The minimum binding sequence is in bold. (B) BCL9 peptide K_i values determined using competitive FP-based assay with 1-F (50 nM) and β -catenin (1,000 nM). (C) Table of BCL9 peptide K_i values (averages and standard deviations of 3 or more experiments).

Finally, removal of P375 at the C-terminus of **18** had no detrimental effect on the binding of the resulting BCL9 peptide to β -catenin (Figure 2.3, peptide **15**). Similar results were obtained when P375 was removed from the longer peptide **12** (Appendix 1 peptide **16**). We concluded from the peptide truncation studies that the minimal domain in BCL9 responsible for its high affinity binding to β -catenin involves residues 351-374.

2.2.4 Re-optimization of BCL9-competitive FP assay

Having determined the minimal binding sequence of BCL9 required for high affinity binding to β -catenin and identified certain non-natural amino acids that could further increase the peptide binding affinity, we sought to further optimize the fluorescently-labeled tracer used in the FP assay. We synthesized a series of shortened peptide tracers that spanned the minimal binding sequence of BCL9 (residues 351-374) and included the F374(2-Nal) mutation alone or in combination with the I369Hle mutation (Appendix 1, peptides **3-F** - **8-F**). We also examined the effects of having the fluorescein

tag at either the N- or C-terminus, and of using β -alanine or 6-aminohexanoic acid as the spacer between the peptide and the tag.

As shown in Figure 2.4, attaching fluorescein to the N-terminus of the peptide (peptides **6-F**, **7-F**) resulted in a narrow dynamic range of ~ 70 mP, whereas labeling on the C-terminus gave an excellent dynamic range of over 160 mP (**4-F**, **5-F**, **8-F**). Furthermore, relatively high concentrations (50 nM) of N-terminally labeled peptides were required to achieve adequate fluorescence signal, while C-terminally labeled tracers gave excellent fluorescence signal at concentrations as low as 5 nM (data not shown).

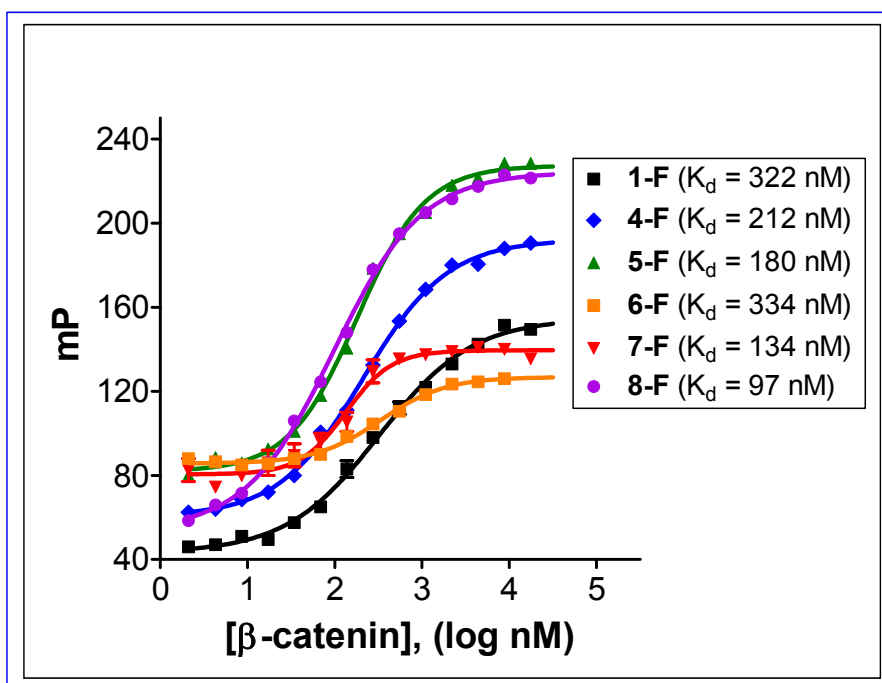


Figure 2.4 K_d and dynamic range for shortened BCL9-derived peptide tracers. Saturation experiments were performed by titrating each tracer (50 nM for **1-F**, **6-F** and **7-F**; 5 nM for **4-F**, **5-F**, and **8-F**) with β -catenin ranging from 2 nM-18 μ M in assay buffer containing 0.01% Triton X-100 and 4% DMSO.

Inclusion of the I369Hle mutation in addition to the F374(2-Nal) mutation (peptides **3-F** - **6-F**) resulted in no additional enhancement in binding affinity as compared to peptides with only the F374(2-Nal) mutation (peptide **7-F** versus peptide **8-F**; Figure 4). In comparing the type of linker used to attach fluorescein we found that the two β -alanine spacer on the C-terminus of the peptide to link the lysine(FAM) conjugate was slightly better than the 6-aminohexanoic acid spacer (data not shown). We therefore chose **8-F** as the optimized tracer for the FP assay.

Saturation experiments showed that **8-F** has a K_d value of 101 ± 42 nM to β -catenin. Furthermore, the FP signal and K_d were stable over 29 hours (Figure 2.5A) and were not affected by 4% of DMSO (Figure 2.5B). For the purpose of high throughput screening, we tested the effect of the surfactant Triton X-100, which can minimize aggregation effects by hydrophobic molecules. Our data showed that 0.01% of the Triton X-100 had no significant effect the FP signal and K_d but higher concentrations (0.05% and 0.1%) caused a decrease in K_d and assay dynamic range (Figure 2.5C).

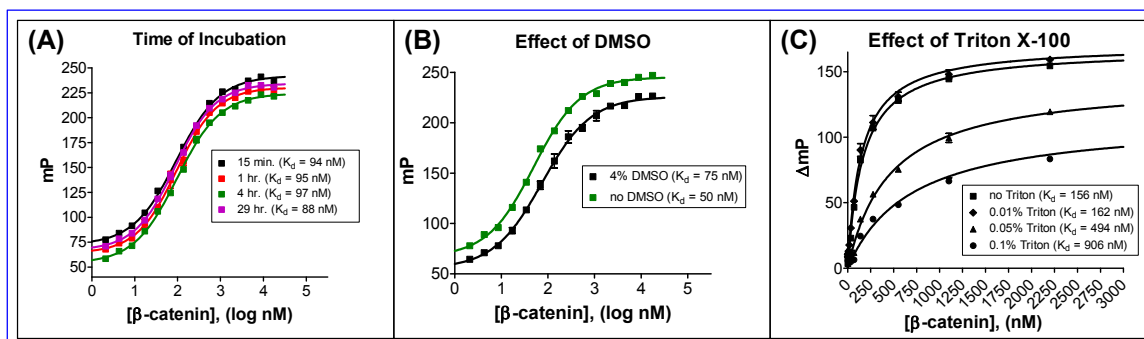


Figure 2.5 Stability of BCL9 FP assay. (A) Saturation experiment with **8-F** to monitor the K_d and dynamic range over an extended time period. **8-F** (5 nM) was titrated with β -catenin (2 nM-18 μ M) in assay buffer containing 4% DMSO and the plate was read at the indicated time points. (B) Saturation experiments with **8-F** to determine the effect of DMSO. Experiments were performed as in (A) in the presence of 0 or 4% DMSO. (C) Saturation experiments with **8-F** to determine the effect of adding Triton X-100 to the assay buffer. Saturation experiments were performed as in (A) using assay buffers containing 0, 0.01, 0.05 or 0.1% Triton X-100. In all experiments, the FP signal was measured after 3 hours and the K_d value was calculated by non-linear least squares analysis.

In re-optimizing our competitive FP assay, we selected a concentration of 250 nM β -catenin and 5 nM of **8-F**. Similar to the results from the saturation experiments, the optimized competitive assay with **8-F** demonstrated a marked improvement in the assay dynamic range (84 mP) compared to the original assay with **1-F** (dynamic range 49 mP). To assess the quality of our re-optimized assay for use as a high throughput screening assay, we calculated the statistical parameter Z' which reflects the dynamic range of the assay as well as the deviation in the controls¹⁵⁷. High quality assays should have Z' -factors nearing the maximum value of 1, with a typical cutoff value for acceptable HTS assays of $Z' = 0.5$. As shown in Figure 2.6, the re-optimized competitive FP assay has a Z' of 0.72 compared to a Z' of 0.29 for the original assay using **1-F**, thus indicating the suitability of our optimized FP assay for HTS purposes.

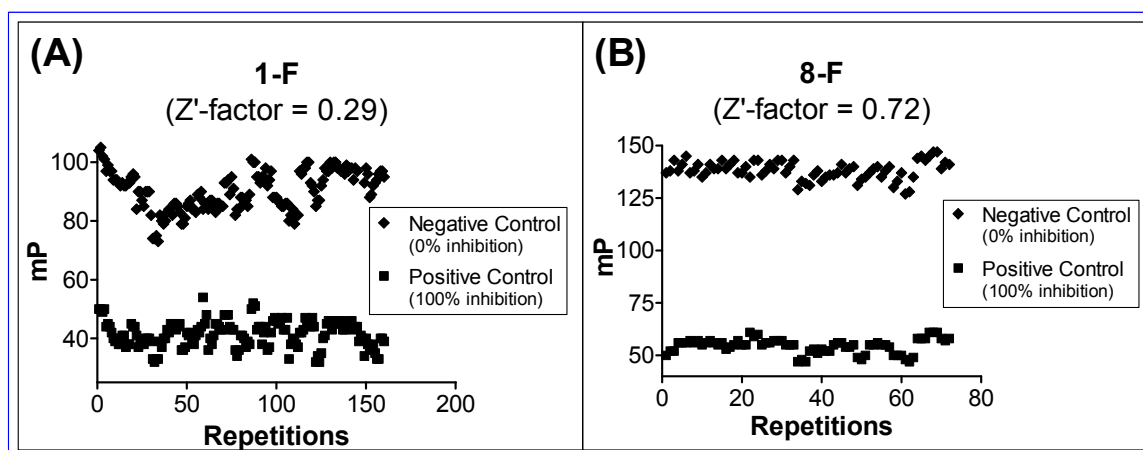


Figure 2.6 Calculated Z'-factors for competitive FP-based assays. (A) Controls and Z'-factor for original competitive FP assay using **1-F** (50 nM) and β -catenin (1 μ M). (B) Controls and Z'-factor for re-optimized competitive FP assay using **8-F** (5 nM) and β -catenin (250 nM). Positive controls representing 100% inhibition contain only tracer. Negative controls representing 0% inhibition contain tracer and β -catenin. Points represent the control wells from experiments performed in separate 96-well plates.

2.2.5 Development of a SPR-based binding assay.

In addition to having a HTS-worthy primary assay, it is critical to have an effective secondary assay to confirm potential screening hits. We therefore designed and optimized a SPR-based BCL9 binding assay. Since SPR-based assays are based on biophysical principles distinct from those involved in fluorescence-based techniques they are not affected by issues of autofluorescence or quenching by the compounds being tested.

For our SPR-based assay, we immobilized recombinant BCL9 protein on the surface of the SPR sensor chip using standard EDC/NHS amide coupling chemistry. BCL9 protein was immobilized at different densities on the Fc2 (4,000 response units), Fc3 (2,200 response units) and Fc4 (1,600 response units) surfaces of the chip, while the Fc1 surface was used as a control surface to account for non-specific binding to the chip.

We evaluated the binding of recombinant β -catenin to immobilized BCL9 using several different concentrations of β -catenin ranging from 500 nM to 8 μ M and determined that β -catenin binds to immobilized BCL9 with a K_d value of 2.9 μ M (Figure 2.7A). This value is in good agreement with the binding affinity of the BCL9 peptide in our FP assay (K_i = 1.1 μ M; Figure 2.1C), suggesting that immobilized and free BCL9 proteins interact with β -catenin very similarly.

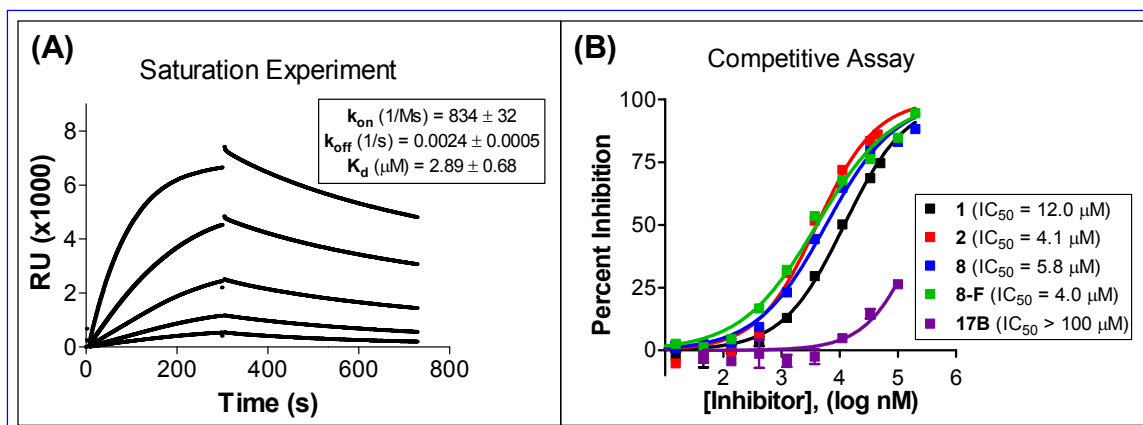


Figure 2.7 SPR-based BCL9 binding assays. (A) Determination of kinetic and steady state parameters for β -catenin binding to immobilized BCL9 protein. The sensograms indicate the responses when varying concentrations (from bottom to top: 0.5, 1, 2, 4, 8 mM) of β -catenin were injected over immobilized BCL9. The k_{on} , k_{off} and K_d were calculated by simultaneous non-linear regression. (B) Competitive binding experiment to determine the ability of synthetic BCL9 peptides to inhibit the binding of β -catenin to BCL9 protein. β -Catenin (300 nM) was preincubated with varying concentrations of peptide inhibitors for at least 30 minutes and then 20 μ L of the reaction mixture was injected at 20 mL/minute over the immobilized BCL9. IC_{50} values were determined by non-linear least squares analysis.

To validate the SPR assay, we tested if our synthetic BCL9 peptides can disrupt the binding of β -catenin to immobilized BCL9 protein. β -Catenin protein was preincubated with varying concentrations of synthetic BCL9 peptides and then injected over the surface of the chip. As shown in Figure 2.7B, the wild type BCL9 35-mer (**1**) inhibits the binding of β -catenin to BCL9 with an IC_{50} value of 12 μ M, which is in reasonable agreement with the determined IC_{50} of 3.5 μ M (K_i = 0.96 μ M) from our FP experiments. Furthermore, peptides bearing the 2-naphthylalanine substitution at F374 (**2**, **8**, **8-F**) show the same 2-3-fold enhancement in binding affinity, consistent with our data obtained in our FP experiment. The specificity of our competitive SPR-based assay was confirmed using peptide **17B** as a negative control. This peptide, which contains known inactivating alanine mutations at residues L366 and I369⁸⁰ and which is inactive in our FP assay (Appendix 1), was likewise found to be more than 10-fold less potent than the wild type peptide **1** in our competitive SPR-based assay. Thus, our competitive SPR-based assay can quantitatively determine the binding affinities of BCL9 peptides to β -catenin in competition with the recombinant BCL9 protein and the results are consistent with those obtained using our FP assay. Therefore, this SPR assay can serve as a useful secondary assay with which to confirm the inhibition of BCL9 binding to β -catenin by compounds identified in our FP-based HTS assay.

2.3 Discussion

2.3.1 **Development and optimization of a high throughput BCL9/B9L-competitive FP binding assay and analysis of the BCL9 binding interaction with β -catenin**

There is much interest in identifying inhibitors of the canonical Wnt signaling pathway and our focus is on the BCL9/B9L binding interactions with β -catenin. BCL9 and B9L primarily bind to a unique binding site located at the N-terminal armadillo (arm) repeat of β -catenin. Analysis of the crystal structure of β -catenin in complex with BCL9 and TCF (PDB code 2GL7) indicates that the α -helical HD2 region of BCL9 binds in a well defined groove in the first arm repeat of β -catenin and does not make any observable contacts with TCF or its binding site on β -catenin⁸⁰. Therefore, inhibitors that bind at the BCL9 binding site may have little or no effect on the interactions of β -catenin with its cytosolic binding partners^{80,84}. Despite this key advantage, no inhibitors of the BCL9 interaction with β -catenin have been reported. This could be, in part, due to the relatively recent discovery of BCL9 as a required component of the β -catenin transcriptional activation complex in human cells. Recently, BCL9 was shown to specifically enhance β -catenin-mediated transcriptional activation in lymphoid cells⁸⁵. BCL9 and its closely related partner B9L were also shown to be crucial to the activity of β -catenin in SW480 colon cancer cells with constitutively activated β -catenin and in Wnt3A-stimulated HEK 293 cells⁸⁴. Additionally, siRNA knockdown of B9L was shown to reduce cell migration, induce an epithelial-like phenotype and inhibit colony formation in colon cancer cell lines¹⁴⁸. Our own results from BCL9/B9L siRNA experiments further support notion that BCL9 and B9L are involved in β -catenin-mediated activation of Wnt target genes. These studies have thus suggested that blocking the BCL9/ β -catenin interaction using small-molecule inhibitors represents an attractive anticancer strategy.

Toward the discovery of small-molecule inhibitors of the BCL9/ β -catenin interaction, we initially developed a reliable and quantitative FP-based binding assay employing a fluorescently-labeled 35-residue BCL9 peptide (**1-F**) and recombinant β -catenin protein and determined that they have a K_d value of 0.62 μ M. This first competitive FP assay, however, had a narrow dynamic range (~45 mP) and a calculated Z' -factor of 0.29, making it unsuitable as a HTS assay. We therefore performed extensive mutational analysis on four critical binding residues (L366, I369, L373, and F374) and showed that while the first three sites were intolerant to mutation, the substitution of 2-

naphthylalanine at F374 could increase the binding affinity of the peptide by 3-fold. We also sought to reduce the overall length of our tracer and subsequently mapped the minimal binding sequence of BCL9 to residues 351-374. Our minimal binding sequence is consistent with the recent report by de la Roche *et al.*⁸⁴, which demonstrated that L351, despite being distant from the β -catenin binding pocket, was critical for the binding of BCL9. Using the results of our peptide mapping and mutation experiments, we were able to develop an optimized tracer (**8-F**) that is 9-residues shorter than **1-F** and had a K_d value of 101 nM. This led to an optimized FP-based competitive assay using **8-F**, which has a large dynamic range, an excellent signal-to-noise ratio and a calculated Z' -factor to 0.72, making this assay suitable for HTS.

Also noteworthy was the fact that our optimized FP assay utilized a more stable preparation of purified recombinant β -catenin. During our original experiments, we found that the β -catenin protein was unstable and tended to precipitate after one to two months of storage at -80°C , even in the presence of 10% glycerol. This was a contributing factor to the higher than normal standard deviations in our initial assays (Figure 2.6). To address this issue, we found that adding 50 mM glutamine and 50 mM arginine to the purification buffer helped stabilize the protein, giving higher yields of soluble protein that did not show signs of precipitation after more than six months of storage. Using this more stable preparation of β -catenin, we also found that the K_d and K_i values of our peptides were on average twice as potent (compare **1-F** from Figure 2.1A and Figure 2.4); however the same trends in potencies for mutated peptides and wild-type peptides of varying lengths remained unchanged.

2.3.2 Development and optimization of a BCL9-competitive SPR-based secondary assay

Since fluorescence-based FP assays are prone to having false positive results due to autofluorescent compounds, we also developed an SPR-based binding assay to complement our FP assay. SPR-based techniques, which are not reliant on molecular fluorescence, are useful for discriminating between compounds that truly inhibit protein-protein binding and eliminate false positives arising from compounds that absorb light or fluoresce at wavelengths similar to those of the fluorescent probe in the FP assay. For our SPR-based assay, we immobilized recombinant BCL9 protein (residues 347-393) and demonstrated that it binds to β -catenin with a K_d value of 2.9 μM . This value was in good agreement with the K_i value of 1.1 μM for the recombinant BCL9 protein

determined in our FP assay and suggested that the immobilized BCL9 protein binds to β -catenin in a manner similar to the recombinant BCL9 protein in solution.

We next developed and optimized the conditions for a competitive SPR assay. Using our BCL9-derived peptides, we showed that BCL9 peptides effectively inhibit the binding of β -catenin to the immobilized BCL9 protein in a dose-dependent manner and the determined IC_{50} values in the SPR assay are in good agreement with those measured in our FP assay.

2.4 Summary

Thus, we now have developed the first set of complementary BCL9/B9L-competitive binding assays. Our FP assay is quantitative, robust and easily adaptable to HTS conditions. Our SPR-based assay has been validated using BCL9 peptides and is an ideal secondary assay since it relies on completely separate biophysical principles for measuring BCL9- β -catenin binding. Together, these assays have laid the groundwork for future HTS campaigns and BCL9/B9L-competitive inhibitor development. Furthermore, our mutational analysis of several key binding residues of BCL9 has helped define the size and scope of residues able to be substituted at those positions. The finding that indole and naphthyl-type moieties are tolerated in place of F374 is intriguing in the context of *de novo* design of small molecule inhibitors, since related ring systems can be useful core scaffolds.

2.5 Experimental Methods

2.5.1 General procedure for peptide synthesis

Peptides were synthesized using standard Fmoc solid-phase peptide synthesis techniques. Briefly, Rink amide resin with either 0.2 mmol/g (for peptides ≥ 24 residues in length) or 0.7 mmol/g (for peptide < 24 residues in length) substitution levels were used to prepare all C-terminal amide capped peptides. Standard side chain protecting groups were used for all amino acids with the exception of N^{ϵ} -4-methyltrityl-lysine (Lys(Mtt)), which was used for coupling to fluorescein. Peptides were synthesized using an ABI 433A automated peptide synthesizer, FastMoc Chemistry and 4-5 equivalents of each amino acid.

Certain unnatural and problematic amino acids such as homoleucine (Hle) and *t*-butyl-leucine (Tle) were coupled manually as follows. The resin-bound peptide was placed in a 5 mL disposable polypropylene column (Fisher Scientific), deprotected with 20% piperidine (2 x 3 mL x 15 minutes) and then washed with DMF (3 x 3 mL), MeOH (3 x 3 mL) and DMF (3 x 3 mL). The Fmoc-amino acid (4 equivalents) was preactivated with HATU (4 equivalents) and HOAt (6 equivalents) in DMF (3 mL) for 10 minutes, and then treated with DIEA (6 equivalents) and added to the resin. The reaction was mixed by inverting for 1 hour or until the resin tested negative in the Kaiser ninhydrin test¹⁵⁸. The remaining residues in the peptide were then coupled using the ABI 433A peptide synthesizer.

For fluorescein labeling, resin-bound peptides were treated with 1% TFA/DCM (5 x 1.5 mL x 15 minutes) to deprotect Lys(Mtt). The peptide was then treated with 5-carboxyfluorescein (5-FAM) N-hydroxysuccinimidyl ester (2 equivalents) and DIEA (3 equivalents) in dry DMF (3 mL). The reaction was covered in aluminum foil and mixed by rocking on a Clay Adams NutatorTM for 4 hours.

Peptides were cleaved from the resin using 87.5% TFA, 5% DTT, 5% H₂O, 2.5% TIS (3 x 2 mL x 10 minutes). The combined filtrates were allowed to stand at room temperature for 2 hours and then concentrated *in vacuo* and precipitated with cold diethyl ether. The crude peptides were purified by semi-preparative reverse-phase high performance liquid chromatography (RP-HPLC) using a Waters Delta 600 HPLC equipped with a Waters 19 x 150 mm SunfireTM C₁₈ column and a Waters 2489 UV detector. Peak fractions were concentrated and lyophilized for 16-24 hours. The pure peptides were characterized by analytical RP-HPLC and electrospray ionization mass spectrometry (ESI-MS). The results are presented in Table S1.

2.5.2 Recombinant proteins

The β -catenin and BCL9 cDNAs were kind gifts from Dr. Wenqing Xu at the University of Washington and Dr. Konrad Basler of the Institut für Molekularbiologie at the Universität Zürich, respectively. β -Catenin (residues 138-686) and BCL9 (residues 347-393) were cloned into a pHis-TEV vector and transformed into BL21 DE3 *Escherichia coli*. Cells were cultured in LB media with 30 μ g/mL kanamycin until the OD₆₀₀ was approximately 0.6 and then protein expression was induced with 200 μ M IPTG at 20°C overnight. Cells were lysed by sonication and the proteins were purified by two steps of chromatography

including Ni-NTA agarose affinity chromatography and size-exclusion chromatography using an Amersham Biosciences P-920 FPLC equipped with a Superdex 200 (for β -catenin) or Superdex 75 (for BCL9) column. β -Catenin was eluted in 30 mM bis-Tris (pH 6.5), 200 mM NaCl, 10% glycerol, 1 mM DTT with or without 50 mM glutamine and 50 mM arginine. BCL9 was eluted in 30 mM Tris (pH 7.5), 200 mM NaCl, 50 mM glutamine, 50 mM arginine, 1 mM DTT. Proteins were aliquotted and stored at -80°C .

2.5.3 FP assays

FP experiments were performed in Microfluor® 2, 96-well, black plates (Thermo Fisher Scientific) and read using a Tecan Ultra plate reader (Tecan U.S. Inc., Research Triangle Park, NC). Saturation experiments to determine the K_d values of fluorescently-labeled tracers with β -catenin protein used 50 nM (**1-F**) or 5 nM (**8-F**) tracer and serial dilutions of β -catenin protein (e.g. 1 nM - 10 μM) in assay buffer (100 mM Na_2PO_4 , pH 7.4, 100 $\mu\text{g}/\text{mL}$ bovine gamma globulin, 0.01% Triton X-100; Invitrogen) with 4% DMSO to produce a total reaction volume of 125 μL . Competitive FP binding experiments used 50 nM (**1-F**) or 5 nM (**8-F**) tracer, 5 μL of compound in DMSO, and a fixed concentration of β -catenin (typically $1.5\text{-}3 \times K_d$ of the tracer; e.g. $K_d = 0.616 \mu\text{M}$, β -catenin concentration used = 1.0 μM) in assay buffer to produce a final volume of 125 μL . Dose-dependent experiments are performed in the same manner using no fewer than 10 concentrations of compound diluted by serial dilution. For each assay, negative controls (equivalent to 0% inhibition) contain tracer, β -catenin and 5 μL DMSO, while positive controls (equivalent to 100% inhibition) contain only tracer and DMSO in a final volume of 125 μL . Each assay plate was covered with adhesive aluminum foil and gently mixed on an orbital shaker for at least 3 hours to reach equilibrium before reading polarization values using 485 nm and 535 nm excitation and emission wavelengths, respectively. Percent inhibition was calculated from equation 1,

$$\% \text{ inhibition} = 100[1 - (\text{mP} - \text{mP}_{\text{free}}) / (\text{mP}_{\text{bound}} - \text{mP}_{\text{free}})] \quad (\text{eq. 1})$$

where mP_{free} is the signal for the free probe (positive control) and mP_{bound} is the signal for the bound probe (negative control). The IC_{50} , the concentration of inhibitor required to displace 50% of the tracer, was determined by non-linear least squares analysis using GraphPad Prism® software. The K_i values for the compounds were calculated using the equation for FP assays¹⁵⁹. Values reported in Appendix 1 represent the averages and

corresponding standard deviations of three or more independent experiments. The Z'-factor for the competitive FP assay was calculated as reported previously¹⁵⁷.

2.5.4 SPR binding assays

SPR experiments were performed at room temperature using Biacore 2000 and 3000 optical biosensors. Recombinant BCL9 (residues 347-393) in sodium acetate buffer (pH 5.0) was immobilized at different densities on the Fc2 (4,000 response units), Fc3 (2,200 response units) and Fc4 (1,600 response units) surfaces of a CM-5 sensor chip using standard EDC/NHS coupling chemistry followed by ethanolamine deactivation of the surfaces. The Fc1 surface was used as a control surface and was treated in the same manner as the Fc2 and Fc3 surfaces but in the absence of BCL9.

The binding affinity of recombinant β -catenin (residues 138-686) to immobilized BCL9 was determined by injecting β -catenin solutions with different concentration from 500 – 8,000 nM in HBS-EP buffer (10 mM HEPES pH 7.4, 150 mM NaCl, 3 mM EDTA, 0.005% v/v P20) over the surfaces at a constant flow rate of 20 μ L/min. During each injection, the protein/protein complex was allowed to associate/dissociate for 300 s and 420 s, respectively. The chip surfaces were regenerated by injecting 50 mM NaOH (2 x 5 μ L) followed by washing with the running buffer (2 x 10 μ L). The measured response units from the Fc4 surface were normalized by subtracting the signal obtained from the Fc1 control surface. The kinetic and binding parameters, k_{on} , k_{off} and K_d , were calculated by globally fitting the data to a 1:1 interaction model using BIAEvaluation software.

SPR competitive solution binding experiments were performed using a constant concentration of β -catenin protein (300 nM). The protein was preincubated at room temperature for at least 30 minutes with varying concentrations of synthetic BCL9 peptides. The reaction mixture (20 μ L) was injected over the surfaces of the chip at a flow rate of 20 μ L/minute. Response units were measured at 3 minutes in the dissociation phase and the specific binding was calculated by subtracting the signal from the control surface (Fc1) from the surfaces with immobilized BCL9. Percent inhibition was calculated from equation 2,

$$\% \text{ inhibition} = 100[1 - (RU_{\text{complex}})/(RU_{\beta\text{-cat}})] \quad (\text{eq. 2})$$

where RU_{complex} is the specific binding signal for β -catenin protein in the presence of the inhibitor and $RU_{\beta\text{-cat}}$ is the specific signal for the β -catenin alone (negative control). For maximum signal-to-noise ratio, the surface with the highest density of immobilized BCL9 (i.e. Fc2) was used for IC_{50} determinations. IC_{50} values were calculated by non-linear least squares analysis using Graph Pad Prism 5.0 software.

Chapter 3

HTS for inhibitors of the BCL9/B9L binding interaction with β -catenin

3.1 Background

HTS started becoming a regular part of drug discovery research during the early to mid 1990's¹⁶⁰. HTS is typically defined by the ability to perform 10,000 – 40,000 assay reactions in a single day. More recently, ultra-high throughput screening (uHTS) has been put into practice with researchers being able to screen over 100,000 compounds in a 24 hour period. For HTS, the typical assay format utilizes either 384- or 1536-well plates with typical working volumes of 10-20 μ L or 2.5-10 μ L, respectively. Performing screening assays on such small scale and with such large numbers of compounds requires simple, robust assays that are amenable to miniaturization.

FP assays meet these criteria exceptionally well and have become a cornerstone of HTS methodology in pharmaceutical research¹⁵⁴. The assays are both homogeneous (do not require a separation step) and extremely sensitive with some assays reported to use picomolar concentrations of fluorophore probes¹⁵⁴. In addition, the reproducibility and often large dynamic ranges of FP assays lead to assays with high Z'-factors making it easier to distinguish actives from false positives during HTS. As demonstrated in Figure 2.6B, our optimized BCL9/B9L-competitive FP assay has a calculated Z'-factor of 0.72 and a reasonably large dynamic range (~80 mP) making it suitable as a primary HTS assay.

Although FP assays can make ideal primary screening assays, HTS often produces hundreds to thousands of initial "active" compounds that require additional follow-up in order to confirm them as "hits." Thus, it is imperative that every HTS campaign have complementary secondary assays to eliminate false positives and confirm active compounds. For our system, we chose an SPR-based assay to confirm our active compounds. We developed and optimized our BCL9/B9L-competitive SPR-based assay

and validated it using our BCL9 peptide-based inhibitors (Figure 2.7B). Our FP and SPR-based assays, therefore, laid the foundations for employing HTS to identify compounds that could potentially be inhibitors or scaffolds for designing inhibitors of the BCL9/B9L binding interaction with β -catenin.

With our high throughput FP assay we screened an in-house collection of 54,000 compounds at the Center for Chemical Genomics at the University of Michigan. Several compounds had confirmed dose-dependent inhibition in our FP and SPR-based assays and are currently being characterized in additional *in vitro* and cell-based selectivity and counter screening assays.

3.2 Results

3.2.1 Optimization of BCL9/B9L-competitive FP assay for HTS

Before moving on to using our FP assay for HTS, we chose to perform additional optimization of the assay to employ the red-shifted fluorophore 5-carboxy tetramethyl rhodamine (5-TAMRA). The 5-TAMRA fluorophore has excitation and emission wavelengths of 540 and 590 nm, respectively, compared to 490 and 520 nm, respectively for 5-FAM. The longer wavelengths employed in the use of the TAMRA-labeled probe help minimize interference from autofluorescent and quenching compounds. Thus, we synthesized the 5-TAMRA analog (**8-R**) of our previously optimized probe **8-F**. Interestingly, we found that **8-R** was extremely sensitive to the presence of bovine gamma globulin (BGG; 100 μ g/mL) in the assay buffer and appeared to show concentration-dependent non-specific binding to either BGG or bovine serum albumin (BSA; Figure 3.1A). When titrated with BSA, **8-R** showed much higher non-specific binding than **8-F**. BGG or BSA are typically included in FP assay buffers as additives to reduce non-specific binding to the surface of the plates. However, in this situation it appeared that the TAMRA fluorophore caused an unacceptably high level of binding of **8-R** to BGG.

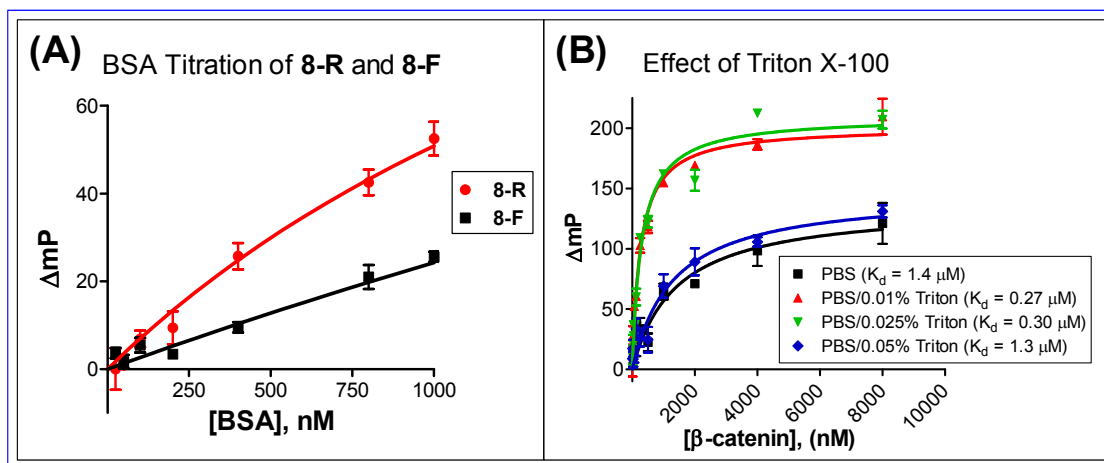


Figure 3.1 Effects of BSA and Triton X-100 on the signal and binding affinity of 8-R. (A) BSA titration of 8-R and 8-F. Tracers (5 nM) in PBS with 0.01% Triton X-100 were titrated with BSA (25-1,000 nM). (B) Saturation experiments with 8-R (5 nM) and β -catenin (250 nM) to determine the effect of adding Triton X-100 (0-0.05%) to the assay buffer without BGG.

By omitting BGG from the assay buffer and using only PBS with 0.01% Triton X-100, we determined 8-R to have a K_d value of 0.26 μM . However, the binding affinity of 8-R was also sensitive to the concentration of detergent. As shown in Figure 2.7B, the binding affinity of 8-R was in good agreement with that of 8-F at Triton X-100 concentrations of 0.01 and 0.025%. In contrast, at concentrations of 0 or 0.05% Triton X-100 the dynamic range of 8-R was reduced dramatically and the K_d value decreased by over 4-fold (Figure 3.1B). Thus, for HTS with 8-R we chose to use PBS with 0.025% Triton X-100 as the assay buffer.

After optimizing the conditions for our FP assay using 8-R, we needed to scale down the reaction volume for performing the screening in low volume 384-well plates. As a testament to the robustness of FP assays in general, we were able to directly scale down the reactions from a working volume of 125 μL to a volume 15 μL . Due to the high molar extinction coefficient of TAMRA ($\epsilon = 65,000 \text{ cm}^{-1}\text{M}^{-1}$) 5 nM 8-R was still sufficient for achieving acceptable fluorescence intensity. In addition, the miniaturized BCL9 HTS assay maintained a Z' -factor of 0.72 (Figure 3.2)

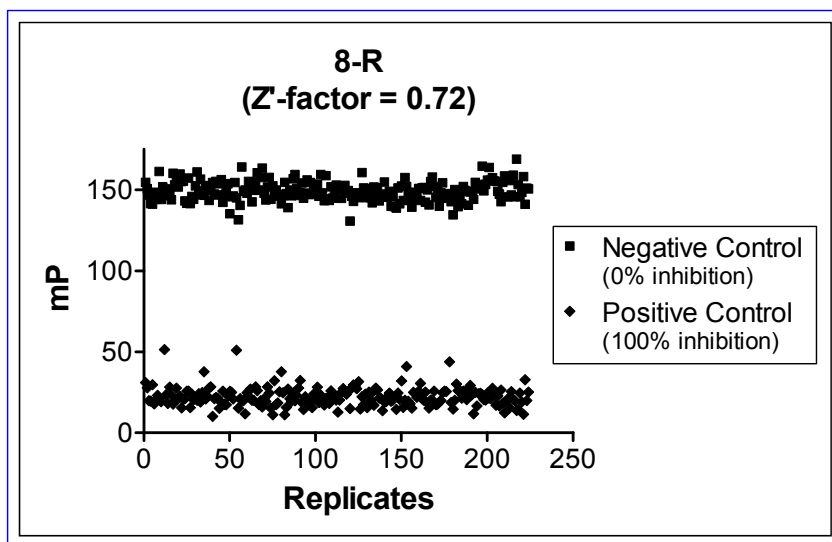


Figure 3.2. Calculated Z'-factor for competitive FP-based assay using 8-R. Competitive FP-based assay using 8-R (5 nM) and β -catenin (250 nM) in a total volume of 15 μ L. Positive controls representing 100% inhibition contain only tracer. Negative controls representing 0% inhibition contain tracer and β -catenin.

3.2.2 HTS for inhibitors of the BCL9/B9L binding interaction with β -catenin

Using our optimized BCL9-competitive FP assay and 8-R as the probe, we screened the in-house library of 54,000 small molecules at the Center for Chemical Genomics at the University of Michigan. The primary screen identified 965 potential active compounds, of which, 170 compounds were discarded as autofluorescent (total fluorescence intensity > 3 standard deviations above that of the controls).

The remaining 795 compounds (1.5% hit rate) were rescreened with our FP assay and 183 (23% confirmation rate, 0.3% overall) were confirmed. After removing additional autofluorescent and known toxic compounds, 176 active compounds were assessed for dose-dependent activity in our FP assay. At the same time, compounds were tested for their ability to quench the fluorescence of 8-R. Compounds deemed to be fluorescence quenchers were eliminated. Of the remaining compounds, 17 (Appendix 1) demonstrated dose-dependent inhibition in our FP assay. Fifteen compounds were obtained as dry stocks. These compounds were retested in our FP assay using 8-F as the probe, and 5 compounds demonstrated reproducible dose-dependent inhibition (Figure 3.3A). Several of these compounds also appeared to quench the fluorescence of 8-F. Nevertheless, they were taken forward and tested in our secondary BCL9-competitive SPR-based assay.

As shown in Figure 3.3B, compound 5480481 demonstrated dose-dependent inhibition of BCL9 binding to β -catenin in our SPR-based secondary assay with an IC_{50} value of 6 μ M. This compound is currently being evaluated in affinity precipitation and cell-based assays.

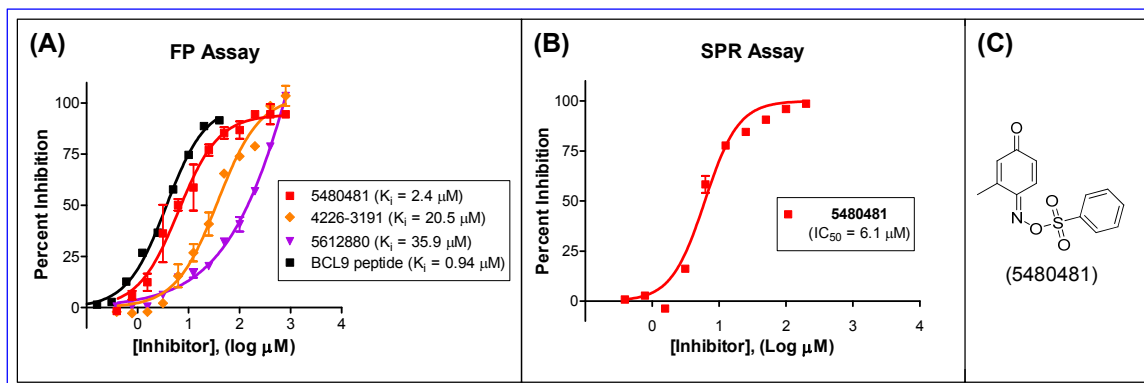


Figure 3.3. Dose-response assays for HTS active compounds. (A) BCL9-competitive FP primary assay. Potential actives identified during HTS were purchased and retested in our FP assay using either **8-F** or **8-R** (5 nM) and β -catenin (250 nM). (B) BCL9-competitive SPR secondary assay to test actives from (A). (B) β -catenin (250 nM) was preincubated with varying concentrations of compounds for at least 30 minutes and then 20 μ L of the reaction mixture was injected at 20 μ L/minute over the immobilized BCL9. K_i values were calculated from the IC_{50} values determined by non-linear least squares analysis using GraphPad Prism software. (C) Structure of active compound from part (B).

3.3 Discussion

3.3.1 Optimization and miniaturization of our FP assay for HTS

As described in Chapter 2 we optimized our FP assay using the FAM-labeled BCL9 peptide probe **8-F**. During assay development FAM was used due to its inexpensive cost. However, the excitation/emission wavelengths (485/525 nm) of FAM are such that its FP signal often is affected by autofluorescence or quenching from many small molecule compounds that appear in HTS collections. Thus, FAM is not an optimal fluorophore for HTS. We therefore further optimized this assay by making a new probe **8-R**, which employs the red-shifted fluorophore 5-TAMRA (excitation/emission wavelengths of 540/590 nm). This new probe was shown to have very similar binding affinity ($K_d = 259$ nM) compared to **8-F**, excellent dynamic range and a comparable Z' -factor of 0.72. Interestingly, the **8-R** probe was sensitive to the presence of BGG in the assay buffer and required that we switch the assay buffer to PBS with 0.02% Triton X-100 for our optimized HTS conditions.

3.3.2 HTS to identify inhibitors of the BCL9/B9L binding interaction with β -catenin

Using our HTS optimized BCL9-competitive FP assay and our new **8-R** probe, we screened the in-house library of 55,000 compounds at the Center for Chemical Genomics at the University of Michigan. Our first round of screening identified 965 potential active compounds. However, even with our TAMRA-labeled probe, we still encountered numerous compounds that interfered with the assay either through autofluorescence or fluorescent quenching. Thus, for future rounds of HTS, we will work to further optimize our FP assay to use even more red-shifted fluorophores such as the BODIPY series of dyes that have typical excitation wavelengths of over 600 nm^{161,162}.

Despite the challenges presented by autofluorescent and quenching compounds, we were able to narrow our list of active compounds. After confirmation screening and dose-response experiments we were left with 17 compounds that required further follow up. Fifteen compounds were obtained from commercial sources and five showed confirmed dose-dependent inhibition in our BCL9-competitive FP assay. Of these five compounds 5480481 demonstrated dose-dependent inhibition in both our FP assay ($K_i = 2.4 \mu\text{M}$) and our SPR-based secondary assay ($\text{IC}_{50} = 6 \mu\text{M}$).

Compound 5480481 was a surprising inhibitor of the BCL9 binding interaction with β -catenin due to its small molecular size and lack of polyaromatic ring systems. At this time, it is unclear where or how this compound binds on β -catenin. Due to its highly electrophilic structure, it is quite possible that this compound acts as a Michael acceptor and is forming a covalent adduct with β -catenin that inhibits the binding of BCL9. Further experiments are clearly needed in order to determine the mechanism of action of 5480481.

Although we were somewhat disappointed by the result of our initial HTS endeavors, there are several possible explanations for small number of active compounds identified and poor chemical structures of those that were identified. First and foremost, the quality of the library being screened can have a significant impact on the types of chemical entities that are identified. Second, the library we screened only contained 54,000 compounds, which is relatively small in comparison with the number of compounds screened (millions) for high-profile targets in the pharmaceutical industry. Third, it is possible that the BCL9/B9L binding site on β -catenin is too big or too shallow to be

targeted by small molecule inhibitors. This is always a concern in targeting protein-protein interactions, which can often have an enormous interaction surface area. In our case, however, we don't believe this to be the case since our mutational analysis of the BCL9 peptide in addition to a detailed analysis of the BCL9- β -catenin co-crystal structure indicates that the binding pocket for L366-F374 of BCL9 is an attractive site for small molecule binding.

3.4 Summary

Our FP and SPR-based assays have laid the groundwork for the design and discovery of potent and specific small-molecule inhibitors of the BCL9/ β -catenin interaction. In this study, we re-optimized our FP assay to employ the red-shifted 5-TAMRA fluorophore and eliminated BGG from our assay buffer due to its non-specific binding to our new tracer. We then demonstrated that our assay is suitable for HTS conditions by screening a 55,000 compound library. After confirmation screening and dose response we identified 17 compounds that merited additional follow up. One of these compounds demonstrated dose dependent inhibition in our secondary SPR-based assay and is now being evaluated in cell-based assays. Although the structure of 5480481 is not an ideal scaffold for drug design, this initial screening has demonstrated our assays can in fact identify inhibitors that block the binding of β -catenin to BCL9 under two different experimental conditions. Future large scale HTS campaigns utilizing far red-shifted fluorophores such as BODIPY and involving more diverse libraries will hopefully prove to be even more fruitful than our initial HTS.

3.5 Experimental Methods

3.5.1 HTS

FP assays were performed in Costar low volume 384-well black plates and FP measurements were recorded using a BMG Pherastar microplate reader with excitation and emission wavelengths of 540 and 590 nm, respectively. Reactions were prepared in assay buffer (PBS, 0.02% Triton X-100) and contained 5 nM **8-R**, 250 nM recombinant β -catenin and 0.4 μ L of compound in DMSO to produce a final volume of 15.4 μ L. The order of addition was: protein (10 μ L), compound (0.4 μ L; 2 dips using a automated pin tool instrument) and then **8-R** (5 μ L). For each assay, negative controls (equivalent to 0% inhibition) contain tracer, β -catenin and 0.4 μ L DMSO, while positive controls

(equivalent to 100% inhibition) contain only tracer and DMSO in a final volume of 15.4 μ L. Plates were incubated at room temperature for at least 30 minutes prior to reading the FP signal.

Primary HTS was performed with the 55,000 in-house library of compounds at the Center for Chemical Genomics (Life Sciences Institute, University of Michigan) which was comprised of commercial screening libraries from ChemBridge Corp. (San Diego, CA), ChemDiv, Inc. (San Diego, CA), Maybridge (Fisher) and MicroSource Discovery Systems, Inc (Gaylordsville, CT). Compounds were screened at approximately 40 μ M concentration. For the primary screen, actives were defined on a plate by plate basis with a cutoff of ≥ 2.5 SD of the negative controls (0% inhibition; tracer and protein). Autofluorescent compounds that exhibited parallel fluorescence >3 SD of the mean of the controls were eliminated. The remaining compounds were then rescreened under the same conditions as the primary screen. Actives that were confirmed in the second screen using the same triage criteria were then assayed for dose-dependent inhibition. Additionally, compounds with known reactive or toxic functional groups were eliminated. For dose-dependent experiments, a separate control plate was prepared containing only compound and **8-R** to identify fluorescent quenchers. Compounds that were not quenchers and demonstrated dose-dependent inhibition were purchased from commercial sources and retested in our FP assay using both **8-F** and **8-R** as probes. Confirmed active compounds were then tested in our SPR-based competitive assay as described for SPR binding assays in Chapter 2.

Chapter 4

siRNA and stabilized BCL9 peptides for validating BCL9 and B9L as targets for inhibiting Wnt signaling

4.1 Background

4.1.1 Biomolecular Inhibition of BCL9/B9L

To help elucidate the functional importance of BCL9/B9L in Wnt signaling, a number of genetic mutants and siRNAs have been developed in both vertebrate and invertebrate model systems. Several studies have demonstrated that the D164A mutation in β -catenin/arm, which disrupts a critical salt bridge with BCL9/Igs, abolished the binding interaction with BCL9/Igs and inhibited β -catenin-mediated transcriptional activation^{80,146}. Dominant negative constructs of BCL9/B9L that lacked the C-terminal portion of protein were also shown to inhibit β -catenin activity⁸³⁻⁸⁵. Brembeck *et al.* also demonstrated that expression of only the B9L HD2 region was sufficient for blocking β -catenin activity¹⁴⁸.

siRNA-mediated knockdown of BCL9/B9L has also been shown to inhibit β -catenin activity in cell-based reporter assays and to block the transcription of known Wnt target genes^{83,84,147}. In transformed colon cancer cells, knockdown of B9L inhibited β -catenin transcriptional activation, cell migration, and also induced an epithelial-like phenotype¹⁴⁸. Our work with BCL9/B9L siRNAs in colon cancer cells further supports these reports. The drawback to siRNA approaches, however, is that it inhibits the expression of the entire BCL9/B9L protein and therefore inhibits all BCL9/B9L protein-protein interactions. To date, the only known protein-protein interactions with BCL9/B9L are with β -catenin and Pygo. Nevertheless, it is unlikely that these are the only interactions in which BCL9/B9L are involved. Thus, to more precisely determine the effects of specifically inhibiting the BCL9/B9L interaction with β -catenin, peptide and small molecule approaches are preferred.

4.1.2 Peptide as tools for studying the specific inhibition of protein-protein interactions

In the absence of validated specific small molecule inhibitors, peptides become the preferred tool for modulation of a particular protein-protein interaction. The challenge with using peptides in cell-based and *in vivo* models is their lack of cell permeability and often rapid proteolysis. To overcome difficulties with cell permeability, cell penetrating peptide (CPP) motifs are often attached to the molecules in order to gain access to the cell. CPPs are cationic peptides that are able to be internalized by cells through a variety of mechanisms including endocytosis and direct uptake (recently reviewed by Fonseca *et al.*¹⁶³). Some of the most common CPPs are penetratin (RQIKIWFQNRRMKWKK) identified from the *Drosophila* Antennapedia homeodomain, TAT (RKKRRQRRR) from HIV-1, and poly-arginine (R₆-R₁₀)¹⁶⁴. CPPs have been used to increase the cell penetration of numerous drugs and biomolecules including peptides, antibodies, oligonucleotides and small molecules¹⁶³.

Although CPPs have been shown to be useful for increasing the delivery of peptides to the cell interior, they do not overcome the barriers presented by the numerous endogenous proteases present in the cellular environment. Cleavage of peptide-based inhibitors can lead to extremely short compound half life ($T_{1/2}$) and is a major reason why peptides find little use as clinical agents. To increase protease resistance, peptide inhibitors often incorporate non-natural residues, D-amino acids, β -amino acids, or are cyclized in one form or another to prevent access to the peptide backbone by proteases^{165,166}.

Cyclization of peptides has been investigated for decades with emphasis on disulfide linkages, amide linkages and other strategies¹⁶⁷. The advantages of peptide cyclization arise from conformational restriction of the peptide backbone, which can lead to enhanced binding and protease resistance. For the stabilization of peptide helices, numerous approaches have been studied including use of non-natural amino acids, helix capping and various cyclization methods (reviewed by Haridas¹⁶⁸ and Henchey *et al.*¹⁶⁹). In the past decade, one of the most notable methods of helix stabilization has been the use of ring-closing metathesis (RCM) to link the side chains of the *i* and *i*+4 or *i*+7 positions (Figure 4.1A)¹⁷⁰. This method of producing “stapled” α -helical peptides, introduced by Verdine and co-workers, has been shown to increase helical propensity and peptide binding affinity, while decreasing the rate of peptide cleavage by

proteases^{170,171}. A separate approach was recently reported by Arora and colleagues which employs the use of RCM to replace the internal hydrogen bond between the carbonyl and amide of the N-terminal *i* and *i*+4 residues of the helix, respectively, with a covalent hydrocarbon linkage (Figure 4.1B)¹⁷². NMR studies demonstrated that this hydrogen bond surrogate (HBS) method creates a nucleation site at the N-terminus of the helix that induces the formation of the remaining helical turns¹⁷³. Although the HBS approach is limited to only being used at the N-terminus of helices, it was still shown to increase peptide helicity and protease resistance similar to stapled peptides¹⁷⁴. Furthermore, the approach does not require the replacement of two peptide side chains making it useful for peptides that bind in less well-exposed pockets.

<p>(A) Hydrogen-Bond Surrogate</p>	<p>Advantages</p> <ul style="list-style-type: none"> -Simple, 4 step dipeptide synthesis, no chirality issues -No side chains replaced -High helix stabilization reported -Protease resistance reported <p>Disadvantages</p> <ul style="list-style-type: none"> -Different dipeptides required for different peptides -Cyclization difficult for hindered N-allyl amino acids, low yields for long peptides -Cell permeability not reported -Expensive, toxic Ru catalysts
<p>(B) Hydrocarbon Stapling</p>	<p>Advantages</p> <ul style="list-style-type: none"> -Synthesis of only 1 non-natural amino acid required -High helix stabilization reported -Cell permeability reported -Protease resistance reported <p>Disadvantages</p> <ul style="list-style-type: none"> -Tedious, 5 step asymmetric amino acid synthesis -Two side chains replaced -Low yields of cyclized product for long peptides -Expensive, toxic Ru catalysts
<p>(C) Triazole (Click Chemistry) Stapling</p>	<p>Advantages</p> <ul style="list-style-type: none"> -Simple 2-step azide amino acid synthesis -Cheap, non-toxic Cu catalysts -High yields of cyclized product (40-90%) <p>Disadvantages</p> <ul style="list-style-type: none"> -Two side chains replaced -Helix stabilization <u>not reported</u> -Cell permeability <u>not reported</u> -Protease resistance <u>not reported</u>

Figure 4.1 Comparison of selected techniques for stabilizing peptide helices. (A) Hydrogen-bond surrogate (HBS). An N-allyl amino acid is synthesized and coupled to the next (*i* – 1) amino acid. The Fmoc-dipeptide containing the N-allyl amino acid is then incorporated at the end of the synthesized peptide, followed by the last amino acid and 4-pentenoic acid. While still attached to the resin, the peptide is subjected to RCM conditions (e.g. Hoveyda-Grubbs II or Grubbs II catalyst, microwave or refluxing benzene) and then cleaved, deprotected and purified. (B) Hydrocarbon stapling. A Fmoc- α -disubstituted olefin amino acid is synthesized and incorporated into the peptide at the *i* and *i*+4 (or *i* and *i*+7) positions. While still attached to the resin, the peptide is subjected to RCM conditions (e.g. Grubbs I, DCM, r.t.) and then cleaved, deprotected and purified. (C) Triazole stapling. Fmoc-L-lysine is converted to its azide derivative Fmoc-L-Nle(ϵ N₃) and, along with Fmoc-propargylglycine (Pra), is incorporated at the *i* and *i* + 4 positions. The linear peptide is then cleaved, deprotected and purified. The linear peptide is cyclized (e.g. CuSO₄, ascorbic acid, H₂O/*t*-BuOH) and then purified. Product formation is detected by a 0.2-1.0 minute shift in analytical RP-HPLC retention time. In figures A-C, amino acid residues are represented by spheres. Non-natural residues and covalent linkages are shown in red.

In addition to peptide cyclization through disulfide, amide or RCM methods, the use of the Huisgen Cu(I)-mediated 1,3-dipolar cycloaddition reaction has recently been described (Figure 4.1C)¹⁷⁵⁻¹⁷⁷. This reaction has been popularized by Sharpless and co-workers in the past decade and has been dubbed a “click” reaction due to its simplicity, high yields, mild reaction conditions and biocompatibility¹⁷⁸. The use of cheap, less-toxic copper reagents instead of expensive, toxic ruthenium-based catalysts also makes click-mediated stapling an attractive alternative to RCM-type cyclization methods. Unlike the hydrocarbon stapling and HBS approaches however, this method of triazole stapling has not been rigorously tested and its influence on peptide helicity and protease resistance has not been examined previously. Thus, our goal was to compare these three methods of stabilizing peptide α -helices and determine which was best suited for our BCL9/B9L peptides. We also investigated the use of CPP tags for our BCL9/B9L peptides. In the process of characterizing these classes of peptides we found that peptide solubility was a major limiting factor, which led us to also perform additional mutational analysis of our BCL9/B9L peptides to improve their solubility.

4.2 Results

4.2.1 **siRNA knockdown of BCL9 and B9L inhibits β -catenin activity and Wnt target gene expression**

In our own studies, we have employed siRNAs against BCL9 and B9L to assess their role in Wnt signaling in SW480 colon cancer cells, which have constitutively activated β -catenin. Knockdown of either gene resulted in a reduction in the expression of the Wnt target genes axin2 and survivin, while simultaneous knockdown of both BCL9 and B9L resulted in nearly complete inhibition of gene expression (Figure 4.2A). These results are consistent with the report by de la Roche *et al.* that showed inhibition of axin2 and c-myc by siRNA-mediated knockdown of BCL9 or B9L⁸⁴.

To further confirm that loss of BCL and B9L inhibits β -catenin activity, we used a cell-based β -catenin luciferase reporter assay. For our reporter constructs, we examined the classic synthetic TOP Flash promoter and the endogenous *siamois* promoter isolated from *Xenopus laevis*^{179,180}. Both promoters contain three TCF/LEF binding sites upstream of the luciferase gene, however, the TCF binding motifs in the TOP Flash promoter have been optimized for maximum sensitivity. Recent work by Sustmann *et al.* has suggested that in the context of highly sensitive synthetic TCF/LEF promoters the

effect of BCL9 enhancement of β -catenin activity is small⁸⁵. Such an artificial system may arguably misrepresent the true activity of the β -catenin transcriptional activation complex. Thus, we wanted to compare the synthetic TOP Flash promoter to the endogenous *siamois* promoter to determine whether they were able to detect the effects of decreased BCL9/B9L expression levels. For our transfection experiments, we used SW480 colon cancer cells that contain constitutively activated Wnt signaling due to the activating S33Y mutation in β -catenin.

From our experiments we confirmed that the *siamois* promoter was significantly less sensitive than the TOP Flash promoter and required the transfection of five times more DNA to achieve a similar signal as from TOP Flash. Despite the need for extra transfected reporter construct, the *siamois* reporter appeared to be more sensitive than TOP Flash to siRNA-mediated knockdown of BCL9. As shown in Figure 4.2B, TOP Flash-driven luciferase activity was unaffected by siRNA knockdown of BCL9 alone, but was greatly inhibited when both BCL9 and B9L were knocked down. *Siamois*-driven luciferase activity, on the other hand, was partially inhibited by BCL9 knockdown but drastically inhibited when both BCL9 and B9L were knocked down. Our results are consistent with previous findings^{83,84,146,148} and suggest that BCL9 is important for β -catenin-mediated Wnt signaling. Nevertheless, the effects of inhibiting the BCL9/B9L interaction with β -catenin can only be inferred using siRNA methods since this approach eliminates all interactions of a multi-functional protein. Since BCL9 and B9L are large proteins with other interactions (e.g. Pygo, C-terminal transcriptional activation domain) besides its binding to β -catenin, specific information will only be gleaned from the use of direct inhibitors of BCL9/B9L binding with β -catenin.

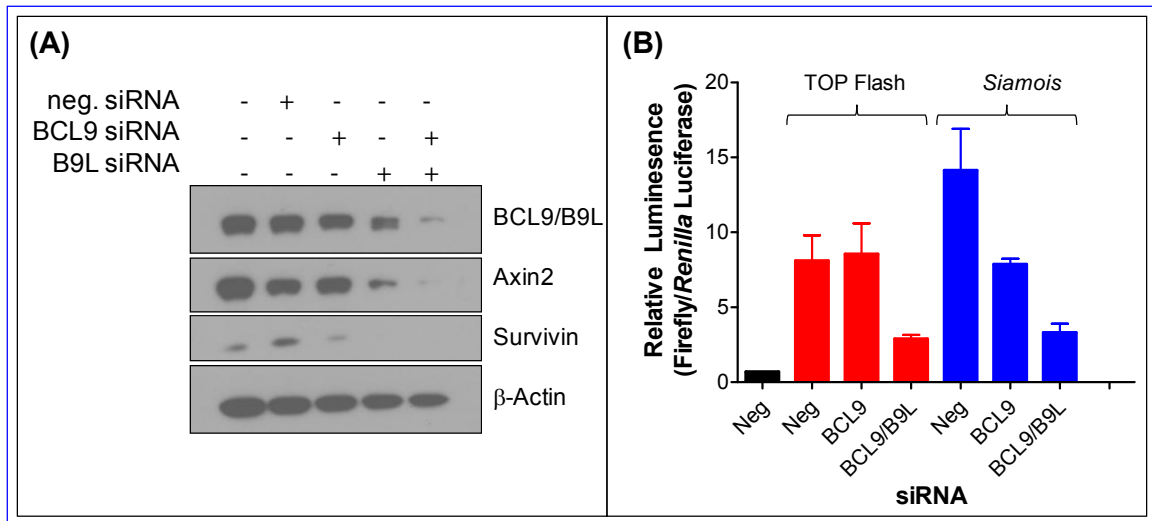


Figure 4.2 Effects of siRNA knockdown of BCL9 and B9L. (A) Immunoblot of cell lysate from SW480 cells transfected with BCL9 and B9L siRNAs. Cells were transfected with siRNAs for 24 hours and then harvested. Cleared cell lysate (25 μ g) was separated by SDS-PAGE and analyzed by immunoblotting with the indicated antibodies. (B) Reporter assay to measure β -catenin mediated transcriptional activity. Cells were transfected with siRNAs for 24 hours and then co-transfected with siRNAs and reporter constructs for an additional 24 hours prior to measuring luminescence. Experiments were performed in triplicate.

4.2.2 Synthesis and evaluation of CPP-tagged BCL9 peptides

To specifically probe the effects of interrupting this interaction, we sought to develop cell-permeable peptide-based inhibitors by tagging our BCL9-derived peptides with Antennapedia (Ant) or polyarginine (Arg_8). To minimize the overall length of our peptides, we tagged our peptides with the truncated Ant 8-mer (Ant_8) peptide, which was shown to retain over 60% of the cell penetrating effectiveness as the longer Ant 16-mer¹⁸¹. For polyarginine, oligomers of 6 to 10 arginines have been shown to be effective^{163,164}. Thus, to maintain a peptide of the same length as our Ant_8 -tagged peptide we chose to use Arg_8 . For both peptides we also synthesized inactive controls that contained double alanine mutations at the key residues L366 and I369.

To ensure that the CPP tags did not affect the binding affinity of our optimized BCL9 peptide **8**, we tested them all in our BCL9-competitive FP binding assay (Figure 4.3B). As expected, the inactive peptides showed no appreciable binding (data not shown) and the Arg_8 -tagged peptide (**8-Arg₈**) was only 2-fold weaker than **8**. The Ant_8 -tagged peptide (**8-Ant₈**) was more potent than **8** having an K_i value lower than the detection limit of the assay (~100 nM).

After confirming the binding affinity of **8-Arg₈** and **8-Ant₈** we tested their effects on cell proliferation in two different cultured cell lines (SW480 and IEC-18). Human colon cancer SW480 cells have constitutively activated β -catenin and are dependent on β -catenin signaling for cell survival. Rat colonic epithelial IEC-18 cells are not derived from a cell line bearing constitutively activated β -catenin and are presumed to be dependent on β -catenin signaling for cell survival and proliferation. As shown in Figures 4.3C both **8-Arg₈** and **8-Ant₈** inhibited SW480 cell growth with IC₅₀ values of 13 and 69 μ M, respectively, while their inactive analogs showed no effect. However, when we tested the peptides against presumed insensitive IEC-18 cells we found the same trends (Figure 4.3D). Human embryonic kidney (293FT) cells also showed nearly identical trends (data not shown). Moreover, we observed that when adherent cells were treated with dilutions of the peptides, within 5 minutes the cells appeared to show membrane abnormalities and other morphologic changes indicative of treatment with cytotoxic agents.

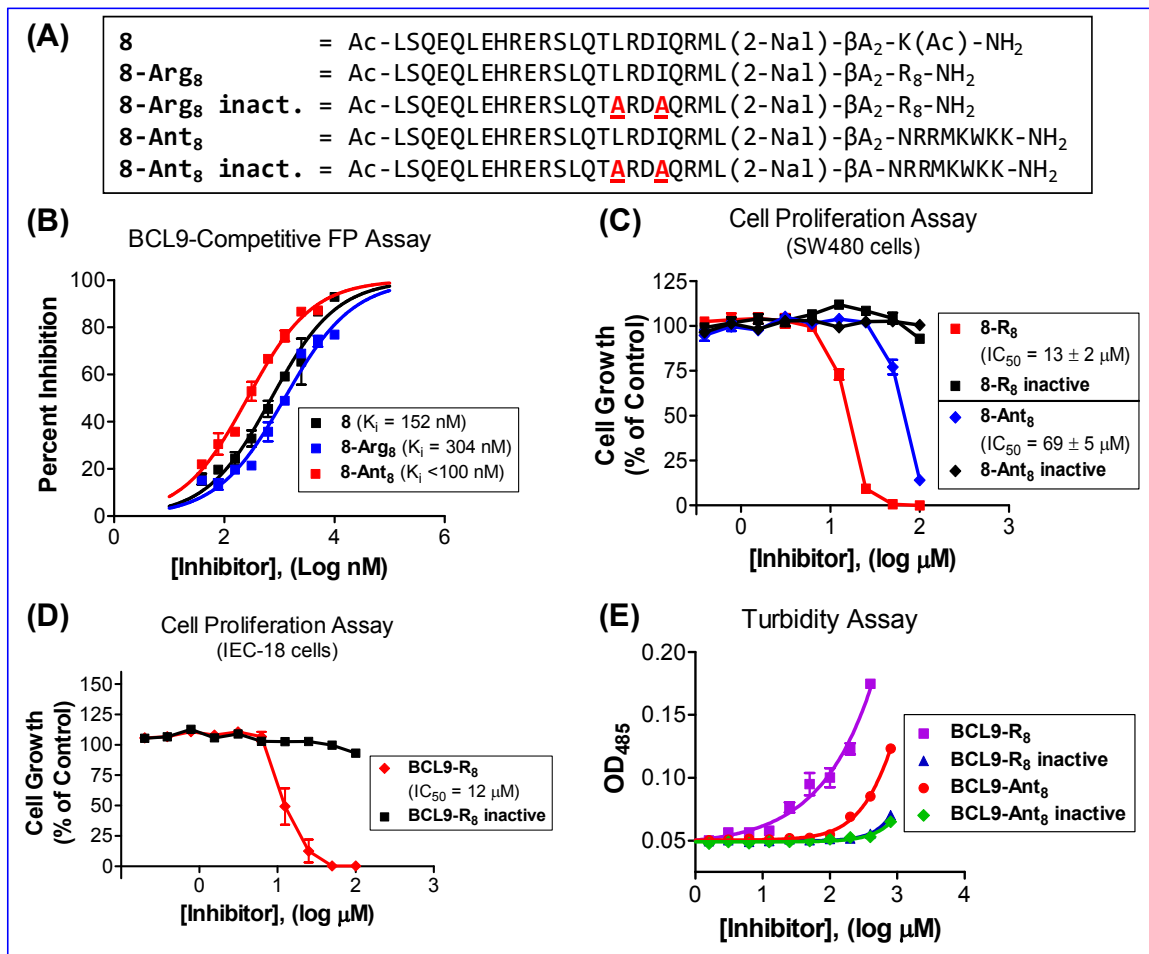


Figure 4.3 *In vitro* characterization of CPP-tagged BCL9 peptides. (A) Sequences of CPP-tagged BCL9 peptides. (B) BCL9-competitive FP assay. Binding affinities of CPP-tagged BCL9 peptides were determined using 5 nM **8-F** and 250 nM β-catenin. (C,D) WST-8 cell proliferation assay. Cells were seeded in 96-well plates in the presence of CPP-tagged BCL9 peptides. After 24 hours, percent cell growth (relative to control) was calculated. Results were the same for adherent cells treated with CPP-tagged BCL9 peptides. (E) Turbidity assay. Compound solubility was qualitatively assessed by diluting compounds in FP assay buffer, shaking vigorously at room temperature for 10 minutes and then measuring the OD₄₈₅. Compound precipitation results in an increase in OD₄₈₅ relative to the baseline.

The apparent non-specific cytotoxicity of **8-Arg₈** and **8-Ant₈** occurred much faster than anticipated for compounds whose mechanism of action requires that they be internalized, translocate to the nucleus and inhibit transcriptional activation and downstream gene expression. Thus, we questioned peptide aggregation or precipitation could be involved in the observed cellular effects of our peptides. To help address this issue, we performed a qualitative turbidity assay in which various concentrations of compound is diluted in FP assay buffer and mixed for 10 minutes. The optical density is then measured at 485 nm (i.e. OD₄₈₅). As suspected, we found that **8-Arg₈** and **8-Ant₈**

appeared to begin precipitating at concentrations approximately equal to their IC₅₀ values in the cell proliferation assays (Figure 4.3E). In contrast, the inactive peptides appeared to be more soluble and did not begin to precipitate until concentrations of over 100 μM, thus explaining why these compounds did not show cytotoxicity. Due to the apparent issues with peptide solubility and the extremely long size of the CPP-tagged peptides (34 residues), we decided to focus our efforts on trying to make stabilized BCL9 α-helical peptides that were also cell-permeable.

4.2.3 Synthesis of HBS-stabilized BCL9 α-helical peptides

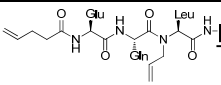
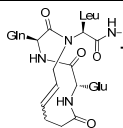
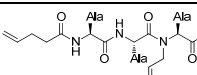
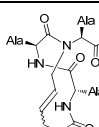
In contrast to CPP-tagged peptides, stabilized α-helical peptides are expected to be resistant to protease cleavage. Unlike linear peptides, helical peptides are more compact and possess an ordered arrangement of internal CO-NH hydrogen bonds, preventing access to the peptide backbone by proteases. In addition, helices stabilized by hydrocarbon stapling have been shown to be cell-permeable when their net charge is neutral or positive^{153,182}. It is believed that their reinforced α-helical secondary structure, a common motif in membrane interacting proteins, contributes to their cell permeability via a pinocytotic pathway¹⁸³. In addition, cell permeability has recently been demonstrated for a HBS-stabilized CBP-derived peptides¹⁸⁴. We reasoned that HBS-stabilized α-helical peptides with neutral or positive net charge would likely be cell-permeable. Thus, we employed this approach for synthesizing stabilized BCL9 α-helical peptides.

From the crystal structure of BCL9 in complex with β-catenin (PDB code 2GL7) it appeared that only a core region of 19 residues (residues 356-374) from BCL9 is responsible for binding to β-catenin. However, from our mutational analysis and peptide mapping, we knew that this short sequence had approximately 15-30-fold weaker binding affinity than the 25-mer (residues 351-374; Table 4.1, peptides **1**, **12**, **18**). We hypothesized that the additional 4 residues on the N-terminus may only be required for increasing helical propensity. Thus, we decided to use several of these residues to create the HBS macrocycle on the N-terminus of the shortened BCL9 20-mer.

We synthesized Fmoc-Gln-N-allyl-Leu-OH (Appendix 4) and coupled it to the resin bound BCL9 peptide. Additional coupling of glutamic acid and 4-pentenoic acid led to the linear peptide **51**. The fully protected resin-bound peptide was treated with Hoveyda-Grubbs 2nd generation catalyst (30 mole %) and heated at reflux in 1,2-dichloroethane

for 16 hours. Cleavage from the resin, deprotection and purification gave the HBS-stabilized BCL9 peptide **51H**, albeit in very low yield. When tested in our BCL9-competitive FP assay, we found that the linear precursor **51** had a K_i value of 48 μM which was in good agreement with the binding affinity of the BCL9 20-mer **18**. However, we were disappointed to find that the cyclized peptide **51H** was only 3-fold more potent ($K_i = 15.7 \mu\text{M}$) than the linear peptide and was still 8-fold weaker than the 25-mer **12**. Furthermore, the extremely low yield of **51H** along with unsuccessful attempts to resynthesize **51H** prevented further analysis by circular dichroism.

Table 4.1. Binding affinities of HBS-stabilized BCL9 peptides.

Peptide	Sequence	$K_i \pm \text{SD}$ (μM)
1	NPDGLSQE <u>QLEHRERSLQTLRDIQRM</u> LPDEKEFT- β A-K(Ac)	0.96 ± 0.40
12	LSQE <u>QLEHRERSLQTLRDIQRM</u> LP	1.9 ± 0.1
18	<u>LEHRERSLQTLRDIQRM</u> LP	28.8 ± 10.2
51	 <u>EHRERSLQTLRDIQRM</u> LP	48.0 ± 9.1
51H	 <u>EHRERSLQTLRDIQRM</u> LP	15.7 ± 1.8
52	 <u>LSQEQLEHRERSLQTLRDIQRM</u> LP	$0.19 \pm 0.05^*$
52H	 <u>LSQEQLEHRERSLQTLRDIQRM</u> LP	$1.5 \pm 0.2^*$

K_i values are the averages and standard deviations of 3 or more independent experiments and were determined using the original BCL9-competitive FP assay with 50 nM **1-F** and 1 μM β -catenin. * indicates K_i values that were determined using the optimized FP assay with 5 nM **8-F** and 250 nM β -catenin. K_i values determined using the optimized conditions are approximately 2-fold more potent than those determined using the original conditions due to a change in the preparation of β -catenin. All peptides are acetylated and amidated on their N- and C-termini, respectively, unless otherwise indicated. The underlined sequence corresponds to the core 19 residues observed to be in contact with β -catenin in the co-crystal structure (PDB code 2GL7).

The 8-fold weaker binding affinity of **51H** relative to the BCL9 25-mer **12** suggested that helical propensity was not the only factor contributing to the higher potency of **12**. Based on the results of our peptide mapping experiments (Figure 2.3) along with a recent report indicating that L351 was important for high affinity binding of BCL9 to β -catenin⁸⁴, we

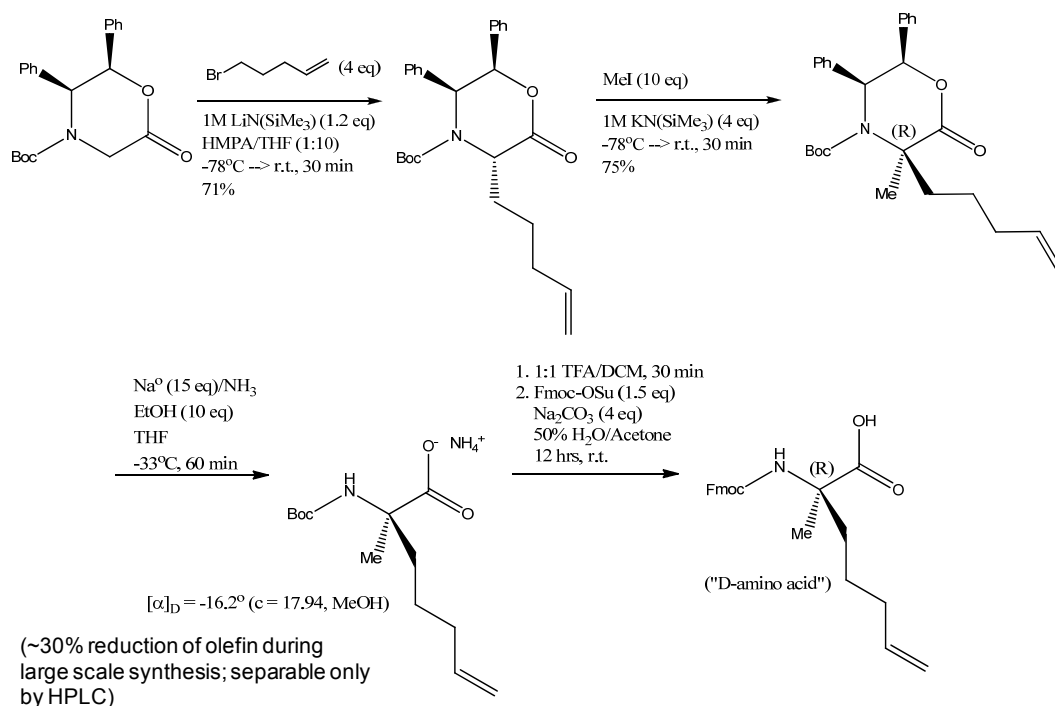
hypothesized that L351 may be critical for peptide binding for reasons besides helix induction. Thus, we redesigned a new HBS-stabilized BCL9 peptide that would incorporate L351. Initial attempts to cyclize a new peptide that utilized N-allyl-Leu at position 351 were unsuccessful. We suspected that the sterically hindered Leu side chain was the cause of the failed cyclization attempts along with the extremely low yield of **51H**. Therefore, we incorporated an all-alanine sequence before L351 and cyclized the peptide through N-allyl-alanine. The resulting linear and cyclized peptides **52** and **52H** were both more potent than **51H** (Table 4.1). The linear peptide **52** was nearly as potent as our optimized BCL9 24-mer **8** ($K_i = 0.16 \mu\text{M}$, Appendix 2) that harbors the 2-Nal mutation at F374. Surprisingly, the HBS-stabilized BCL9 peptide **52H** was actually 8-fold *less* potent than its linear precursor even though CD spectroscopy indicated that it was more helical (Appendix 3B). These results suggested that the importance of L351 may be due to additional binding interactions which are not possible when in an α -helical secondary structure. Although such an interaction was not captured in the co-crystal structure, it is possible that its absence is merely an artifact of the crystallization itself. If L351 is indeed required to be in a non-helical conformation for binding, then the HBS method of helix stabilization is not appropriate for our BCL9/B9L system. Thus, we next focused on the stapling methods for helix stabilization.

4.2.4 Synthesis of hydrocarbon stapled BCL9 peptides

Since its introduction ten years ago hydrocarbon stapling through the use of the RCM reaction has been demonstrated to stabilize α -helices, increase protease resistance and promote cell permeability of helical peptides^{153,170,182,185,186}. Such cell-permeable peptides are useful as biochemical tools to probe the effects of inhibiting certain protein-protein interactions. Due to their protease resistance, stapled peptides have longer half-lives than normal linear peptides which also makes them valuable for *in vivo* studies^{185,186}. Although hydrocarbon stapling is the most well-known method of stabilizing α -helical peptides, its usefulness and notoriety stems from the fact that the peptides become cell-permeable, which may actually be an attribute of a neutral or positively charged stabilized α -helix and not necessarily the method of stabilization per se. In principle, when all else is held constant, any method that stabilizes an α -helix should promote cell permeability. With this concept in mind, we sought to identify the most simple, robust and cost effective method of stabilizing our BCL9/B9L α -helical peptides to increase protease resistance and promote cell permeability.

First, we examined the popular hydrocarbon stapling approach. Several advantages have been pointed out by the authors including the fact that the disubstituted olefin amino acid is both insensitive to racemization and also appears to have an intrinsic ability to promote helix formation¹⁷⁰. These advantages, however, are offset by the limited number of methods for asymmetrically synthesizing the α,α -disubstituted olefin amino acid. To the best of our knowledge, the only way to synthesize the amino acid with a high degree of stereoselectivity is through the method reported by Williams *et al.*¹⁸⁷. This protocol, which is also used by Verdine and colleagues, involves a five to seven step synthesis (Scheme 1), depending on whether the chiral starting material is purchased or synthesized.

Scheme 1. Synthesis of Fmoc-disubstituted olefin amino acid



We performed the synthesis and found that the major drawback came during the cleavage of the 1,2-diphenylethyl chiral auxiliary, which requires a carefully controlled dissolving metal reduction. Although the reaction worked well on small scale, upon scale up we found it difficult to selectively cleave the auxiliary without reducing the olefin. Typically, we found that at a 1-3 gram scale, up to 30% of the olefin was reduced during this step. Furthermore, the reduced side product, which was now useless, could only be

removed by preparative RP-HPLC. Verdine and co-workers have also encountered this same problem, for which they have no easy solution (personal communication).

Despite these obstacles, we synthesized the (R)-enantiomer of the α,α -disubstituted olefin amino acid and incorporated it into our BCL9 20-mer replacing the solvent exposed residues E360 and Q364. The crystal structure of BCL9 in complex with β -catenin (PDB code 2GL7) shows these two residues are not involved in binding interactions (Figure 4.4). In the case of E360, the side chain is not even resolved. These two residues are located at the i and $i+4$ positions relative to each other and would serve to link one full turn of the helix. Other residues are also available for use in stapling, however, we chose E360 and Q364 due to their central location within the BCL9 sequence and because their replacement would eliminate one negative charge, thereby increasing the overall net positive charge of the peptide.

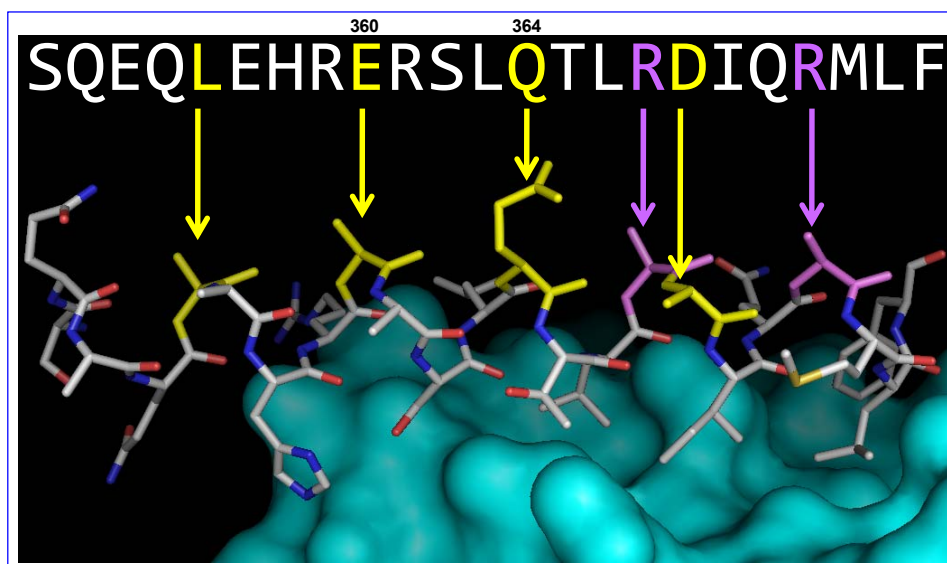


Figure 4.4 Solvent-exposed residues in BCL9. The crystal structure of BCL9 in complex with β -catenin (PDB code 2GL7) shows that L356, E360, Q364, R367, D368 and R371 are solvent exposed with Q364 having the only fully resolved side chain. Residues that correspond to potential i and $i+4$ combinations are shown in yellow. Residues that correspond to potential $i+7$ positions are shown in purple. β -Catenin is shown as a cyan surface contour model. The BCL9 sequence is shown at top with the corresponding solvent-exposed residues colored yellow or purple.

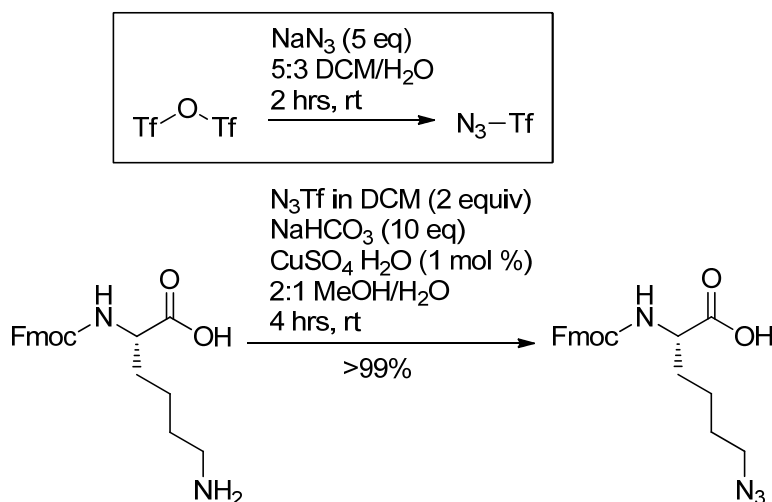
Cyclization of the resin-bound peptide with Grubbs 1st generation catalyst, followed by cleavage, deprotection and purification gave the cyclic peptide (Ac-LEHR*RSL*TLRDIQRMLF-NH₂; * = olefin residue) in very low yield (~1 mg). Attempts to characterize the percent helicity of this peptide were hampered, however, by the

extremely poor aqueous solubility of the peptide. We speculated that the insolubility of the peptide may be in part due to a hydrophobic staple. Thus, the tedious and expensive synthesis of the α,α -disubstituted olefin amino acid, and the low yield and poor aqueous solubility of the cyclized product indicated that we should examine another approach.

4.2.5 Synthesis of triazole stapled BCL9 peptides

Since the hydrocarbon stapled BCL9 peptide had poor aqueous solubility, we decided to investigate the use of the triazole stapling approach, hoping that that the dipole of the triazole would improve solubility. In contrast to the synthesis of the disubstituted olefin amino acid, the synthesis of the requisite azide modified amino acid is accomplished in two simple steps, only one purification step and with excellent yield (Scheme 2). The second half of the staple, Fmoc-propargylglycine (Pra), is commercially available.

Scheme 2. Synthesis of Fmoc-L-Nle(ϵ N₃)-OH



Once the azide and terminal alkynyl amino acids are incorporated into the peptide, the full length peptide can be cleaved from the resin, deprotected and cyclized in solution^{175,176,188}. Cyclization can also be done on the resin; however, issues with oligomerization can occur depending on the substitution level of the resin, proximity of the cyclization site relative to the resin and the reaction conditions¹⁸⁹. Oligomerization is minimized in solution when using concentrations of less than or equal to 1 mg/mL in a H₂O/*t*-BuOH mixture. The use of 33% *t*-BuOH likely helps induce helix formation in solution bringing the azide and alkyne functional groups closer together and promoting intramolecular cyclization^{190,191}.

In contrast to hydrocarbon stapling, the triazole stapling method has not been extensively studied and there has been little investigation into the optimal length of the linker, order of the azide and alkynyl residues, or use of L or D enantiomers. Cantel *et al.* demonstrated that cyclization of L-Nle(ϵ N₃) and L-Pra substituted at the *i* and *i*+4 positions, respectively were a good mimic of the amide-stapled peptide inhibitor of parathyroid hormone-related peptide (PTHrP), albeit with minor differences in the peptide backbone¹⁸⁸. Using this combination as a starting point, we systematically examined the effect of linker length, position of the triazole ring within the staple, and use of L or D-enantiomers.

Having selected E360 and Q364 as the positions for introducing our triazole staple, we determined the distance between the side chains of both amino acids and constructed the linker with appropriate length triazole bridge using computational modeling (Figure 4.5). Various combinations of Nle(ϵ N₃) or Nva(δ N₃) and L- or D-Pra were examined and the locally minimized structures of the triazole-stapled peptides and BCL9 peptide from the crystal structure of BCL9 in complex with β -catenin showed the least amount of distortion in the backbone of peptides utilizing D-Pra (Figure 4.5, right side). Using all L-amino acids or shortening the length of the staple by using Nva(δ N₃) caused noticeable perturbations in the backbone conformation. Thus, we began our synthesis of triazole-stapled peptide using the Nle(ϵ N₃)xxxL/D-Pra combination.

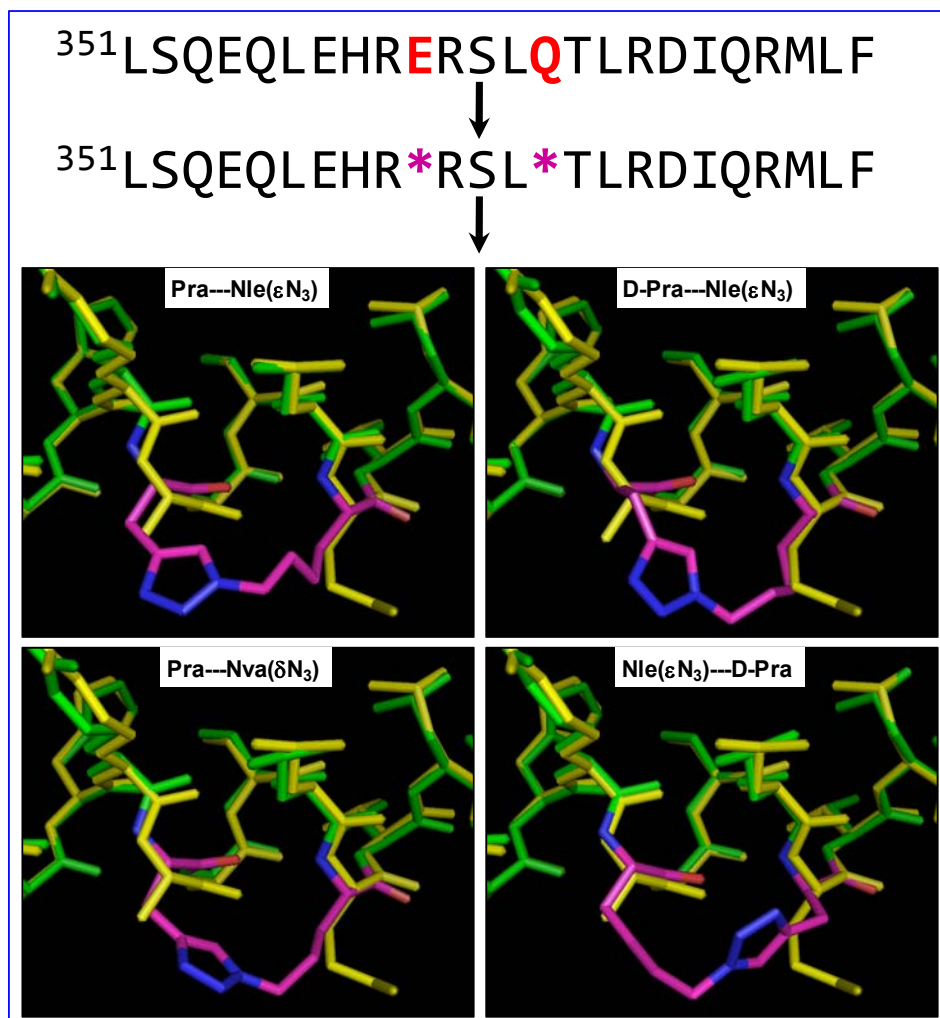


Figure 4.5. Computational modeling of possible triazole-stapled BCL9 peptides. Top: The BCL9 24-mer. Highlighted in red are residues to be replaced by azido and alkynyl amino acids (magenta *). Bottom: Locally minimized structures of triazole-stapled BCL9 peptides using various combinations of Nle(ϵ N₃) or Nva(δ N₃) and L- or D-Pra. BCL9 peptide from the reported co-crystal structure with β -catenin (PDB code 2GL7) is shown in yellow. Energy minimized BCL9 peptides are shown in green with the triazole staple highlighted in magenta/blue.

Cyclization of the peptides was monitored by analytical RP-HPLC. We found that the conditions of Cantel *et al.*¹⁸⁸, which employed 4.4 equivalents of CuSO₄ and ascorbic acid, and a peptide concentration of 1 mg/mL in 2:1 H₂O/*t*-BuOH worked well for our system. As a testament to the ease of this click reaction, we observed that reaction overnight as previously reported was not necessary. Instead the reaction appeared to go to completion within 20-60 minutes at room temperature. We did observe oxidation of our BCL9 peptides, presumably at M372. Mutation of M372 to Leu (the corresponding

residue in B9L) in later peptides eliminated this problem and did not affect the binding affinity of our peptides (Figure 4.8A, peptide **70**).

Using these reaction conditions, we synthesized two sets of cyclized peptides bearing either L- or D-Pra at position 364 (**53T** and **54T**, respectively, Figure 4.6A). As shown in Figure 4.6B, the L-Nle(ϵN_3) and L-Pra combination (peptides **53** and **53T**) gave a linear peptide with a binding affinity 2-fold weaker than the wild type BCL9 24-mer (Figure 4.6B). The triazole-stapled peptide **53T** was 2-fold more potent than the wild type and 4-fold more potent than its linear precursor. When we switched to the L-Nle(ϵN_3) and D-Pra combination (peptides **54** and **54T**), the linear peptide was 8-fold weaker than the wild type, which was not surprising due to the introduction of a D-amino acid in the sequence. More interestingly, the triazole-stapled peptide **54T** was 4.5-fold more potent than the wild type BCL9 24-mer and 38-fold more potent than its linear precursor.

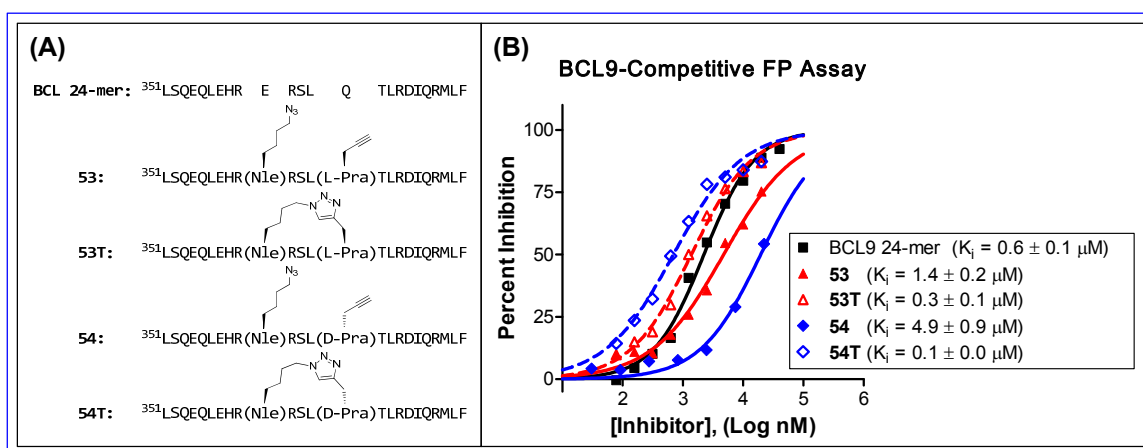


Figure 4.6 Triazole-stapled BCL9 peptides and their β -catenin binding affinities. (A) Linear and triazole stapled BCL9 peptides. All peptides are acetylated and amidated on their N- and C-termini, respectively. All amino acids are L-enantiomers except Pra, in which the stereochemistry is indicated for each peptide. (B) Peptide binding affinities as determined in the BCL9-competitive FP assay. The FP assay was performed with 5 nM **8-F** and 250 nM β -catenin. K_i values are the averages and standard deviations of 3 or more independent experiments.

These results supported our computational modeling results which indicated that the use of D-Pra may give the least distortion of the α -helical peptide backbone in the triazole-stapled peptide. CD spectroscopy confirmed that the triazole stapled peptide **54T** was 63.7% helical in PBS compared to 35.3% and 43.4% for the wild-type and uncyclized **54**, respectively (Figure 4.7). Furthermore, the large difference in binding affinities between the linear and cyclic peptides bearing the D-Pra residue can serve as a reliable control

for ensuring that the cyclization procedure was successful. The weaker binding affinity **54** relative to the BCL9 24-mer suggests that the D-Pra is likely inducing a local conformational change that affects the overall spatial arrangement of the binding residues but doesn't affect the helicity (i.e. a "kink" in the helix).

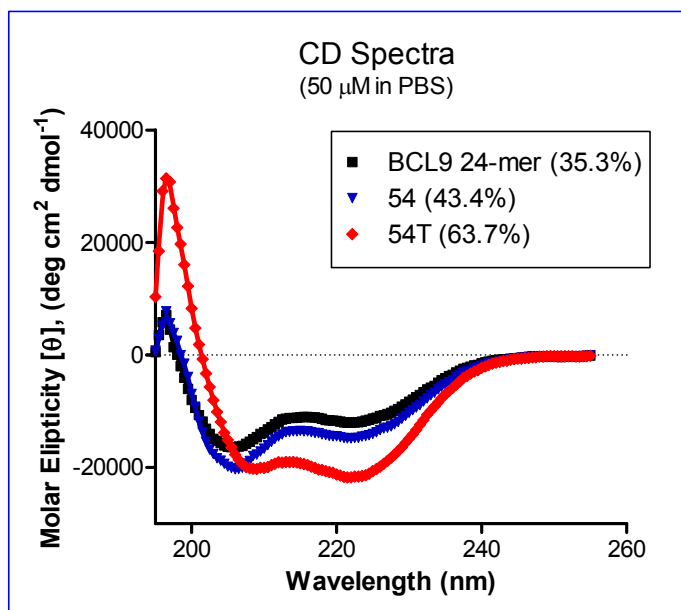
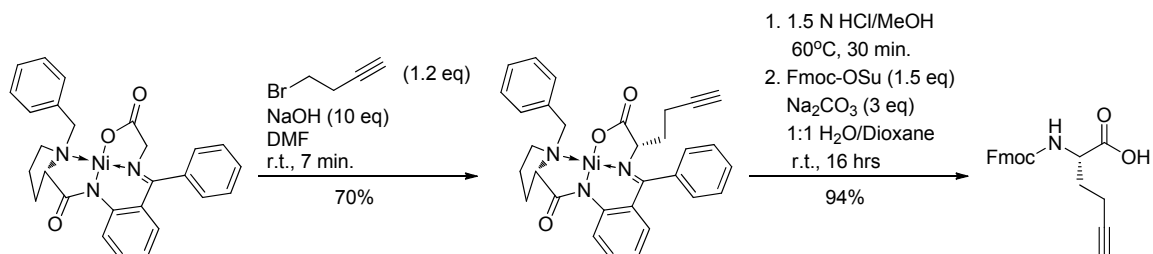


Figure 4.7. CD spectra of triazole-stapled BCL9 peptides. Peptides were dissolved in PBS at a final concentration of 50 μM . The spectra were averaged over 10 scans. Percent helicity was calculated from the molar ellipticity θ at 222 nm as previously reported¹⁹²⁻¹⁹⁴.

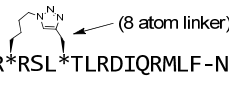
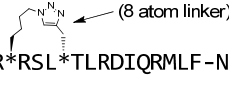
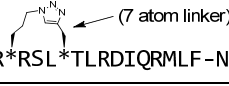
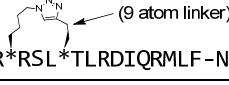
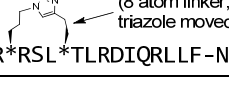
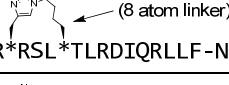
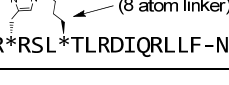
Next we worked to determine the optimal length of the triazole staple and position of the triazole ring within the staple. For shortening the length of the azido linker, we started with Fmoc-ornithine and converted it to the corresponding norvaline(δN_3) [i.e. $\text{Nva}(\delta\text{N}_3)$] by the same method as illustrated in Scheme 2. To lengthen the alkynyl linker, we synthesized propargylalanine (Paa) using a Ni(II) complex of a glycine Schiff's base with (*S*)-2-[*N*,(*N'*-benzylpropyl)amino]benzophenone (BPB; Scheme 3)^{195,196}. The starting complex is relatively simple to synthesize on large scale and its use for the synthesis of mono-substituted amino acids is straightforward and gives acceptable yields.

Scheme 3. Synthesis of Fmoc-propargylalanine (Paa)



With several different azido and alkynyl amino acids in hand, we systematically examined the effect of shortening or lengthening the staple, moving the triazole within the staple, and reversing the direction of the triazole staple. As shown in Table 4.2, all linear uncyclized peptides had low micromolar binding affinities. When the peptides were cyclized, significant differences became apparent. Shortening the length of the linker by one carbon (**55T**) resulted in complete loss of binding affinity for β -catenin. Lengthening the linker by one carbon (**56T**) also resulted in weaker binding affinity (2-fold weaker than uncyclized, 5-fold weaker than BCL9 24-mer). In addition, shifting the position of the triazole by one atom (**57T**) severely reduced the binding affinity (50-fold weaker than BCL9 24-mer) and resulted in significantly worse peptide solubility. Reversing the linker did not significantly affect the binding affinity when using both L-Pra and L-Nle(ϵ N₃) (**58T**), however, using D-Pra at position 360 (**59T**) resulted in 6-fold weaker binding affinity. Work is currently in progress to examine the effects of using the L-Pra and D-Nle(ϵ N₃) combination.

Table 4.2. Binding affinities of triazole-stapled BCL9 peptides with different linkers.

Peptide	Sequence	Triazole-Stapled $K_i \pm SD$ (μM)	Linear $K_i \pm SD$ (μM)
BCL9 24-mer	Ac- ³⁵¹ LSQEQLEHRERSLQTLRDIQRMLF-NH ₂	--	0.6 \pm 0.1
53T	Ac- ³⁵¹ LSQEQLEHR*(RSL)*TLRDIQRMLF-NH ₂ 	0.3 \pm 0.1	1.4 \pm 0.2
54T	Ac- ³⁵¹ LSQEQLEHR*(RSL)*TLRDIQRMLF-NH ₂ 	0.1 \pm 0.0	4.9 \pm 0.9
55T	Ac- ³⁵¹ LSQEQLEHR*(RSL)*TLRDIQRMLF-NH ₂ 	NB	2.4 \pm 0.2
56T	Ac- ³⁵¹ LSQEQLEHR*(RSL)*TLRDIQRMLF-NH ₂ 	3.0 \pm 0.3	1.4 \pm 0.1
57T	Ac- ³⁵¹ LSQEQLEHR*(RSL)*TLRDIQRLLF-NH ₂ 	30 \pm 5*	1.9 \pm 0.4
58T	Ac- ³⁵¹ LSQEQLEHR*(RSL)*TLRDIQRLLF-NH ₂ 	0.8 \pm 0.2	3.6 \pm 1.0
59T	Ac- ³⁵¹ LSQEQLEHR*(RSL)*TLRDIQRLLF-NH ₂ 	4.3 \pm 0.4	2.2 \pm 0.2

K_i values are the averages and standard deviations of 3 or more independent experiments and were determined using the BCL9-competitive FP assay with 5 nM **8-F** and 250 nM β -catenin. All peptides are acetylated and amidated on their N- and C-termini, respectively. NB indicates no binding was observed up to 40 μM . * indicates K_i value was extrapolated because of an incomplete binding curve due to poor peptide solubility.

From this work we concluded that for triazole stapling of consecutive turns of an α -helix, the optimal staple consists of an 8 atom linker comprised of L-Nle(ϵN_3) and D-Pra at the i and $i+4$ positions, respectively. However, we were disappointed to find that our triazole-stapled peptides were still displaying poor aqueous solubility above 10 μM . Thus, we next focused on identifying residues within the BCL9/B9L peptide sequence that could be mutated to improve peptide solubility.

4.2.6 Additional mutational analysis of BCL9/B9L peptides to improve aqueous solubility.

Using our qualitative turbidity assay, we were able to estimate the aqueous solubility of our BCL9/B9L peptides. We found that the wild type BCL9 24-mer and the M372L mutant peptide (**70**) both appeared to precipitate at approximately 50 μM (Figure 4.8A,B). Removal of the N-terminal acyl cap of BCL9 (**BCL9-N**) appeared to cause a slight increase in peptide solubility. Interestingly, the corresponding B9L 24-mer

(residues 394-417) was completely soluble up to 800 μM , the highest concentration tested. B9L differs by only four residues (Figure 4.8A), however two of the residues are charged (K396 and E413) which likely contribute to its enhanced solubility.

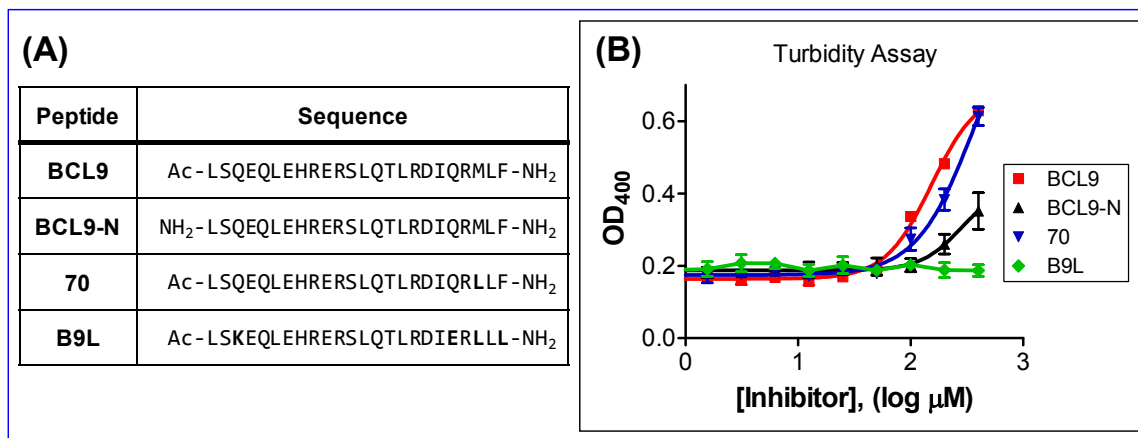


Figure 4.8. Aqueous solubility of BCL9 and B9L peptides. (A) BCL9 and B9L peptide sequences. B9L residues that differ from BCL9 are in bold. (B) Turbidity assay. Peptides were serially diluted (in duplicate) in DMSO in 96-well plates and then diluted with FP assay buffer to a final volume of 125 μL . Plates were shaken vigorously for 10 minutes at room temperature and then light absorbance was recorded at 400 nm.

Since our ultimate goal was to design cell-permeable peptides with neutral or positive overall charge, additional acidic residues were not desired in our BCL9 sequence. Instead, we systematically made lysine mutations at various points throughout the BCL9 peptide **70** (Figure 4.9A; peptides **71-73**) and tested their effect on peptide solubility. Peptide **70** was our standard of comparison because M372 was mutated to avoid future issues with oxidation during triazole stapling. Surprisingly, the incorporation of an additional lysine was not as important as the location in which the lysine was introduced. As shown in Figure 4.9B, the introduction of lysine only improved the solubility when it was introduced in or on the C-terminus of the hydrophobic triplet LLF (peptides **73** and **76**). This effect was also seen when introducing a polar serine or threonine residue at position 372 (**74** and **75**, respectively). However, introducing a charged or polar residue at position 372 also resulted in a 3-fold decrease in binding affinity (Figure 4.9A). The same trend was also observed when the charged and polar residues α,γ -diaminobutyric acid and homoserine, respectively, were introduced at position 372 (data not shown).

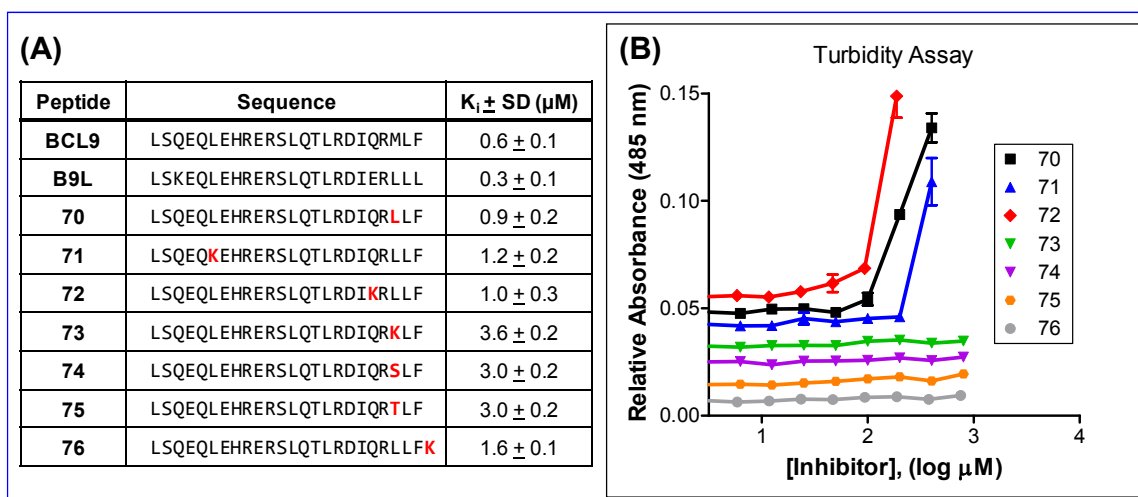


Figure 4.9. Binding affinities and aqueous solubility of mutated BCL9 peptides. (A) BCL9 and B9L peptide sequences and binding affinities. Mutated BCL9 residues are in bold. All peptides are acetylated and amidated on their N- and C-termini, respectively. K_i values were determined in the BCL9-competitive FP assay and represent the averages and standard deviations of three or more independent experiments. (B) Turbidity assay. Peptides were serially diluted (in duplicate) in DMSO in 96-well plates and then diluted with FP assay buffer to a final volume of 125 μL . Plates were shaken vigorously for 10 minutes at room temperature and then light absorbance was recorded at 485 nm. In order for all data sets to be visualized, each data set has been shifted by an arbitrary value and therefore represents relative absorbance values.

We hypothesized that the hydrophobic triplet on the C-terminus of the BCL9 peptide was causing aggregation and precipitation of the peptides. From our experiences with CPP-tagged peptides, we knew that this could potentially lead to issues with non-specific toxicity and limit the usefulness of a cell-permeable BCL9 peptide-based inhibitor. Thus, we decided to further investigate the requirement of a hydrophobic residue at position 372. Shown in Figure 4.10A, we started with leucine (**70**), and sequentially shortened the side chain at position 372 to norvaline (3 carbons, **77**), α -aminobutyric acid (2 carbons, **78**) and finally alanine (**79**). As suspected, the solubility and binding affinity of the BCL9 peptides were inversely correlated such that decreasing the number of carbons increased solubility but decreased the binding affinity with β -catenin (Figure 4.10B). While **70** and **77** retained wild-type-like binding affinity, they both showed signs of precipitation at 50-100 μM . On the other hand, **78** and **79** both showed complete solubility to 800 μM , but showed a progressive decrease in binding affinity. We concluded that the optimal residue for position 372 of BCL9 is a hydrophobic residue with a side chain of approximately two carbons. However, it is possible that other non-natural amino acids such as dimethylglycine or cyclobutylglycine may also work at this position. Residues of this type are currently being investigated.

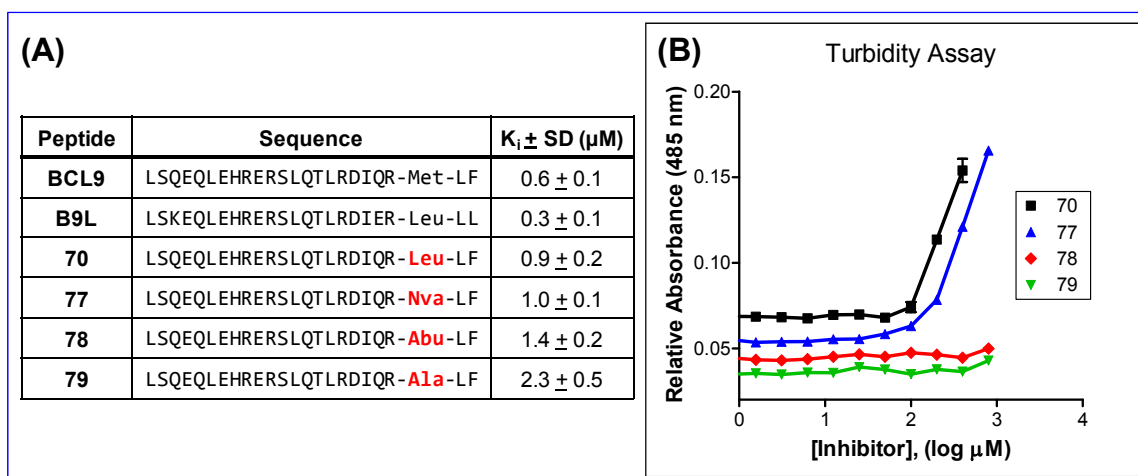


Figure 4.10. Binding affinities and aqueous solubility of BCL9 M372 mutant peptides. (A) BCL9 and B9L peptide sequences and binding affinities. Mutated BCL9 residues are in bold red. All peptides are acetylated and amidated on their N- and C-termini, respectively. K_i values were determined in the BCL9-competitive FP assay and represent the averages and standard deviations of three or more independent experiments. (B) Turbidity assay. Peptides were serially diluted (in duplicate) in DMSO in 96-well plates and then diluted with FP assay buffer to a final volume of 125 μL . Plates were shaken vigorously for 10 minutes at room temperature and then light absorbance was recorded at 485 nm. In order for all data sets to be visualized, each data set has been shifted by an arbitrary value and therefore represents relative absorbance values.

In a slightly different approach to improving peptide solubility and increasing the overall positive charge of our peptides, we mutated one or more of the acidic (with the exception of E360) and glutamine residues to arginine (Figure 4.11A). Single and double mutations did not affect peptide binding affinity (**80-83**); however, combined arginine mutations caused a 2-5-fold decrease in binding affinity for β -catenin (**86-88**). The quadruple arginine mutant **85**, which was not mutated at Q355, was an exception and showed no difference in binding affinity. Additionally, these mutations did not enhance the solubility, and in the case of the combined arginine mutations, typically decreased the peptide solubility.

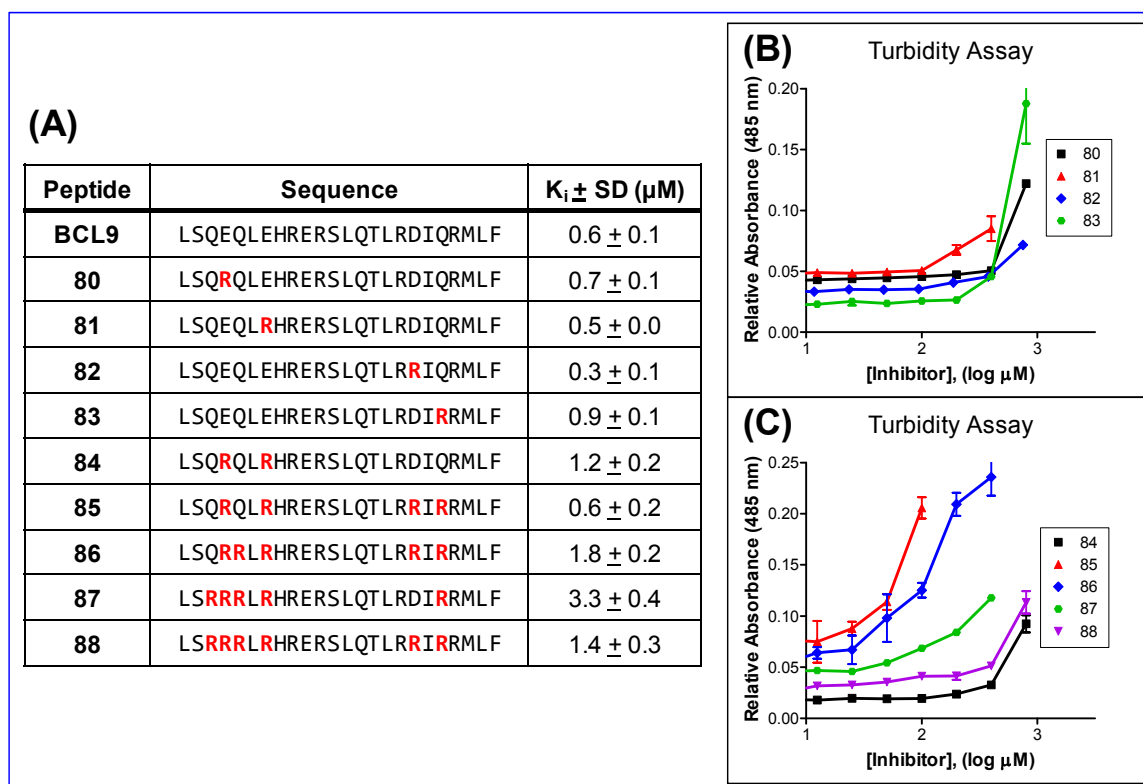


Figure 4.11. Binding affinities and aqueous solubility of arginine mutated BCL9 peptides. (A) BCL9 and B9L peptide sequences and binding affinities. Mutated BCL9 residues are in bold red. All peptides are acetylated and amidated on their N- and C-termini, respectively. K_i values were determined in the BCL9-competitive FP assay and represent the averages and standard deviations of three or more independent experiments. (B) Turbidity assay. Peptides were serially diluted (in duplicate) in DMSO in 96-well plates and then diluted with FP assay buffer to a final volume of 125 μL . Plates were shaken vigorously for 10 minutes at room temperature and then light absorbance was recorded at 485 nm. In order for all data sets to be visualized, each data set has been shifted by an arbitrary value and therefore represents relative absorbance values.

From our combined results with improving peptide solubility, we attempted to make several optimized triazole-stapled peptides (Figure 4.12A). These peptides contained the F374(2-Nal) mutation known to enhance binding affinity by 2-3-fold (Figure 2.2B), lacked N-terminal acetylation and contained the M372(2-Abu) mutation which was shown to increase peptide solubility (Figure 4.10B). Since the combined arginine mutants did not show improved solubility, we instead made two peptides in which only the acidic residues were mutated to either lysine (**60T**) or arginine (**61T**). In **60T**, we used the B9L sequences as a template and also included an additional lysine on the C-terminus. As shown in Figure 4.12B, the lysine mutant **60T** demonstrated reasonable solubility with precipitation beginning around 50-100 μM . In contrast, the arginine mutant **61T** showed decreased solubility and appeared to precipitated at concentrations lower than 10 μM .

Simply mutating the acidic residues to their corresponding amides (**62T**) also did not increase solubility.

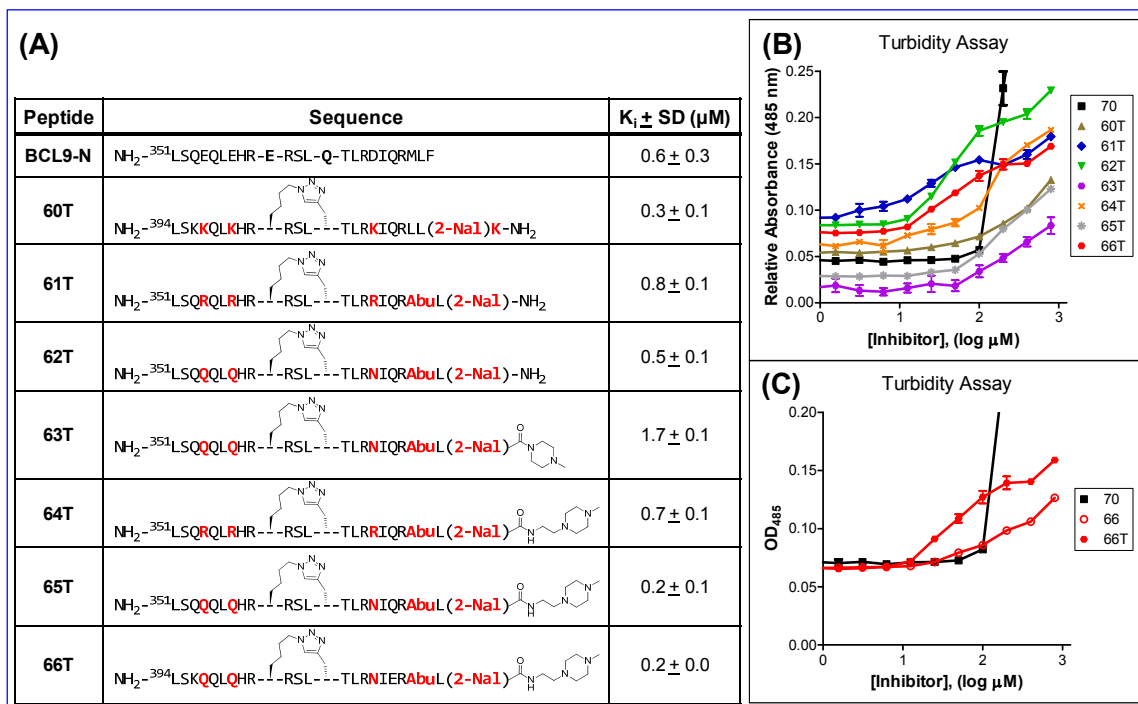


Figure 4.12. Binding affinities and aqueous solubility of triazole-stapled BCL9 peptides. (A) BCL9 and B9L peptide sequences and binding affinities. Mutated BCL9 residues are in bold red. All peptides have free N-termini. C-termini are amidated as indicated. K_i values were determined in the BCL9-competitive FP assay with 5 nM 8-F and 250 nM β -catenin and represent the averages and standard deviations of three or more independent experiments. (B,C) Turbidity assays. Peptides were serially diluted (in duplicate) in DMSO in 96-well plates and then diluted with FP assay buffer to a final volume of 125 μL . Plates were shaken vigorously for 10 minutes at room temperature and then light absorbance was recorded at 485 nm. In order for all data sets to be visualized, each data set in (B) has been shifted by an arbitrary value and therefore represents relative absorbance values.

Finally, we chose to incorporate piperazine moieties at the C-terminus to help improve solubility. From peptide **76**, we knew that incorporating charged groups at the C-terminus could help improve solubility. When 1-methylpiperazine was coupled directly to the C-terminus (**63T**), we achieved improved solubility (Figure 4.12B), but the binding affinity decreased by 3-fold (Figure 4.12A, compare to **62T**). The decrease in binding affinity was likely due to interference from the piperazine preventing the proper binding of the 2-Nal moiety. Thus, we switched to using 1-(2-aminoethyl)-4-methylpiperazine, which incorporated a 2-carbon spacer and an additional amine. This functionalization

was well tolerated, showing no signs of decreasing the binding affinity. Furthermore, **65T** showed reasonable solubility with no significant precipitation up to 50 μM (Figure 4.12B).

An additional trend we observed was the marked decrease in solubility upon cyclization of the triazole-stapled peptides (Figure 4.12C). This is most likely due to the loss of hydrogen bonding with the solvent in favor of forming internal hydrogen bonds upon helix formation. This decrease in solubility will likely be a hurdle for any peptide being stabilized in an α -helical conformation. As such, we were not able to achieve the fully soluble triazole-stapled peptides as we were with the linear peptides. However, we decided to move forward with several peptides to test their ability to inhibit protease cleavage of the peptides in solution.

4.2.7 Trypsin cleavage of linear and triazole-stapled BCL9 peptides

Proteolysis is a major limitation of peptide-based inhibitors and is a reason why peptides are not commonly pursued as therapeutic agents. However, previous work has demonstrated that stabilization of α -helical peptides inhibits their cleavage by proteases such as trypsin and chymotrypsin^{153,170,174,186}. This effect is presumably due to the formation of internal hydrogen bonds between backbone carbonyls and amide protons that prevents easy access to the peptide backbone by proteases. We tested our linear and triazole-stapled BCL9 peptides for their resistance to trypsin cleavage. To our disappointment, we found that **65T** was cleaved at the same rate or faster than the wild-type BCL9 and B9L peptides (Figure 4.13B,C). Using both L-enantiomers of Nle(ϵN_3) and L-Pra (**53T**) also resulted in a similar cleavage rate, as did the use of the longer staple (**56T**). The only peptide to possibly show resistance to trypsin cleavage was the one with direction of the triazole staple reversed (**58T**); however, this result is still being confirmed.

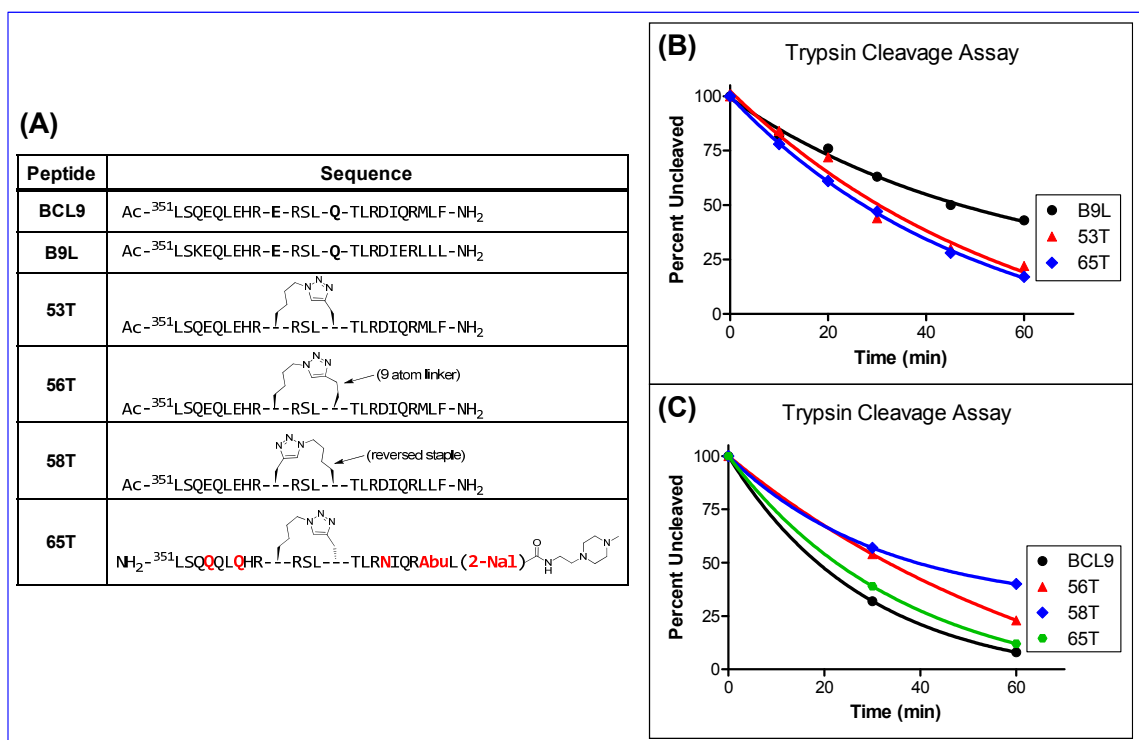


Figure 4.13. Trypsin cleavage of triazole-stapled BCL9 peptides. (A) B9L and triazole-stapled peptide sequences. Mutated residues are shown in bold red. (B,C) Trypsin cleavage assays. Peptides (100 μ M) were dissolved in buffer (10% EtOH/PBS, pH 7.4 or PBS, pH 7.4 only for B and C, respectively) and trypsin (1 nM) was added. Reactions were incubated at 37°C and aliquots were periodically removed and quenched with 1 volume of 20% TFA and then analyzed by RP-HPLC. Tryptophan (150 μ M) was used as an internal control in the assay buffer.

4.3 Discussion

4.3.1 siRNA knockdown of BCL9/B9L inhibits Wnt signaling in colon cancer cells

The siRNA knockdown of BCL9 and B9L demonstrated that reducing the expression levels of only one of the two homologs was insufficient for the full inhibition of β -catenin-mediated transcriptional activity and Wnt target gene translation. Our immunoblotting results showed that after knockdown of either BCL9 or B9L, Axin2 and Survivin protein are still detectable, albeit at lower levels. By comparison, when both BCL9 and B9L levels are knocked down, Axin2 and Survivin expression are nearly completely inhibited. Axin2 has been suggested to be the ideal endogenous marker of Wnt signaling activity due to its near ubiquitous expression in a variety of tissues and the presence of up to eight putative TCF binding motifs in its promoter region⁶⁶. Thus, inhibition of Axin2 expression by siRNA-mediated depletion of BCL9/B9L strongly supports a role for BCL9/B9L in canonical Wnt signaling.

Our reporter assays have also demonstrated that reduction of BCL9/B9L protein levels inhibits β -catenin-mediated transcriptional activation. In addition, we determined that both the highly sensitive TOP Flash and the endogenous siamois promoters are capable of detecting the effects of BCL9/B9L protein depletion; however, the endogenous promoter appears to be more sensitive to changes in BCL9/B9L expression.

The results from both the immunoblotting and reporter assays also indicate that BCL9 and B9L may have some level of redundancy in terms of their roles in the β -catenin transcriptional activation complex. The fact that knockdown of BCL9 alone had little or no effect on the expression of Axin2 or TOP Flash reporter activity, suggests that either B9L is the more important of the two homologs or is at least able to compensate for loss of BCL9.

Nevertheless, one must be cautioned in over-interpreting these results, since they are only from the immortalized SW480 colon cancer cell line that is known to have at least one mutation in the APC gene and likely additional mutations in other genes. It is certainly possible that the roles of BCL9 and B9L are different in other tissue types. In addition, the mechanism by which BCL9/B9L enhance β -catenin-mediated gene transcription is still not fully understood. In *Drosophila*, BCL9/Lgs is required for recruiting Pygo to the β -catenin complex^{61,81,147}. However, in humans the evidence for Pygo being a critical cofactor is less compelling^{84,85}. On the other hand, the C-terminus of BCL9/B9L appears to harbor an additional transactivation domain that may represent its critical contribution to the β -catenin-TCF complex^{84,85}. However, this transactivation domain was mapped to a region between the HD4 and HD5 regions. Thus, there are still three conserved HD regions in these 1400 amino acid proteins that, to date, have no known function. Clearly, additional investigation will be required to elucidate the full functional roles of BCL9 and B9L.

4.3.2 CPP-tagged BCL9 peptides

To specifically inhibit the binding of BCL9/B9L to β -catenin in cells, we investigated the use of CPPs to enhance the cell permeability of our BCL9 peptides. CPPs such as polyarginine, TAT and Antennapedia (a.k.a. Penetratin) have been shown to be effective at delivering large macromolecular cargo to the interior of cells. Although the exact mechanisms of cell penetration are still unclear, it is believed that the positively charged side chains characteristic of CPPs interact with the phospholipid membrane and induce

uptake via various endocytotic mechanisms^{163,197}. We synthesized the CPP-tagged BCL9 peptides **8-Arg₈** and **8-Ant₈** and determined that the binding affinity was unaffected (possibly increased for **8-Ant₈**) by the tags. When we tested these compounds in cell proliferation assays, we were disappointed to find that the compounds displayed non-specific toxicity and were killing various cell lines regardless of their dependence on β -catenin-mediated signaling. Furthermore, adherent cells treated with our compounds showed morphologic changes indicative of cell death within 5 minutes, which would not be expected for inhibitors of Wnt signaling. Further investigation revealed that both peptides had very poor aqueous solubility and their IC₅₀ values in the cell proliferation assays appeared to correlate with their solubility. A recent report by Cardozo *et al.* also found that the Antennapedia CPP has toxic side effects in cells at concentrations above 10-30 μ M¹⁹⁸. These findings led us to look for another method of creating cell-permeable peptides.

4.3.3 Stabilized α -helical BCL9 peptides

In addition to having potential cytotoxicity issues, CPP-tagged peptides do not offer any resistance to protease cleavage. In fact, the additional basic residues in the tag would likely promote cleavage by proteases such as trypsin. Stabilization of the α -helical secondary structure has been shown to increase peptide binding affinity, cell permeability and protease resistance^{153,170,172,174,182,186}, and is therefore a more attractive method of generating cell-permeable BCL9 peptides. We examined several approaches to stabilizing our BCL9 α -helical peptides. First we tried the HBS method which uses RCM to generate a covalent linkage in place of the internal hydrogen bond between the carbonyl and amide at the *i* and *i*+4 positions in the peptide backbone. The first peptide we synthesized included the core 20 residues that appear to be involved in binding interactions as seen in the BCL9 co-crystal structure with β -catenin (PDB code 2GL7). The cyclized peptide (**51H**), however, was only 3-fold more potent than its linear precursor and still 8-fold weaker than the longer BCL9 peptides and BCL9 protein. The second stabilized peptide we synthesized (**52H**) included the entire 24 amino acids (residues 351-374) that we previously determined to be the optimal binding sequence of BCL9 (Figure 2.3). We observed that this cyclized peptide was actually 8-fold less potent than its linear precursor, indicating that the stabilization of the helical structure at the N-terminus of the BCL9 peptide is detrimental to the binding of BCL9 to β -catenin.

Although surprising, these results help piece together the puzzle regarding the requirement of L351 for BCL9 binding to β -catenin. Our peptide mapping studies (Figure 2.3) determined that although L351 is over 10 Å away from the edge of β -catenin in the co-crystal structure, deletion of L351 results in a 38-fold decrease in binding affinity. In addition, mutation of L351 to alanine was reported to result in loss of binding to β -catenin⁸⁴. In addition, L351 is conserved across BCL9, B9L and Lgs homologs in humans, mice, zebrafish and flies⁸⁰. Thus, our results from the HBS-stabilized peptide **52H** suggest that, in contrast to that observed in the co-crystal structure, when in solution the N-terminus of the BCL9 HD2 α -helix is not helical at residue L351. It is possible that this residue is actually involved in another, yet to be determined, binding interaction that is not possible when L351 is part of the helix.

Since HBS stabilization at the N-terminus of our BCL9 peptides was not possible, we instead decided to synthesize stapled BCL9 peptides, which are stabilized through covalent linkage between the side chains of the *i* and *i*+4 or *i*+7 positions. Our modeling studies identified a number of residues in which the solvent exposed side chains could be modified and used for stapling. We chose E360 and Q364 due to its central location within our BCL9 peptide sequence. For stapling one turn of the helix, several strategies exist that involve different methods (e.g. disulfide, amide, olefin RCM, triazole) of linking the side chains. First we examined the hydrocarbon stapling method that employs RCM conditions to link the two olefin side chains^{170,186}. Our first observation was that the 5-7 step stereoselective synthesis of the requisite α,α -disubstituted olefin amino acid was tedious, expensive and not easily scaled up. We also had very low yields of the cyclized peptide, although the yields could probably have been improved upon further optimization. Finally, the hydrocarbon stapled peptide was insoluble in water making analysis and characterization difficult.

To circumvent many of the problems we encountered with hydrocarbon stapling, we decided to utilize the less-well studied method of triazole stapling¹⁸⁸. This approach employs the copper catalyzed Huisgen 1,3-dipolar cycloaddition reaction between an azide and a terminal alkyne¹⁹⁹. In addition, the synthesis of the azido amino acid can be achieved in a two-step, one purification synthesis from commercially available Fmoc-amino acids. The cyclization reaction also utilizes cheap, non-toxic copper sulfate/ascorbic acid reagents and is performed in aqueous solution.

Molecular modeling of possible linker combinations for triazole stapling indicated that the Nle(ϵ N₃)/D-Pra combination at the $i/i+4$ positions, respectively, would likely have the least distortion of the α -helical peptide backbone observed in the BCL9 co-crystal structure. We started with this combination and found that, while the linear peptide had diminished binding affinity due to the presence of a D-amino acid, cyclization resulted in an increase in helicity (from 43% to 64%) and a 38-fold increase in binding affinity. Overall, the triazole stapled peptide was 4.5-fold more potent than the wild-type BCL9 peptide. Examination of L- and D-Pra, different length linkers, moving the location of the triazole within the staple, and reversing the direction of the staple, led to the conclusion that the L-Nle(ϵ N₃) and D-Pra combination of residues at the i and $i+4$ positions, respectively, gave the optimal triazole staple for stabilizing one full turn of the BCL9 α -helix.

Unfortunately, our triazole-stapled BCL9 peptides were not completely soluble and showed signs of precipitation at 10-100 μ M. Since the CPP-tagged BCL9 peptides had demonstrated non-specific toxicity likely due to aggregation and precipitation, we focused on increasing the solubility of our peptides without disrupting their binding affinities. First, we found that removing the N-terminal acyl cap had a slight improvement in solubility. Although this modification will remove one internal hydrogen bond and destabilize the N-terminus of the helix, our HBS peptides indicated that the N-terminus (L351) was not supposed to be helical anyways. Next we focused on reducing the hydrophobicity of the C-terminal MLF triplet. M372 was previously mutated to leucine (corresponding residue in B9L) to avoid oxidation of the sulfide during cyclization. Through mutational analysis of M372, we determined the optimal residue to be one with a non-polar, 2-carbon side chain (i.e. 2-Abu). This residue increased the solubility of the peptide without causing a significant reduction in binding affinity.

While attempting to increase the solubility of our peptides, we also wanted to increase the overall positive charge. Verdine and co-workers have previously reported that hydrocarbon-stapled peptides are only soluble when neutral or positively charged¹⁵³. We experimented with making single or multiple arginine mutations at all acidic and glutamine residues. To our surprise, these peptides were, in general, less soluble than the wild-type peptide. Instead, we mutated all acidic residues to their corresponding amides and then focused on incorporating charged groups at the C-terminus of the peptide. We found that coupling N-methylpiperazine directly to the C-terminus increased

solubility, but decreased the binding affinity. We assumed that the piperazine was affecting the binding of the C-terminal 2-Nal moiety. Therefore, we added an ethyl spacer and found that peptide solubility was moderately increased and that binding affinity was unaffected.

Even with all of the modifications made to the BCL9 peptides, we were never able to achieve complete solubility of the triazole stapled peptides. The stapled peptides were always equal or less soluble than their linear precursors. This effect is due to the loss of hydrogen bonding between the peptide backbone and the solvent upon helix formation²⁰⁰. Nonetheless, our best triazole-stapled peptides lack N-terminal acylation, contain the M372(2-Abu) and F374(2-Nal) mutations, and have 1-(2-aminoethyl)-4-methylpiperazine coupled to the C-terminus (e.g. peptide **65T**).

4.3.4 Trypsin stability

The ultimate goal for our triazole-stapled BCL9 peptides is to use them as biochemical tools to inhibit the BCL9 binding interaction with β -catenin in cells and animal models. One hurdle for achieving this goal is to make the peptides resistant to protease cleavage. We tested the stability of our peptides in the presence of trypsin, a serine protease that cleaves after basic residues. Unfortunately, we found that our triazole-stapled peptides were not resistant to trypsin cleavage to any considerable degree.

Although the results of the trypsin cleavage assays were disappointing, there are several reasonable explanations for the lack of protease resistance exhibited by our triazole stapled peptides. The most plausible explanation is that triazole stapling of only one turn of the BCL9 α -helix is insufficient to stabilize the entire length of the helix. This problem has also been encountered by Verdine and co-workers during the synthesis of hydrocarbon stapled p53 and RNase A peptides^{153,170}. For these peptides, it was determined that stapling of two consecutive turns, via the *i* and *i*+7 positions was required. Thus, it is possible that this same strategy may need to be employed for the triazole stapling of BCL9/B9L peptides. Additional support for this strategy comes from the fact that our best triazole-stapled peptides are on average only 2-4-fold more potent than their analogous BCL9 peptides. If the triazole was stabilizing the full helix, a larger increase in binding affinity might be expected.

A second explanation for the lack of protease resistance of our triazole stapled BCL9 peptides is that the staple may not be in the optimal location. Support for this argument can be found in the design of hydrocarbon-stapled BID BH3 peptide, in which only two of the four tested stapling sites resulted in high levels (>60%) of helix stabilization¹⁸⁶. In addition, certain amino acids such as threonine are also known to reduce helical propensity^{200,201}, and the current location of our triazole staple is adjacent to T365. Thus it is possible that the T365 is counteracting the stabilizing effect of the staple. To address this issue, studies are currently in progress to determine if repositioning the triazole staple (positions 364 to 368) so that it encompasses T365 will enhance the binding affinity and protease stability of our BCL9 peptides.

A third possibility is that the triazole ring itself is influencing the stability of the helix or altering its mode of binding to trypsin. From our experiments in optimizing the length and composition of the triazole-staple (Table 4.2) we observed that the binding affinity, and presumably the stability of the helix, is extremely sensitive to the location of the triazole within the staple (compare **53T** and **57T**). The question of the influence of the triazole ring will be addressed by performing the analogous hydrocarbon stapling with a mono-substituted olefin amino acid synthesized using the same Ni(II) complex used in Scheme 3.

4.4 Summary

In summary, we have investigated a number of methods for synthesizing cell-permeable BCL9 peptide inhibitors. Our attempts at using CPP-tagged peptides were hindered by poor peptide solubility and non-specific toxicity. We therefore evaluated three different methods of synthesizing stabilized BCL9 α -helical peptides with the hope that we will eventually be able to make them cell-permeable. The HBS method did not work well for our peptides, but helped shed light on the role of L351 in BCL9 binding to β -catenin. Examination of hydrocarbon stapling versus triazole stapling led us to conclude that triazole stapling is a more facile, robust method of stabilizing the helix and our studies helped determine the optimal combination of linkers for stabilizing one turn of the helix. Although we were not completely successful in maximizing the solubility of our stapled peptides, the further mutational analysis of specific BCL9 residues has increased our understanding of the BCL9 binding interaction with β -catenin. Finally, our triazole-stapled peptides did not show resistance to trypsin cleavage. Whether this is an intrinsic flaw of

the triazole stapling method or merely due to incorrect placement of the staple is undetermined at this time.

4.5 Experimental Methods

4.5.1 Immunoblotting

SW480 cells in culture media (Lebovitz's-15 media (Gibco) supplemented with 10% fetal bovine serum and 50 units/mL penicillin/streptomycin) were cultured overnight in 6-well plates at 37°C, 5% CO₂ to 60% confluency. The media was then decanted and replaced with Opti-MEM I (2 mL/well). BCL9 and B9L ON-TARGET SMART pool and negative control siRNAs (80 pmol each; Dharmacon) and Lipofectamine 2000 (10 µL) were diluted in Opti-MEM I media (0.25 mL each; Gibco), then combined and incubated at room temperature for 30 minutes. Cells were treated with siRNA/Lipofectamine 2000 complexes to give a final volume of 2.5 mL/well. Cells were transfected for 24 hours and then harvested and washed once with PBS (0.5 mL). The cells were resuspended in cold lysis buffer (PBS, 1% Triton X-100, 2 mM PMSF, Roche mini Complete protease inhibitor cocktail), incubated on ice for 30 minutes and then lysed by flash freezing in liquid nitrogen and thawing on ice. Cell lysates were cleared by ultracentrifugation and total protein concentration was determined using the BCA protein assay kit (Pierce). Total proteins (20 µg) were separated by SDS-PAGE and transferred to 0.2 µm PVDF membranes at 100V for 2.5 hours in cold transfer buffer (Tris-Glycine buffer, 20% methanol, 0.025% SDS). Membranes were treated for 30 minutes with blocking buffer (Tris-buffered saline, 0.5% Tween-20, 5% milk) and then probed overnight at 4°C with antibodies against BCL9 (R & D Systems), B9L (R & D Systems), Axin2 (Cell Signaling Technology), Survivin (Cell Signaling Technology) or β-Actin (Sigma). The membranes were then treated with secondary antibodies conjugated to horseradish peroxidase and visualized by chemiluminescent detection.

4.5.2 Reporter assays

Reporter assays were performed in clear-bottom white 96-well plates (Fisher). Transfections were performed exactly as described for immunoblotting experiments, but all reagents were scaled down 16.7-fold to account for the reduced well volume (150 µL/well). SW480 cells were seeded in 96-well plates and transfected with siRNAs for 24 hours. The media was then decanted and siRNAs were co-transfected with either TOP Flash (6 ng/well) or *siamois* (30 ng/well) reporter plasmids and pTK-*Renilla* luciferase

control plasmid for an additional 24 hours. The media was then decanted and the cells were washed once with PBS (30 μ L/well). Luciferase activities were measured using the Dual-Luciferase® Reporter Assay system (Promega) according to the manufacturer's protocol. Firefly luciferase luminescence was normalized against *Renilla* luciferase luminescence.

4.5.3 Cell proliferation assays

Cells (3000-5000/well) are seeded in 96-well culture plates (Corning) and incubated for 1-3 days with different concentrations of inhibitors. Cell growth inhibition is measured using the Cell Counting Kit-8 (Dojindo Molecular Technologies Inc., Maryland) according to the manufacturer's protocol.

4.5.4 Synthesis of Fmoc-protected HBS peptides

General. Solvents were used without further purification. When necessary, commercial anhydrous grade DMF was used. Thin-layer chromatography (TLC) was performed on silica-coated glass plates and visualized with ultraviolet light. Solvents were removed using a rotary evaporator and when necessary, compounds were further dried by vacuum pump. NMR spectroscopy was performed using a Bruker 300 MH NMR. Mass spectrometry was performed with a Finnigan LCQ Deca electrospray ionization mass spectrometer. Optical rotation measurements were performed using a Rudolph Research Analytical Autopol® III automatic polarimeter. Spectral data for individual compounds is listed in Appendix 6.

o-NBS-amino acid-OtBu general synthesis. *o*-NBS-amino acids were synthesized using a previously described method²⁰². Briefly, amino acid-OtBu·HCl (1.5 equivalents) and *o*-nitrobenzenesulfonyl chloride (1 equivalent) were dissolved in dichloromethane (1 mL/mmol) and treated with pyridine (1.5 equivalents). The reaction was stirred under N₂ at 23°C for 24 hours and then poured into ether (4.5 mL/mmol) and washed with 0.5 N HCl (3 x 2 mL/mmol). The combined aqueous washes were back-extracted with ether (1 x 2 mL/mmol) and the combined organic extracts were dried (MgSO₄), filtered, concentrated *in vacuo* and purified by flash column chromatography (3:1 hexanes/ethyl acetate) to afford the product as an off-white crystalline solid (yield 65%).

Fmoc-N-allyl-amino acid-OtBu general synthesis. *o*-NBS-amino acid-OtBu and K₂CO₃ (2 equivalents) in dry DMF (5.5 mL/mmol) were treated with allyl bromide (1.5 equivalents)

and stirred overnight at 23°C and then quenched with H₂O (7 mL/mmol), extracted with ether (3 x 3.5 mL/mmol). The combined organic extracts were washed with H₂O (3 x 3 mL/mmol), dried (MgSO₄), filtered, concentrated *in vacuo* and dried under high vacuum to afford the product as a light yellow solid (yield 97%).

N-allyl-amino acid-OtBu general synthesis. *o*-NBS-*N*-allyl-amino acid-*OtBu* and K₂CO₃ (3 equivalents) were dissolved/suspended in dry DMF (8.4 mL/mmol), treated with thiophenol (1.3 equivalents) and stirred vigorously at room temperature for 3 hours. The reaction was then poured into 1:1 ether/H₂O (28 mL/mmol) and separated. The aqueous portion was extracted with ether (3 x 14 mL/mmol) and then the combined organic extracts were extracted with 1 N HCl (5 x 8.4 mL/mmol). The acidic aqueous extracts were adjusted to pH 8.0 with Na₂CO₃ and then extracted with ether (5 x 8.4 mL/mmol). The combined organic extracts were dried (MgSO₄), filtered, concentrated *in vacuo* and dried under high vacuum to afford a yellow oil (yield 90%).

Fmoc-amino acid-N-allyl-amino acid-OtBu general synthesis. Fmoc-amino acid-OH (1.5 equivalents), HATU (1.5 equivalents) and HOAt (1.5 equivalents) were dissolved in dry DMF (5 mL/mmol) and stirred for 10 minutes and then treated with DIEA (2 equivalents) and added to the *N*-allyl-amino acid-*OtBu*. The reaction was stirred under an atmosphere of nitrogen at room temperature for 16 hours and then poured into H₂O (10 mL/mmol) and extracted with ether (3 x 10 mL/mmol). The combined organic extracts were dried (MgSO₄), filtered, concentrated *in vacuo* and purified by flash column chromatography (3:1 hexanes/ethyl acetate) to afford the product as a colorless solid (yield 74%).

Fmoc-amino acid-N-allyl-amino acid-OH general synthesis. Fmoc-amino acid-*N*-allyl-amino acid-*OtBu* 50% TFA/DCM (20 mL/mmol) with 5% triethylsilane and stirred at room temperature for 25 minutes. The reaction was then concentrated *in vacuo*, dissolved in ether (20 mL/mmol), washed with H₂O (3 x 12 mL/mmol), extracted with saturated NaHCO₃ (4 x 8 mL/mmol). The combined aqueous extracts were acidified with concentrated HCl and extracted with ether (3 x 12 mL/mmol). The combined organic extracts were dried (MgSO₄), filtered, concentrated *in vacuo* and dried under high vacuum to afford the product as a colorless solid (yield 95%).

4.5.5 Synthesis of azido and alkynyl amino acids

Fmoc-azido amino acids general synthesis. Fmoc-Nle(eN₃)-OH and Fmoc-L-Nva(dN₃)-OH were synthesized from Fmoc-L-Lys-OH·HCl and Fmoc-Orn-OH·HCl, respectively according to the previously reported protocol²⁰³.

Paa-Ni-BPB. (S)-Gly-Ni-BPB¹⁹⁶ (2.78 mmol) and crushed NaOH (27.8 mmol) were dissolved/suspended in anhydrous DMF under vacuum. The flask was purged with nitrogen and the reaction was stirred at room temperature for 7 minutes. 4-Bromo-1-butyne (3.83 mmol) was added via syringe and the reaction was stirred for an additional 6 minutes, and then poured into 5% acetic acid (120 mL) and extracted with toluene (3 x 40 mL). The combined organics were washed with brine (20 mL), dried (MgSO₄), filtered, concentrated *in vacuo* and purified by flash column chromatography (4:1 ethyl acetate/acetone) to afford the product as a red solid (1.94 mmol; 70%).

Fmoc-Paa-OH. (S)-Paa-Ni-BPB (4.8 mmol) was dissolved in 2:1 MeOH/DCM (15 mL) and added dropwise over 10 minutes to a refluxing solution of 3 N HCl/MeOH at 60°C. The reaction was stirred for an additional 20 minutes and then concentrated to dryness, redissolved in H₂O (10 mL), and evaporated to dryness again. The crude residue was dissolved in H₂O (30 mL), washed with CHCl₃ (6 x 20 mL). The combined organic washes were extracted with H₂O (15 mL) and the combined aqueous extracts were neutralized with Na₂CO₃. Additional Na₂CO₃ (15 mmol) was added and the solution was cooled to 0°C. Fmoc-N-hydroxysuccinimide ester (7.5 mmol) in dioxane (45 mL) was added dropwise and the reaction was then allowed to warm slowly to room temperature and stir overnight. The reaction was then diluted with H₂O (100 mL), acidified with concentrated HCl and extracted with EtOAc (3 x 40 mL). The combined organic extracts were dried (MgSO₄), filtered, concentrated *in vacuo*, and purified by flash column chromatography (1:1 EtOAc/hexanes, 1% AcOH) to afford the product as a colorless solid (4.5 mmol; 94%). The product redissolved in an ether/hexane mixture, concentrated *in vacuo* and dried under high vacuum to remove all traces of AcOH.

4.5.6 Peptide synthesis

General. Automated solid-phase peptide synthesis was performed on an Applied Biosciences 433A peptide synthesizer unless otherwise indicated. Manual solid-phase peptide synthesis was performed in sealed 10 mL disposable polypropylene columns (Fisher Scientific). Peptides were deprotected with 20% piperidine/DMF (2 x 6 mL x 10

minutes). Amino acid couplings were accomplished by preactivating the amino acid (5 equivalents) with HATU (5 equivalents) and HOAt (7.5 equivalents) in DMF (5 mL) for 15 minutes and then treating with DIEA (7.5 equivalents), adding to the resin and shaking for 60 minutes or until the resin tested negative by the Kaiser ninhydrin test¹⁵⁸. All peptides were cleaved and deprotected with 87.5% TFA, 5% DTT, 5% H₂O, 2.5% TIS, and then purified by semi-preparative RP-HPLC using a Waters Sunfire™ 19x150 C₁₈ column followed by lyophilization for 16-24 hours. Mass spectrometry was performed with a Finnigan LCQ Deca electrospray ionization mass spectrometer. Purity and mass spectral data are listed in Appendices 1 and 2.

CPP-tagged peptides. Peptides were synthesized by automated solid phase peptide synthesis as previously reported²⁰⁴. Ant₈- and Arg₈-tagged peptides were cleaved and deprotected with cleavage cocktail for 8 and 16 hours, respectively, prior to purification by semi-preparative RP-HPLC.

HBS peptides. The peptide was synthesized by automated peptide synthesis until the coupling of the N-allyl-dipeptide. The resin was then transferred to a 10 mL and Fmoc-N-allyl-dipeptide the following amino acid and 4-pentenoic acid were coupled manually. The protected, resin-bound peptide was then transferred to a 25 mL flask and purged with N₂. Hoveyda-Grubbs 2nd generation catalyst (30 mole %) in freshly distilled benzene (20 mL) was added under an atmosphere of N₂ and the resin was stirred for 10 minutes at room temperature and then heated at reflux for 24 hours. The resin was then filtered, washed with MeOH (4 mL), DCM (3 x 4 mL), cleaved/deprotected for 2 hours, concentrated, precipitated with cold ether, centrifuged, redissolved in CH₃CN/H₂O, treated with MP-TMT ruthenium scavenging beads (20 equivalents; Biotage), and purified by semi-preparative RP-HPLC.

Hydrocarbon-stapled peptide. The (R)-Fmoc-disubstituted olefin amino acid was synthesized following to published protocols^{170,187} and is outlined Scheme 1. After automated peptide synthesis, the resin-bound peptide was subjected to RCM conditions as previously described¹⁷⁰. A 10mM solution of bis(tricyclohexylphosphine)/benzylidene ruthenium (IV) dichloride (Grubbs catalyst) in 1,2-dichloroethane (DCE) was prepared as follows: DCE was degassed by distillation, followed by 3 cycles of vacuum evacuation and purging with nitrogen. Grubbs catalyst was added to a dry flask, evacuated and purged with nitrogen 3 times. DCE was then added to the flask and the solution was

evacuated and purged with nitrogen once more. This solution was then used for performing the RCM reaction.

Triazole-stapled peptides general procedure. Pure, lyophilized linear peptide and sodium L-ascorbate (4.4 equivalents) were dissolved in 2:1 H₂O/*t*-BuOH to give a final peptide concentration of 1 mg/mL. CuSO₄·5H₂O (4.4 equivalents) was added and the reaction was stirred at room temperature for 30-60 minutes. The reaction was then concentrated *in vacuo* and purified by semi-preparative RP-HPLC. Typical yields of cyclized product were 40-90%.

4.5.7 Modeling of triazole staples

A helical peptide segment of BCL9 (residues S352 to F374) taken from the crystal structure (PDB code 2GL7) was used as a template for constructing the stapled peptide. A triazole bridge between E360 and Q364 was needed. Different lengths of linker (three and four carbon atoms) on Q364 were tested. Finally, we have determined that a triazole group linking one carbon atom on E360 and four carbon atoms on Q364 is sufficient. Because only beta carbon on E360 is resolved in the crystal structure, different chiral orientation of the beta atom on E360 can be prepared directly from modeling by changing the beta carbon on E360. A one-carbon linked triazole group was first built on E360 and the three carbon linker group was added by modifying the side chain of Q364. After the bridge was formed, local minimization of modified E360 and Q364 was performed. All the computational modeling was done using Sybyl (Tripos, Inc., St. Louis, MO).

4.5.8 Turbidity assay

Compound stock solutions were prepared at 20 mM concentrations in DMSO. Serial dilutions (5 µL) in DMSO were then prepared in 96 clear flat-bottom cell culture plates. FP assay buffer (120 µL) was then added and the plates were mixed vigorously on an orbital shaker for at least 10 minutes. Light absorbance at 485 nm was then measured. The wavelength used for measurement could be any value 400 nm or up without any significant difference in the relative measurement values. Compound precipitation was estimated to be the point at which the curve begins to rise above the baseline. However, compound aggregation (which does not absorb light) likely begins at lower concentrations.

Chapter 5

Conclusions and Future Directions

5.1 Importance of Wnt signaling and the role of BCL9/B9L

Over the past 30 years, the Wnt signaling pathway has received much attention and has been extensively studied due to its involvement in numerous cellular processes ranging from embryonic development and cell differentiation to tissue homeostasis and cell motility^{4,6}. The realization that Wnt signaling is involved in human diseases such as cancer and osteoporosis has only increased the interest in understanding the mechanisms of Wnt signaling. Research has revealed that the primary effector of canonical Wnt signaling is β -catenin, a multi-functional protein involved in both cell adhesion and transcriptional activation. To date, there have been over 10,000 peer-reviewed publications regarding β -catenin alone. Yet, despite the exhaustive amount of work that has been put into understanding the functions of β -catenin, new discoveries are still being made.

Recently, BCL9 and its homolog B9L were identified as components of the nuclear β -catenin transcriptional activation complex^{61,81,146}. Originally identified as Lgs in *Drosophila*, the functions of BCL9/B9L in vertebrates are still under debate. These proteins have been shown to bind to β -catenin through their conserved HD2 region. It is postulated that BCL9/B9L serve to recruit the protein Pygo, which has been shown to bind histones¹⁴⁹, to the transcriptional activation complex. This Pygo-recruitment function of BCL9/B9L has been shown to be essential in *Drosophila*; however, in vertebrates the evidence is less concrete^{61,81,82,147,205,206}. On the other hand, BCL9 was shown to also possess a transcriptional activation domain in its C-terminal region which can synergize with the transcriptional activation properties of β -catenin^{84,85}. Besides these functions, it is important to remember that BCL9 and B9L are ~140 kDa proteins that contain six conserved regions (HD1-6)⁸³, of which only HD1 and HD2 have known binding

interactions. Thus, future work will likely reveal additional binding interactions of BCL9/B9L that help delineate their roles in Wnt signaling.

Although the complete list of binding interactions for BCL9 and B9L is far from finished, the functional importance of these co-factors for β -catenin-mediated transcriptional activation has been demonstrated in several different scenarios. Our work and that of others, has shown that siRNA knockdown of BCL9 and B9L in colon cancer and lymphoma cells with activated β -catenin suppresses the transcriptional activity of β -catenin and inhibits the expression of known Wnt target genes (Figure 4.2)^{83,84,148}. Furthermore, knockdown of B9L was shown to inhibit cell invasion of colon cancer cells, however, it is unclear whether this function is controlled by the B9L- β -catenin interaction or is due to another function of B9L¹⁴⁸.

For the design of new therapeutics to treat hyperproliferative diseases such as cancer, targeting the BCL9/B9L binding interaction with β -catenin is an attractive strategy for several reasons. First, the formation of the BCL9- β -catenin-TCF nuclear transcription complex is the most downstream step in the Wnt signaling pathway. Diseases arising from β -catenin activation as a result of overexpression of Wnt ligands, disruption of the β -catenin destruction complex or mutation of β -catenin itself would therefore, all be expected to be sensitive to a BCL9 inhibitor. Second, the BCL9/B9L binding site on β -catenin is unique and is not shared by any other known β -catenin binding partners⁸⁰. Thus, on-target toxicity due to the disruption of other desired β -catenin binding interactions such as those with E-cadherin, APC or Axin, would be expected to be minimal. This is in contrast to TCF inhibitors, which in several cases, have been shown to inhibit the binding of APC, a protein known to have a binding site on β -catenin that overlaps with that of TCF^{45,130,207}. Finally, the α -helical HD2 region of BCL9 binds to β -catenin with a binding affinity of 0.5-1 μ M (Figure 2.1 and Sampietro *et al.*⁸⁰) and our work has demonstrated that BCL9-derived peptides can be designed to have binding affinities as low as 100 nM. Additionally, this binding interaction is primarily mediated by just a handful of closely spaced hydrophobic residues, making the design of small molecule inhibitors a plausible reality.

5.2 Summary and conclusions of our work

5.2.1 Development of BCL9 binding assays, BCL9 mutational analysis, and HTS

The quest for drug-like, cell-permeable inhibitors of the BCL9/B9L binding interaction with β -catenin begins with the development of a reliable and quantitative binding assay. We initially designed a FP-based BCL9-competitive binding assay using a fluorescently-tagged peptide encompassing the entire 35 amino acid HD2 region of BCL9. Although this probe was longer than most typical FP probes, it served as a useful starting point for our in-depth analysis of the BCL9- β -catenin binding interaction. With this initial assay, we performed extensive mutational analysis on four critical binding residues in BCL9, and discovered that the F374 (L417 in B9L) binding pocket was able to accommodate larger bicyclic residues such as naphthylalanine and 5-chlorotryptophan with a corresponding 3-fold increase in binding affinity. Systematic truncation of the unwieldy BCL9 35-mer allowed us to map the minimal binding region of BCL9 to a much shorter and more manageable 24 amino acid sequence (residues 351-374). Combining these results we were able to re-optimize our FP assay with a smaller and more potent tracer, which allows the use of less β -catenin protein, gives a larger signal-to-noise ratio and provides for discrimination between a larger range of compound binding affinities¹⁵⁹. Conversion of our FAM-labeled tracer to TAMRA and re-optimization of our assay buffer provided us with not only a robust, reliable and quantitative binding assay, but also a reliable HTS assay for the screening and potential identification of novel small molecule inhibitors of the BCL9- β -catenin binding interaction.

To complement our FP assay, we also developed a SPR-based BCL9-competitive binding assay and validated it with our BCL9-based peptide inhibitors. This assay is not high throughput, but serves as an invaluable secondary assay to confirm the activity of compounds identified during the course of HTS for BCL9 inhibitors.

We used our fully optimized FP assay to perform HTS of a 54,000 compound library at the Center for Chemical Genomics at the University of Michigan. From this collection we had an initial hit rate of 1.5%, of which 23% were confirmed upon re-screening. After dose-response testing of these compounds, we identified 17 compounds for further follow up. Further testing, revealed that several of these compounds were in fact fluorescence quenchers. However, two compounds showed dose-dependent inhibition of

BCL9 binding in our SPR-based secondary assay and merit further characterization in our cell-based reporter assays.

From this work, we learned two important lessons. First, we found that although TAMRA is excited at longer wavelengths than FAM (540 nm vs. 485 nm, respectively), TAMRA is still subject to significant amounts of interference from autofluorescent and quenching small molecules. This is an intrinsic drawback to fluorescence-based methods and can become more pronounced when trying to identify inhibitors of protein-protein interactions, which often involve larger surface areas than do enzyme binding sites. Nevertheless, the simplicity, high throughput and quantitative nature of FP assays make them prime choices for HTS. Thus, to overcome issues with fluorescence quenching, it will be necessary to utilize even more red or near-infrared-shifted probes such as the Alexa Fluor and BODIPY series of dyes. Second, we concluded that more diverse, and possibly larger, libraries of compounds will likely need to be screened to identify a significant number of BCL9 inhibitors. From our initial screen, our most potent compound (5480481, $K_i = 2.4 \mu\text{M}$) appears to be too small to be a reversible, competitive inhibitor. Based on the electron deficient nature of this compound, it is more likely to be forming a covalent adduct with β -catenin and inhibiting the binding of BCL9. The fact that we were able to regenerate the BCL9-immobilized surface of our SPR-chip after treatment with compound 5480481 indicates that it is not irreversibly bound to BCL9. In addition, it may be necessary to complement our HTS approach with other screening approaches such as NMR fragment-based screening to identify BCL9 inhibitors, since the BCL9 binding site is larger than a typical enzyme active site for which many HTS compounds are better suited. NMR screening methods have been shown to be effective for developing inhibitors of protein-protein interactions as is exemplified by the development of the BCL-2 family inhibitor ABT-737²⁰⁸.

5.2.2 Cell-permeable and stabilized α -helical BCL9 peptides

While working to identify specific inhibitors of the BCL9- β -catenin binding interaction, we also worked toward validating the interaction with specific cell-permeable BCL9 peptide-based inhibitors. In contrast to siRNA methods that reduce the expression of BCL9 and thereby inhibit all of its functions, cell-permeable BCL9-peptides would be extremely useful as tools for studying the specific inhibition of BCL9/B9L binding to β -catenin. In addition, a single inhibitor would be expected to block the functions of both BCL9 and B9L. Our initial attempts to generate cell-permeable peptides using polyarginine or

Antennapedia CPPs as carrier peptides resulted in poorly soluble peptides that demonstrated non-specific toxicity to a range of different cell types. We speculated that the binding of the cationic peptides to the phospholipid membrane and subsequent aggregation of the peptides was causing lethal disturbances in the cellular membrane. This hypothesis was supported by the fact cell death was occurring much more rapidly than would be expected from inhibition of Wnt signaling and that the more soluble inactive peptides did not show non-specific toxicity. In addition, CPPs such as Antennapedia were recently reported to have cytotoxic effects themselves¹⁹⁸.

We therefore focused on eliminating the CPP tags and making stabilized α -helical BCL9 peptides that were cell-permeable. We first tried the RCM-based method of generating HBS-stabilized peptides. This approach featured a relatively straight forward synthesis of the requisite N-allyl-dipeptide, however, we found that the RCM reaction did not work well when the N-allyl-amino acid contained a bulky side chain such as that in leucine. Switching to N-allyl-alanine allowed us to obtain the HBS-stabilized BCL9 peptide, though, the overall yield was still lower than we had hoped. Analysis of the HBS stabilized BCL9 24-mer showed the peptide actually be less potent than its linear precursor. This result was surprising since we had previously believed that the additional non-binding N-terminal residues in the BCL9 helix were only required for helix propagation. In light of this new data, we concluded that the N-terminus of BCL9 around L351 is not helical in its native state and that forcing it to become helical through HBS stabilization is detrimental to the binding of BCL9. We speculate that L351 may actually be involved in an additional binding interaction with β -catenin that was not observed in the reported crystal structure of BCL9 in complex with β -catenin. Thus, the HBS helix stabilization method is not appropriate for our BCL9/B9L system.

Since the BCL9 α -helix could not be stabilized at the N-terminus, we examined both hydrocarbon and triazole stapling techniques for stabilization within the helix. The hydrocarbon stapling technique, also an RCM-based method, is the more studied of the two techniques and has been shown to increase helicity, binding affinity, protease resistance and cell permeability^{153,170,186}. We attempted this approach, but found the disubstituted olefin amino acid to be tedious and expensive to synthesize. Furthermore, the stapled peptide was obtained in low yields after on-resin peptide cyclization and was highly insoluble in aqueous solution. We therefore focused most heavily on the newer, less-well characterized triazole stapling technique¹⁸⁸, which involves the copper-

mediated Huisgen azide/alkyne 1,3-dipolar cycloaddition¹⁹⁹. Synthesis of the azido amino acid was accomplished in two steps with high yield and the reaction was easily scaled up. Furthermore, the cyclization was performed in aqueous solution, at room temperature, with non-toxic, air-insensitive copper reagents and gave good yields (40-90%). CD spectroscopy showed that the triazole stapled peptide was more helical in solution (64% vs 43% for linear). In addition, we experimented with a variety of different length linkers, different combinations of linkers, and both L- and D-enantiomers, and concluded the optimal combination to be L-Nle(eN₃) and D-Pra substituted at the *i* and *i*+4 positions, respectively, for stabilization of one full turn of the BCL9 α -helix.

Unfortunately, our triazole stapled peptides also suffered from poor aqueous solubility. Through a range of peptide mutations we identified the hydrophobic MLF sequence to be the main cause of low peptide solubility. Mutation of M372 to smaller hydrophobic groups such as 2-Abu or the coupling of solubilizing groups (i.e. piperazine) to the C-terminus of the peptide increased peptide solubility. Despite these alterations, the triazole stapled peptides still exhibited lower solubility than their linear counterparts due to the loss of hydrogen bonding between the peptide backbone and the solvent. This effect is likely intrinsic to the stabilization of helices in general and underscores the need for stabilized helices to be very potent.

Finally, we determined that our *i*+4 triazole-stapled BCL9 peptides were not resistant to trypsin cleavage. At this time, we do not believe that this is an intrinsic flaw of the triazole stapling technique, but rather the current location of the staple is not able to stabilize the full helix. Changing the position of the staple is therefore, the obvious next step. After that, cyclization between the *i* and *i*+7 positions for the stapling of two consecutive turns should be investigated. It may also be possible to make a doubly-stapled peptide by incorporating the two sets of azido and alkynyl residues in the peptide.

In summary, we have established a solid foundation for the discovery and development of novel inhibitors of the BCL9/B9L binding interaction with β -catenin. Our binding assays likely will be the cornerstone of future BCL9-competitive inhibitor screening, design and development. Our extensive mutational analysis of the residues mediating the interaction with β -catenin have also helped define the proper residue size and polarity for binding to each pocket, which will aid in the rational structure-based design of inhibitors once an appropriate scaffold is determined. Our detailed study of the triazole

stapling of α -helical peptides has also helped define the proper residue combinations for stapling one turn of an α -helix. Further study of different stapling locations and stapling of consecutive turns is expected to yield protease resistant and cell-permeable peptides that will serve as excellent, metabolically stable biological tools for analyzing the effects of specifically inhibiting the BCL9/B9L binding interaction with β -catenin.

Despite the questions that still remain regarding the complete functional significance of BCL9/B9L in different tissue and cancer types, BCL9/B9L are attractive targets for designing selective inhibitors of β -catenin-mediated Wnt signaling. Because the binding sites for BCL9 and B9L appear to be one and the same and the fact that their binding site is distinct from those of other known β -catenin binding partners, suggests that a class of compounds may exist that is capable of selectively inhibiting the binding of BCL9 and B9L with β -catenin and antagonizing canonical Wnt signaling. Such a class of inhibitors could have tremendous potential in treating countless hyperproliferative human diseases.

5.3 Future Directions

As outlined above, our work has laid the foundation for the thorough study of the BCL9/B9L binding interaction with β -catenin and for the identification, design and development of inhibitors of this interaction. Nevertheless, we have only scratched the surface of what is possible in this field. Thus for the future directions of our work, we envision four major branches of research: 1) Additional FP-based high throughput and NMR fragment-based screening for novel scaffolds and binding motifs that can be used to design small molecule BCL9/B9L inhibitors; 2) *de novo* design of potential small molecule BCL9/B9L inhibitors; 3) additional investigation of triazole stapling for the stabilization of α -helical peptides and the development of metabolically stable, cell-permeable peptides; and 4) Mutational analysis of additional residues of unknown importance in BCL9 binding to β -catenin.

5.3.1 HTS and NMR fragment-based screening for BCL9/B9L inhibitors

Our initial HTS campaign involved the screening of 54,000 compounds. In the realm of HTS, this is a relatively small number of compounds and it is not terribly surprising that we did not identify a potent lead compound. Thus, our first goal is to screen an additional 100,000 compounds that has now become available at the Center for Chemical Genomics. For this next screen we will utilize an improved tracer in which the TAMRA

fluorophore will be replaced with the red shifted BODIPY 630/650 dye. This dye has excitation and emission wavelengths that are 100 nm longer than TAMRA and will result in fewer false positive hits as a result of fluorescence quenching.

In addition to HTS, we will also begin NMR fragment-based screening²⁰⁹. This approach has been used to successfully design and develop novel small molecule inhibitors of the binding interaction between α -helical BH3 peptides and the anti-apoptotic proteins Bcl-2, Bcl-xL and Bcl-w²⁰⁸. In this method, a small library of a few thousand ligands is screened and structure-activity relationships (SAR) are identified between low molecular weight molecules and the particular binding pockets of the target protein. Ligands, often with low to moderate binding affinity, are optimized and then chemically linked to generate larger, often highly potent ligands. The advantage of this approach is that high affinity ligands can be generated from the SAR results of a relatively small library of ligands. This is particularly useful for developing inhibitors of protein-protein interactions, because the binding interaction surface is often larger and shallower than that of enzymes and can therefore require larger molecules for potent activity; molecules that don't typically exist in traditional HTS libraries.

In order to perform protein NMR studies, we will first need to generate a smaller β -catenin construct. Our current construct is 549 amino acids in length making it unwieldy for NMR experiments. Typically, protein NMR studies are performed on proteins of less than 200 amino acids. We are therefore in the process of generating a truncated β -catenin construct that contains only the first four arm repeats (residues 138-307). A similar construct was shown to still bind BCL9/Lgs in immunoprecipitation assays⁶¹. Although the BCL9/B9L binding site is restricted to the first arm repeat, the additional three repeats are likely necessary to stabilize the overall protein structure, since another construct containing only the first two arm repeats did not bind BCL9/Lgs. Once we have generated our construct and purified the recombinant protein, we will test its binding affinity to our BCL9 peptides. If the shorter construct retains similar binding affinity, we will assume it has the same structure as the full length protein. We will then generate a ¹⁵N labeled protein and perform NMR fragment-based screening.

5.3.2 *De novo* design of potential small molecule BCL9/B9L inhibitors

We will also begin the *de novo* design and synthesis of potential BCL9/B9L inhibitors based on the BCL9 co-crystal structure and the results of our BCL9 mutational analysis.

Currently, we have several core scaffolds that, when properly functionalized, have been shown to inhibit the binding of α -helical peptides to their target proteins (e.g. BH3-Bcl-2, p53-MDM2). These scaffolds can serve as useful starting points for the design of BCL9/B9L inhibitors. From our mutational analysis we already know that F374 can be mutated to tryptophan or naphthylalanine. These results are consistent with the crystal structure, which shows a large pocket adjacent to F374 (Figure 5.1). In addition, there is another groove connecting to this pocket that may tolerate a small functional group. Thus, if a scaffold can combine these elements with a mimic of L373 and potentially link out to one or both of the I369 and L366 binding pockets, it may be possible to achieve potent binding affinity.

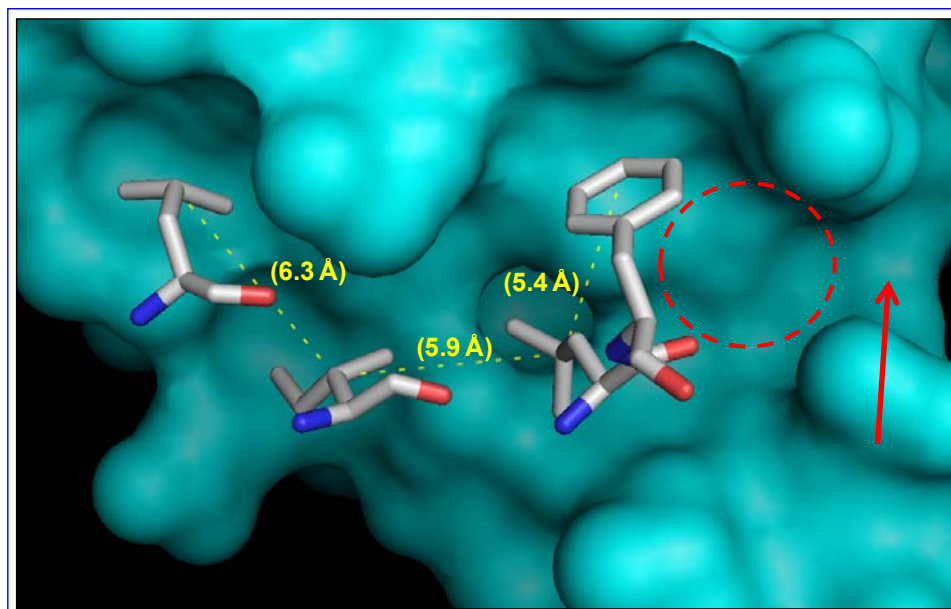


Figure 5.1. BCL9 binding residues. Four of the key BCL9 binding residues (from left to right: L366, I369, L373, F374) are shown in complex with β -catenin (PDB code 2GL7). Measurements between key residues are in yellow. Additional pockets for inhibitor design are indicated by a red oval and arrow.

5.3.3 Further investigation of triazole stapling of BCL9 peptides

Our results from the triazole-stapling of the BCL9 α -helix demonstrate that this method is able to increase helical propensity, is easily performed under mild and non-toxic conditions, and uses easily synthesized reagents. However, from our trypsin cleavage experiments, we found that our peptides were not resistant to proteolysis. We speculate that this is because the current location of the staple (from position 360 to 364) is not optimal for the stabilization of the full helix, and is therefore allowing part of the helix to remain unstructured and accessible to protease cleavage. Thus, we will examine

additional locations (as outlined in Figure 4.4) for the stapling of single turns of the BCL9 helix. We will also use the Ni(II)-glycine-BPB complex to synthesize longer alkynyl amino acids for stapling the *i* and *i*+7 positions. This longer stapling was shown to be more effective for the hydrocarbon stapling of p53 and RNase A peptides^{153,170} and therefore may be equally effective for our BCL9 peptides. Additionally, our BCL9 peptides are long enough to accommodate multiple staples. Incorporating multiple staples was never really an option for hydrocarbon stapling since both sides of the staple are identical. Triazole stapling however, uses complementary azide and alkyne moieties, which can allow for the use of reversed staples. Thus, by switching the direction of the staple (i.e. azide-alkyne; alkyne-azide), which we've shown to not drastically affect binding affinity (Figure 4.6, compare **53T** and **58T**), we can avoid cross stapling and should be able to form two separate staples in the same peptide. This technique has the potential for generating highly stabilized helices that may also demonstrate high levels of protease resistance and cell permeability.

5.3.4 Mutational analysis of other BCL9 residues

Finally, there are several residues in the BCL9 sequence that still require further mutational analysis in order to better define their role in BCL9 binding. Our studies have shown that L351 is required in the linear BCL9 peptides and must not be in a helical conformation. However, this residue does not appear to be close to β -catenin in the co-crystal structure. Thus, we will perform a range of mutations at this position to determine the amino acid requirement and hopefully shed some light on the function of L351.

In addition, we will examine whether T365 can be mutated to other residues. Threonine is known to destabilize helices²⁰¹, and its positioning immediately after the current location of our triazole staple may be a factor in the low trypsin resistance of our triazole-stapled peptides. We will therefore examine the effect of using other residues such as Ser and 2-Abu at this position. In addition, E155 of β -catenin is very close to this position, and although it will be highly solvated, polar or charged residues may still be able to hydrogen bond or form a salt bridge with this residue to increase the binding affinity. Thus, we will also examine the use of both homoserine and diaminobutyric acid at this position as well.

Thus, by taking a multifaceted approach we expect to identify and develop both small molecule and peptide-based cell-permeable inhibitors of the BCL9/B9L binding

interaction with β -catenin. Such inhibitors will certainly serve as useful biological tools for better studying the roles of BCL9/B9L in the Wnt signaling pathway and may also have potential as a new class of anticancer therapeutics.

Appendices

Appendix 1. Table of BCL9 and B9L peptides.

	<u>Sequence</u>	<u>m/z [M+2H]²⁺</u> (<u>calc.</u>)	<u>Purity</u> (%)	<u>K_i</u> (<u>±SD</u>) (<u>μM</u>)
1	Ac-NPDGLSQQLEHRERSLQTLRDIQRM LFPDEKEFT-βA-K(Ac)-NH ₂ (a.a. 347-381)	1513.40 ^a (1513.43)	96.4	0.964 (0.403)
1-F	Ac-NPDGLSQQLEHRERSLQTLRDIQRM LFPDEKEFT-βA-K(5-FAM)-NH ₂ (a.a. 347-381)	1618.93 ^a (1618.78)	98.9	0.616 ^b (0.321)
1B	Ac-NPDGLSQQLEHRERSLQTLRDIQRM LFPDEKEFT-NH ₂ (a.a. 347-381)	1433.00 ^a (1433.05)	91.6	0.366 ^c (0.100)
2	Ac-NPDGLSQQLEHRERSLQTLRDIQRM (2-Nal)PDEKEFT-βA-K(Ac)-NH ₂ (a.a. 347-381)	1530.07 ^a (1530.10)	98.9	0.374 (0.124)
2-F	Ac-NPDGLSQQLEHRERSLQTLRDIQRM (2-Nal)PDEKEFT-βA-K(5-FAM)-NH ₂ (a.a. 347-381)	1635.47 ^a (1635.45)	90.3	0.365 ^b (0.159)
3-F	Ac-LSQQLEHRERSLQTLRD(Hle)QRML(2-Nal)- Ahx-K(5-FAM)-NH ₂ (a.a. 351-374)	1865.93 (1865.94)	90.6	0.375 ^{b,c} (0.113)
4-F	Ac-LSQQLEHRERSLQTLRD(Hle)QRML(2-Nal)- P-(βA) ₂ -K(FAM)-NH ₂ (a.a. 351-375)	1928.80 (1928.97)	>99.0	0.213 ^{b,c}
5-F	Ac-LSQQLEHRERSLQTLRD(Hle)QRML(2-Nal)- βA ₂ -K(FAM)-NH ₂ (a.a. 351-374)	1880.20 (1880.44)	94.2	0.200 ^{b,c} (0.043)
6-F	(FAM)-Ahx-LSQQLEHRERSLQTLRD(Hle) QR ML(2-Nal)-NH ₂ (a.a. 351-374)	1780.80 (1780.89)	95.5	0.299 ^{b,c} (0.036)
7-F	(FAM)-Ahx-LSQQLEHRERSLQTLRDIQRM (2-Nal)-NH ₂ (a.a. 351-374)	1773.80 (1773.88)	94.7	0.137 ^{b,c} (0.004)
8	Ac-LSQQLEHRERSLQTLRDIQRM(2-Nal)- βA ₂ -K(Ac)-NH ₂ (a.a. 351-374)	1715.47 (1715.41)	94.0	0.156 ^c (0.064)
8-F	Ac-LSQQLEHRERSLQTLRDIQRM(2-Nal)- βA ₂ -K(FAM)-NH ₂ (a.a. 351-374)	1873.33 (1873.43)	91.0	0.101 ^{b,c} (0.042)
8-R	Ac-LSQQLEHRERSLQTLRDIQRM(2-Nal)- βA ₂ -K(TAMRA)-NH ₂ (a.a. 351-374)	1900.47 (1900.48)	94.4	0.259 (0.140)
8-Arg ₈	Ac-LSQQLEHRERSLQTLRDIQRM(2-Nal)- βA ₂ -RRRRRRRR-NH ₂ (a.a. 351-374)	1503.53 ^a (1503.51)	95.5	0.272 (0.023)
8-Arg ₈ inact.	Ac-LSQQLEHRERSLQTLRDIQRM(2-Nal)- βA ₂ -RRRRRRRR-NH ₂ (a.a. 351-374)	1475.60 ^a (1475.48)	93.6	NB
8-Ant ₈	Ac-LSQQLEHRERSLQTLRDIQRM(2-Nal)- βA ₂ -NRRMKWKK-NH ₂ (a.a. 351-374)	1463.40 (1463.13)	>99	<0.100
8-Ant ₈ inact.	Ac-LSQQLEHRERSLQTLRDIQRM(2-Nal)- βA ₂ -NRRMKWKK-NH ₂ (a.a. 351-374)	1411.33 ^a (1411.42)	83.4	NB

9	Ac-LEHRERSLQTLRDIQRMLFP <u>DEKEFT</u> -NH ₂ (a.a. 356-381)	1664.93 (1664.87)	>99	16.4 (4.3)
10	Ac- <u>NPDGLSQQ</u> LEHRERSLQTLRDIQRMLFP-NH ₂ (a.a. 347-375)	1774.20 (1774.42)	97.3	1.10 (0.23)
11	Ac- <u>DGLSQQ</u> LEHRERSLQTLRDIQRMLFP-NH ₂ (a.a. 349-375)	1668.80 (1668.86)	>99	3.27 (0.36)
12	Ac- <u>LSQQ</u> LEHRERSLQTLRDIQRMLFP-NH ₂ (a.a. 351-375)	1582.87 (1582.84)	>99	1.90 (0.12)
13	Ac- <u>QQ</u> LEHRERSLQTLRDIQRMLFP-NH ₂ (a.a. 353-375)	1482.80 (1482.78)	>99	34.7 (4.3)
14	Ac- <u>Q</u> LEHRERSLQTLRDIQRMLFP-NH ₂ (a.a. 355-375)	1354.20 (1354.23)	97.5	37.7 (5.8)
15	Ac-LEHRERSLQTLRDIQRMLF-NH ₂	1241.73 (1241.68)	95.5	21.4 (3.3)
16	Ac- <u>LSQQ</u> LEHRERSLQTLRDIQRMLF-NH ₂ (a.a. 351-374)	1534.33 (1534.32)	94.3	0.596 ^c (0.138)
17	Ac-LEHRERSLQT <u>ARDA</u> QRMLFP-NH ₂	1248.07 (1248.16)	>99	>400
17B	Ac-LSQQLEHRERSLQT <u>ARDA</u> QRMLF-NH ₂	1492.27 (1492.27)	97.7	>400
18	Ac-LEHRERSLQTLRDIQRMLFP-NH ₂	1290.20 (1290.20)	>99	28.8 (10.2)
19	Ac-LEHRERSLQT- <u>A</u> -RDIQRMLFP-NH ₂	1269.40 (1269.18)	92.4	>400
20	Ac-LEHRERSLQT- <u>F</u> -RDIQRMLFP-NH ₂	1307.20 (1307.20)	>99	>400
21	Ac-LEHRERSLQT- <u>I</u> -RDIQRMLFP-NH ₂	1290.33 (1290.20)	97.2	78.8 (20.5)
22	Ac-LEHRERSLQT- <u>Nle</u> -RDIQRMLFP-NH ₂	1290.20 (1290.20)	98.0	180 (15)
23	Ac-LEHRERSLQT- <u>Hle</u> -RDIQRMLFP-NH ₂	1297.13 (1297.21)	95.6	259 (40)
24	Ac-LEHRERSLQT- <u>Tle</u> -RDIQRMLFP-NH ₂	1290.33 (1290.20)	97.4	>400
25	Ac-LEHRERSLQT- <u>V</u> -RDIQRMLFP-NH ₂	1283.27 (1283.20)	97.0	>400
26	Ac-LEHRERSLQTLRD- <u>A</u> -QRMLFP-NH ₂	1269.27 (1269.18)	97.8	>400
27	Ac-LEHRERSLQTLRD- <u>F</u> -QRMLFP-NH ₂	1307.20 (1307.20)	93	137 (35)
28	Ac-LEHRERSLQTLRD- <u>Y</u> -QRMLFP-NH ₂	1315.13 (1315.20)	95.3	>400
29	Ac-LEHRERSLQTLRD- <u>Nle</u> -QRMLFP-NH ₂	1290.13 (1290.20)	95	44.0 (2.3)
30	Ac-LEHRERSLQTLRD- <u>Hle</u> -QRMLFP-NH ₂	1297.20 (1297.21)	99	19.9 (5.7)
31	Ac-LEHRERSLQTLRD- <u>Tle</u> -QRMLFP-NH ₂	1290.20 (1290.20)	92	122 (49)
32	Ac-LEHRERSLQTLRD- <u>V</u> -QRMLFP-NH ₂	1283.27 (1283.20)	95.2	>400
33	Ac-LEHRERSLQTLRD- <u>M</u> -QRMLFP-NH ₂	1299.27 (1299.18)	96.9	78.5 (25.7)
34	Ac-LEHRERSLQTLRDIQRM- <u>A</u> -F-P-NH ₂	1269.13 (1269.18)	97.7	>400
35	Ac-LEHRERSLQTLRDIQRM- <u>F</u> -FP-NH ₂	1307.27	99	173

		(1307.20)		(66)
36	Ac-LEHRERSLQTLRDIQRM- Y -FP-NH ₂	1315.33 (1315.20)	95.9	270 (21)
37	Ac-LEHRERSLQTLRDIQRM- I -FP-NH ₂	1290.33 (1290.20)	95.6	129 (20)
38	Ac-LEHRERSLQTLRDIQRM- Nle -FP-NH ₂	1290.13 (1290.20)	99	88.2 (17.4)
39	Ac-LEHRERSLQTLRDIQRM- Hle -FP-NH ₂	1297.20 (1297.21)	99	66.8 (17.2)
40	Ac-LEHRERSLQTLRDIQRM- Tle -FP-NH ₂	1290.13 (1290.20)	96	133 (20)
41	Ac-LEHRERSLQTLRDIQRM- V -FP-NH ₂	1283.27 (1283.20)	>99	>400
42	Ac-LEHRERSLQTLRDIQRML- A -P-NH ₂	1252.20 (1252.18)	99.2	119 (9)
43	Ac-LEHRERSLQTLRDIQRML- Y -P-NH ₂	1298.20 (1298.20)	97.0	95.0 (15.9)
44	Ac-LEHRERSLQTLRDIQRML- Hfe -P-NH ₂	1297.27 (1297.21)	90.2	54.6 (7.4)
45	Ac-LEHRERSLQTLRDIQRML- W -P-NH ₂	1309.73 (1309.71)	93.7	22.1 (7.2)
46	Ac-LEHRERSLQTLRDIQRML- 1-Nal -P-NH ₂	1315.13 (1315.21)	96.7	16.8 (2.9)
47	Ac-LEHRERSLQTLRDIQRML- 2-Nal -P-NH ₂	1315.13 (1315.21)	95.0	8.41 (1.67)
48	Ac-LSKEQLEHRERSLQTLRDIERLLL-NH ₂ (a.a. 394-417 of B9L)	1508.93 (1508.86)	98.4	0.37 ^c (0.17)
49	Ac-LEHRERSLQTLRDIQRML- (5-CIW) -P-NH ₂	1326.80 (1326.69)	93.7	3.61 ^c (1.16)
50	Ac-LSQEQLLEHRERSLQTLRDIQRML- (5-CIW) -NH ₂	1570.80 (1570.80)	96.7	0.345 ^c (0.003)

K_i values were determined using the BCL9-competitive FP assay with **1-F** (50 nM) and β-catenin (1 μM).

^a $m/z = [M+3H]^{3+}$

^b K_d value instead of K_i

^c K_i determined using new preparation of β-catenin (containing 50 mM Gln/Arg) and 8-F (5 nM)

Appendix 2. Table of HBS, stapled and mutant BCL9 and B9L peptides.

	<u>Sequence</u>	<u>m/z [M+2H]²⁺</u> <u>(calc.)</u>	<u>Purity</u> <u>(%)</u>	<u>K_i</u> <u>(±SD)</u> <u>(μM)</u>
51	pen-EQ(N-allyl-L)EHRERSLQTLRDIQRMLFP-NH ₂	1458.73 (1458.78)	98.0	48.0 (9.1)
51H	(HBS)pen-EQ(N-allyl-L)EHRERSLQTLRDIQRMLFP-NH ₂	1444.87 (1444.77)	>99	15.7 (1.8)
52	pen-AA(N-allyl-A)LEHRERSLQTLRDIQRMLF-NH ₂	1680.93 (1680.90)	>99	0.188 (0.053)
52H	(HBS)pen-AA(N-allyl-A)LEHRERSLQTLRDIQRMLF-NH ₂	1666.93 (1666.88)	92.2	1.51 (0.22)
53	Ac-LSQEQL ^ε HR-Nie(εN ₃)-RSL-Pra-TLRDIQRMLF-NH ₂	1530.27 (1530.13)	95.1	1.44 (0.22)
53T	Ac-LSQEQL ^ε HR-Nie(εN ₃)-RSL-Pra-TLRDIQRMLF-NH ₂ triazole-stapled	1530.27 (1530.13)	94.0	0.331 (0.065)
54	Ac-LSQEQL ^ε HR-Nie(εN ₃)-RSL-(D-Pra)-TLRD ^I QRMLF-NH ₂	1530.33 (1530.13)	>99	4.94 (0.92)
54T	Ac-LSQEQL ^ε HR-Nie(εN ₃)-RSL-(D-Pra)-TLRD ^I QRMLF-NH ₂ triazole-stapled	1530.27 (1530.13)	97.8	0.129 (0.047)
55	Ac-LSQEQL ^δ HR-Nva(δN ₃)-RSL-Pra-TLRDIQRMLF-NH ₂	1530.27 (1523.32)	95.3	2.37 (0.16)
55T	Ac-LSQEQL ^δ HR-Nva(δN ₃)-RSL-Pra-TLRDIQRMLF-NH ₂ triazole-stapled	1523.33 (1523.32)	>99	NB
56	Ac-LSQEQL ^ε HR-Nie(εN ₃)-RSL-Paa-TLRDIQRMLF-NH ₂	1537.40 (1537.34)	93.3	1.40 (0.10)
56T	Ac-LSQEQL ^ε HR-Nie(εN ₃)-RSL-Paa-TLRDIQRMLF-NH ₂ triazole-stapled	1534.40 (1537.34)	97.7	3.00 (0.29)
57	Ac-LSQEQL ^δ HR-Nva(δN ₃)-RSL-Paa-TLRDIQRLLF-NH ₂	1521.40 (1521.34)	>99	1.86 (0.38)
57T	Ac-LSQEQL ^δ HR-Nva(δN ₃)-RSL-Paa-TLRDIQRLLF-NH ₂ triazole-stapled	1521.40 (1521.34)	>99	29.5 (4.6)
58	Ac-LSQEQL ^ε HR-Pra-RSL-Nie(εN ₃)-TLRDIQRLLF-NH ₂	1521.47 (1521.34)	94.9	3.59 (0.97)
58T	Ac-LSQEQL ^ε HR-Pra-RSL-Nie(εN ₃)-TLRDIQRLLF-NH ₂ triazole-stapled	1521.47 (1521.34)	94.0	0.770 (0.177)
59	Ac-LSQEQL ^ε HR-(D-Pra)-RSL-Nie(εN ₃)-TLRD ^I QRLLF-NH ₂	1521.33 (1521.34)	98.2	2.22 (0.16)
59T	Ac-LSQEQL ^ε HR-(D-Pra)-RSL-Nie(εN ₃)-TLRD ^I QRLLF-NH ₂ triazole-stapled	1521.47 (1521.34)	>99	4.36 (0.37)
60	NH ₂ -LSK KQLK HR(Nie-εN ₃)RSL(D-Pra)TLR KIKRLL (2-Nal)K-NH ₂ (a.a. 394-417)	1595.07 (1595.02)	>99	6.27 (0.18)
60T	NH ₂ -LSK KQLK HR(Nie-εN ₃)RSL(D-Pra)TLR KIKRLL (2-Nal)K-NH ₂ (a.a. 394-417) triazole-stapled	1595.13 (1595.02)	97.2	0.341 (0.113)
61	Ac-LSQRQL RHR -Nie(εN ₃)-RSL-(D-Pra)-TLR RIQRAbuL (2-Nal)-NH ₂	1559.00 (1558.93)	95.4	5.72 (0.84)
61T	Ac-LSQRQL RHR -Nie(εN ₃)-RSL-(D-Pra)-TLR RIQRAbuL (2-Nal)-NH ₂ triazole stapled	1558.93 (1558.93)	98.1	0.841 (0.066)
62	NH ₂ -LSQQQLQHR-(Nie-εN ₃)-RSL-(D-Pra)-TLRNIQ- RAbu-L (2-Nal)-NH ₂ (a.a. 351-374)	1509.80 (1509.86)	97.0	13.9 (2.6)

62T	NH ₂ -LSQQQLQHR-(Nle-εN ₃)-RSL-(D-Pra)-TLRNIQ-R Abu -L(2-Nal)-NH ₂ (a.a. 351-374) triazole-stapled	1509.93 (1509.86)	98.4	0.513 (0.137)
63	NH ₂ -LSQQQLQHR-(Nle-εN ₃)-RSL-(D-Pra)-TLRNIQ-R Abu -L(2-Nal)-(N-methylpiperazine) (a.a. 351-374)	1551.33 (1551.40)	91.7	20.3 (1.7)
63T	NH ₂ -LSQQQLQHR-(Nle-εN ₃)-RSL-(D-Pra)-TLRNIQ-R Abu -L(2-Nal)-(N-methylpiperazine) (a.a. 351-374) triazole-stapled	1551.33 (1551.40)	79.7	1.72 (0.09)
64T	NH ₂ -LSQRQL RHR -(Nle-εN ₃)-RSL-(D-Pra)-TLR RI Q-R Abu -L(2-Nal)-(1-(2-aminoethyl)-4-methylpiperazine) triazole-stapled	1622.00 (1621.98)	>99%	0.677 (0.058)
65	NH ₂ -LSQQQLQHR-(Nle-εN ₃)-RSL-(D-Pra)-TLRNIQ-R Abu -L(2-Nal)-(1-(2-aminoethyl)-4-methylpiperazine)	1572.87 (1572.92)	92.1	5.54 (0.55)
65T	NH ₂ -LSQQQLQHR-(Nle-εN ₃)-RSL-(D-Pra)-TLRNIQ-R Abu -L(2-Nal)-(1-(2-aminoethyl)-4-methylpiperazine) triazole-stapled	1572.93 (1572.92)	94.9	0.205 (0.091)
66	NH ₂ -LSK QQLQHR -(Nle-εN ₃)-RSL(D-Pra)TLR NI ERLL(2-Nal)-(1-(2-aminoethyl)-4-methylpiperazine)	1587.40 (1587.44)	95.8	2.44 (0.06)
66T	NH ₂ -LSK QQLQHR -(Nle-εN ₃)-RSL(D-Pra)TLR NI ERLL(2-Nal)-(1-(2-aminoethyl)-4-methylpiperazine) triazole stapled	1587.33 (1587.44)	95.7	0.157 (0.043)
70	Ac-LSQEQL HRERSLQTLRDIQR LLF-NH ₂	1525.47 (1525.34)	93.6	0.940 (0.169)
71	Ac-LSQE QKEHRERSLQTLRDIQR LLF-NH ₂	1532.87 (1532.84)	>99	1.19 (0.16)
72	Ac-LSQEQL HRERSLQTLRDIKR LLF-NH ₂	1525.47 (1525.36)	>99	1.03 (0.34)
73	Ac-LSQEQL HRERSLQTLRDIQRK LF-NH ₂	1533.00 (1532.84)	98.0	3.64 (0.21)
74	Ac-LSQEQL HRERSLQTLRDIQRS LF-NH ₂	1512.47 (1512.31)	95.9	3.04 (0.23)
75	Ac-LSQEQL HRERSLQTLRDIQRT LF-NH ₂	1519.40 (1519.32)	95.5	2.99 (0.16)
76	Ac-LSQEQL HRERSLQTLRDIQRLLFK -NH ₂	1589.53 (1589.38)	>99	1.62 (0.08)
77	Ac-LSQEQL HRERSLQTLRDIQRNva LF-NH ₂	1518.40 (1518.33)	98.4	1.02 (0.06)
78	Ac-LSQEQL HRERSLQTLRDIQR(2-Abu) LF-NH ₂	1511.47 (1511.32)	>99	1.40 (0.21)
79	Ac-LSQEQL HRERSLQTLRDIQRALF -NH ₂	1504.47 (1504.32)	95.1	2.34 (0.50)
80	Ac-LS QRQ LEHRERSLQTLRDIQRMLF-NH ₂	1547.93 (1547.84)	>99	0.676 (0.065)
81	Ac-LSQEQL RHRERSLQTLRDIQRMLF -NH ₂	1547.80 (1547.84)	98.4	0.540 (0.012)
82	Ac-LSQEQL HRERSLQTLRRI QRMLF-NH ₂	1554.93 (1554.85)	96.4	0.337 (0.094)
83	Ac-LSQEQL HRERSLQTLRDIR RMLF-NH ₂	1548.27 (1548.34)	>99	0.886 (0.062)
84	Ac-LS RER LEHRERSLQTLRDIQRMLF-NH ₂	1562.33 (1562.36)	>99	1.16 (0.17)

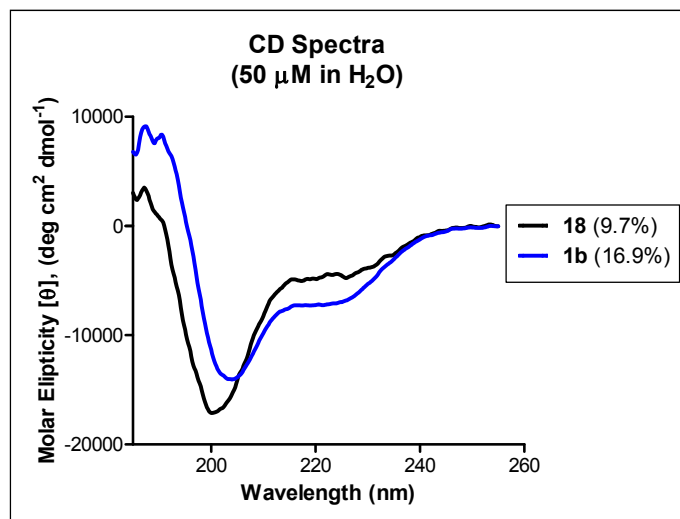
85	Ac-LSQRQLRHRERSLQTLRRIRMLF-NH ₂	1595.93 (1595.93)	95.1	0.621 (0.209)
86	Ac-LSRRQLRHRERSLQTLRRIRMLF-NH ₂	1610.07 (1609.96)	>99	1.81 (0.19)
87	Ac-LSRRRLRHRERSLQTLRDIRMLF-NH ₂	1603.40 (1603.44)	97.2	3.32 (0.40)
88	Ac-LSRRRLRHRERSLQTLRRIRMLF-NH ₂	1624.00 (1623.98)	95.3	1.41 (0.28)

K_i values were determined using the BCL9-competitive FP assay with **8-F** (5 nM) and β-catenin (250 nM, purified with 50 mM Gln, 50 mM Arg).

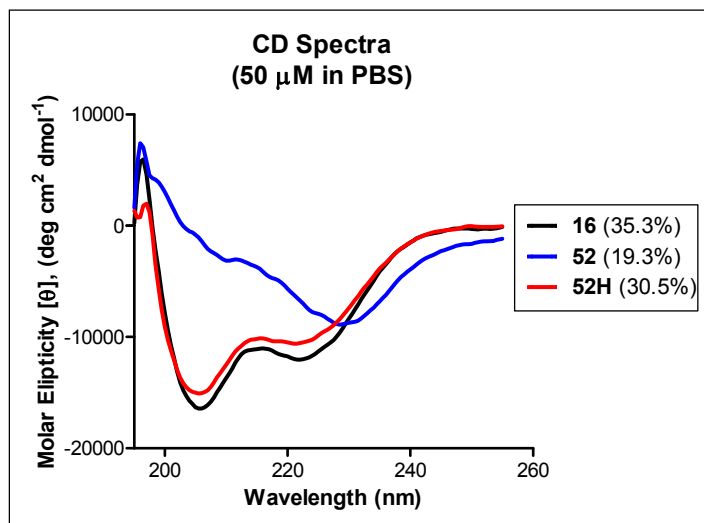
Appendix 3. Circular dichroism experiments with BCL9 peptides

CD measurements were performed at room temperature using a Jasco J-715 and a quartz flow cell with a 1 mm path length. Peptides were dissolved in distilled water or PBS at a concentration of 50 μM . The spectra were averaged over 10 scans collected at 50 nm/min and the baseline (water only) was subtracted from each spectrum. Percent helicity was calculated as reported previously¹⁹²⁻¹⁹⁴.

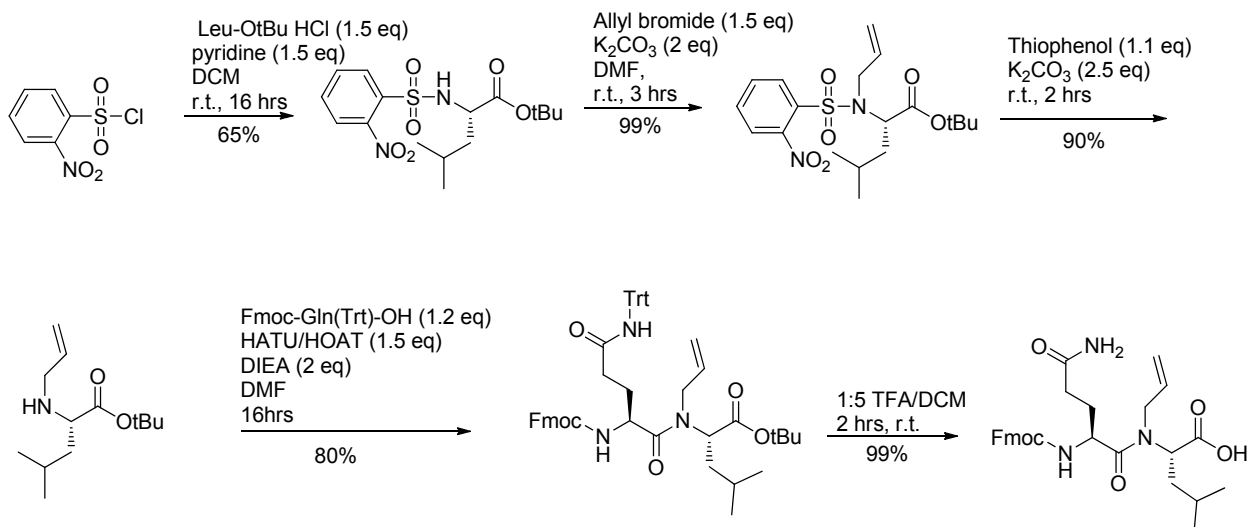
A. BCL9 35-mer and 20-mer



B. BCL9 24-mer and HBS-stabilized BCL9 peptides



Appendix 4. Synthesis scheme for Fmoc-glutaminy-N-allyl-leucine



Appendix 5. Spectral data for synthesized amino acids

o-NBS-Leu-OtBu

R_f 0.5 (3:2 hexanes/ethyl acetate); ¹H NMR (300 MHz, CDCl₃) δ 8.11-8.06 (m, 1H), 7.96-7.91 (m, 1H), 7.74-7.69 (m, 2H), 6.00 (d, J = 10.0 Hz, 1H), 4.08 (ddd, J = 14.8, 8.8, 6.1 Hz, 1H), 1.89 (appar. septet, J = 6.6 Hz, 1H), 1.63-1.48 (m, 2H), 1.18 (s, 9H), 0.98 (d, J = 2.0 Hz, 3H), 0.96 (d, J = 2.1 Hz, 3H); ¹³C NMR (75.5 MHz) δ 170.66, 147.82, 134.50, 133.46, 132.89, 130.52, 125.63, 82.24, 56.19, 42.29, 27.61, 24.39, 22.83, 21.33.

o-NBS-Ala-OtBu

R_f 0.5 (3:2 hexanes/EtOAc); ¹H NMR (300 MHz, CDCl₃) δ 8.11-8.08 (m, 1H), 7.94-7.91 (m, 1H), 7.75-7.69 (m, 2H), 6.11 (d, J = 8.7 Hz, 1H), 4.13 (dq, J = 9.0, 7.2 Hz, 1H), 1.45 (d, J = 7.2 Hz, 3H), 1.26 (s, 9H); ¹³C NMR (75.5 MHz) δ 170.64, 147.82, 134.38, 133.62, 132.95, 130.52, 125.62, 82.56, 53.20, 27.66, 19.92.

o-NBS-N-allyl-Leu-OtBu

R_f 0.6 (3:1 hexanes/ethyl acetate); ¹H NMR (300 MHz, CDCl₃) δ 8.08-8.02 (m, 1H), 7.70-7.64 (m, 2H), 7.61-7.56 (m, 1H), 5.98 (dddd, J = 17.4, 10.0, 7.7, 5.0 Hz, 1H), 5.21 (ddt, J = 17.2, 1.5, 1.5 Hz, 1H), 5.12 (ddt, J = 10.1, 1.1, 1.1 Hz, 1H), 4.60 (dd, J = 8.8, 6.2 Hz, 1H), 4.20 (ddt, J = 16.8, 5.0, 1.1 Hz, 1H), 3.84 (ddt, J = 16.7, 7.8, 1.0 Hz, 1H), 1.81-1.72 (m, 1H), 1.70-1.64 (m, 2H), 1.29 (s, 9H), 0.98 (d, J = 6.3 Hz, 3H), 0.91 (d, J = 6.4 Hz, 3H); ¹³C NMR (75.5 MHz) δ 170.27, 148.20, 135.89, 133.45, 133.30, 131.44, 131.25, 123.90, 117.42, 81.93, 59.58, 49.06, 39.21, 27.76, 24.26, 22.57, 21.19.

o-NBS-N-allyl-Ala-OtBu

R_f 0.55 (3:2 hexanes/EtOAc); ¹H NMR (300 MHz, CDCl₃) δ 8.10-8.04 (m, 1H), 7.71-7.59 (m, 3H), 5.86 (tq, J = 6.3, 10.2 Hz, 1H), 5.20 (dd, J = 17.4, 1.5 Hz, 1H), 5.08 (dd, J = 10.2, 1.5 Hz, 1H), 4.70 (q, J = 7.2 Hz, 1H), 4.16 (dd, J = 16.8, 6.0 Hz, 1H), 3.84 (dd, J = 16.8, 6.3 Hz, 1H), 1.48 (d, J = 7.5 Hz, 3H), 1.36 (s, 9H); ¹³C NMR (75.5 MHz, CDCl₃) δ 170.28, 148.04, 135.13, 134.01, 133.37, 131.61, 131.29, 124.07, 117.87, 82.08, 56.65, 48.53, 27.81, 16.87.

N-allyl-Leu-OtBu

R_f 0.5 (3:1 hexanes/EtOAc); ¹H NMR (300 MHz, CDCl₃) δ 5.87 (ddt, J = 17.1, 10.2, 6.1 Hz, 1H), 5.17 (dq, J = 17.1, 1.6 Hz, 1H), 5.08 (dq, J = 10.2, 1.4 Hz, 1H), 3.26 (ddt, J = 13.7, 5.9, 1.4 Hz, 1H), 3.14 (t, J = 7.3 Hz, 1H), 3.10 (ddt, J = 13.7, 6.2, 1.2 Hz, 1H), 1.74 (septet, J = 7.0, 1H), 1.60-1.50 (bm, 1H), 1.47 (s, 9H), 1.42 (dt, J = 3.6, 7.0 Hz, 2H), 0.93 (d, J = 6.6 Hz, 3H), 0.90 (d, J = 6.6 Hz, 3H); ¹³C NMR (75.5 MHz) δ 175.45, 136.60, 116.21, 80.82, 59.82, 50.70, 43.04, 28.15, 24.98, 22.64, 22.54.

Fmoc-Gln(Trt)-N-allyl-Leu-OtBu

R_f 0.4 (2:1 hexanes/EtOAc); ¹H NMR (300 MHz, CDCl₃) δ 7.75 (d, J = 7.5 Hz, 2H), 7.56 (t, J = 6.5 Hz, 2H), 7.33-7.27 (m, 4H), 7.25-7.19 (m, 15H), 6.84 (s, 1H), 5.80-5.70 (m, 2H), 5.18-5.12 (m, 2H), 4.68 (dd, J = 8.4, 5.4 Hz, 1H), 4.54 (bt, J = 8.8 Hz, 1H), 4.39 (appar. quintet, J = 9.7 Hz, 2H), 4.20 (t, J = 6.9 Hz, 1H), 3.59 (dd, J = 17.3, 5.5 Hz, 1H), 2.40-2.30 (m, 2H), 2.25-2.10 (m, 1H), 1.85-1.64 (m, 2H), 1.63-1.58 (m, 2H), 1.53 (bs, 1H), 1.40 (s, 9H), 1.36 (s, 1H), 0.92 (d, J = 6.3 Hz, 3H), 0.88 (d, J = 6.3 Hz, 3H); ¹³C NMR (75.5 MHz, CDCl₃) δ 172.36, 170.34, 156.23, 144.77, 143.98, 143.74, 141.39, 141.29, 133.80, 128.76, 127.92, 127.70, 127.05, 126.99, 126.92, 125.13, 120.02, 119.98, 118.04, 81.61, 77.22, 70.58, 66.76, 57.24, 51.05, 49.04, 47.28, 37.61, 27.99, 24.96, 22.83, 22.00.

Fmoc-Ala-N-allyl-Ala-OtBu

R_f 0.9 (2:1 hexanes/EtOAc); ¹H NMR (300 MHz, CDCl₃) δ 7.75 (d, J = 7.5 Hz, 2H), 7.59 (d, J = 7.2 Hz, 2H), 7.39 (t, J = 7.2 Hz, 2H), 7.30 (t, J = 7.5 Hz, 2H), 5.92-5.86 (m, 1H), 5.73 (d, J = 8.1 Hz, 1H), 5.29 (d, J = 10.5 Hz, 1H), 5.24-5.10 (m, 1H), 4.77 (q, J = 6.6 Hz, 1H), 4.62 (quintet, J = 7.2 Hz, 1H), 7.34 (d, J = 6.9 Hz, 2H), 4.21 (t, J = 6.9 Hz, 1H), 4.01 (bs, 1H), 3.90-3.66 (m, 1H), 1.44 (s, 9H), 1.41 (d, J = 6 Hz, 3H), 1.38 (d, J = 6.6 Hz, 3H); ¹³C NMR (75.5 MHz) δ 173.14, 170.58, 155.45, 143.96, 143.88, 141.30, 133.87, 127.68, 127.05, 125.18, 119.96, 117.62, 81.57, 66.91, 55.57, 54.35, 48.33, 47.41, 47.17, 27.99, 27.84, 21.05, 19.40, 14.62.

Fmoc-Gln-N-allyl-Leu-OH

R_f 0.4 (9:1 EtOAc/MeOH); ¹H NMR (300 MHz, CDCl₃) δ 7.76 (d, J = 7.6 Hz, 2H), 7.60 (dd, J = 7.0, 4.7 Hz, 2H), 7.40 (t, J = 7.4 Hz, 2H), 7.31 (ddt, J = 1.1, 2.9, 7.4 Hz, 2H), 6.57 (bs, 1H), 6.50 (bs, 1H), 6.03 (d, J = 8.4 Hz, 1H), 5.85 (ddt, J = 17.2, 10.6, 5.4 Hz,

1H), 5.26 (d, J = 17.2 Hz, 1H), 5.23 (d, J = 10.0 Hz, 1H), 5.08 (dd, J = 9.1, 4.5 Hz, 1H), 4.68 (bt, J = 7.7 Hz, 1H), 4.39 (dq, J = 6.6, 10.7 Hz, 2H), 4.20 (t, J = 6.8 Hz, 1H), 3.76 (dd, J = 17.7, 3.6 Hz, 1H), 2.33-2.23 (m, 2H), 2.20-2.13 (m, 2H), 1.90-1.78 (m, 2H), 1.68-1.55 (m, 2H), 0.95 (d, J = 6.2 Hz, 3H), 0.90 (d, J = 6.3 Hz, 3H); ¹³C NMR (75.5 MHz) δ 178.40, 175.37, 173.32, 156.92, 143.64, 143.41, 141.39, 141.31, 132.98, 127.86, 127.13, 127.06, 125.08, 120.09, 118.64, 77.24, 67.40, 56.79, 50.75, 49.13, 47.08, 37.22, 31.05, 29.32, 24.95, 22.67, 21.72.

Fmoc-Ala-N-allyl-Ala-OH

R_f 0.3 (2:1 hexanes/EtOAc, 1% AcOH); ¹H NMR (300 MHz, CDCl₃) δ 8.60 (bs, 1H), 7.75 (d, J = 7.5 Hz, 2H), 7.60 (dd, J = 6.9, 4.2 Hz, 2H), 7.38 (t, J = 7.2 Hz, 2H), 7.29 (t, J = 7.2 Hz, 2H), 6.03 (d, J = 8.4 Hz, 1H), 5.94-5.83 (m, 1H), 5.32-5.09 (m, 2H), 4.70 (q, J = 7.2 Hz, 1H), 4.70-4.54 (m, 1H), 4.33 (d, J = 7.2 Hz, 1H), 4.20 (dt, J = 6.9, 7.2, 2H), 4.0 (apparent q, J = 17.1 Hz, 2H), 1.45 (d, J = 7.2 Hz, 3H), 1.36 (d, J = 6.6 Hz, 3H); ¹³C NMR (75.5 MHz) δ 175.51, 173.96, 155.70, 143.94, 143.83, 141.28, 133.33, 133.12, 127.69, 127.06, 125.23, 119.95, 118.18, 67.04, 54.09, 48.99, 47.41, 47.12, 19.00, 14.39.

Fmoc-L-Nle(ε-N₃)-OH

¹H NMR (300 MHz; CDCl₃) δ 7.77 (d, J = 7.5 Hz, 2H), 7.59 (d, J = 6.9 Hz, 2H), 7.41 (t, J = 7.2 Hz, 2H), 7.32 (t, J = 7.2 Hz, 2H), 5.27 (d, J = 8.4 Hz, 1H), 4.43 (d, J = 6.9 Hz, 2H), 4.23 (t, J = 6.6 Hz, 2H), 3.29 (t, J = 6.3 Hz, 2H), 1.94 (ddt, J = 12.9, 7.0, 7.0 Hz, 1H), 1.74 (ddt, J = 14.1, 7.5, 7.5 Hz, 1H), 1.68-1.59 (m, 2H), 1.52-1.47 (m, 2H); ¹³C (75.5 MHz) d 176.98, 156.16, 143.75, 143.59, 141.29, 127.75, 127.06, 125.02, 120.01, 67.13, 53.51, 50.99, 47.08, 31.78, 28.30, 22.41

Fmoc-L-Nva(δN3)-OH

¹H NMR (300 MHz, CDCl₃) δ 7.76 (d, J = 7.5 Hz, 2H), 7.59 (d, J = 7.3 Hz, 2H), 7.40 (t, J = 7.5 Hz, 2H), 7.31 (t, J = 7.4 Hz, 2H), 6.91 (bs, 1H), 5.35 (d, J = 8.1 Hz, 1H), 4.59 (two m, ratio 1:4, 3H), 4.21 (t, J = 6.6 Hz, 1H), 3.33 (two t, ratio 3:1, J = 6.3 Hz, 2H), 2.08 – 1.90 (m, 1H), 1.86 – 1.31 (m, 3H); ¹³C NMR (75 MHz, CDCl₃) δ 176.41, 156.08, 143.75, 143.57, 141.34, 127.78, 127.10, 125.02, 120.05, 67.13, 53.22, 50.75, 47.13, 29.61, 24.82.

Fmoc-L-Propargylalanine-OH (Fmoc-Paa)

$[\alpha]_D^{20} = -14.64^\circ$ (c = 3.35, MeOH); $^1\text{H NMR}$ (300 MHz, CDCl_3) δ 7.76 (d, J = 7.5 Hz, 2H), 7.59 (d, J = 6.9 Hz, 2H), 7.40 (t, J = 7.5 Hz, 2H), 7.31 (t, J = 7.2 Hz, 2H), 5.40 (d, J = 8.1 Hz, 1H), 4.52-4.39 (m, 3H), 4.23 (t, J = 6.6 Hz, 1H), 2.31-2.28 (m, 2H), 2.20-2.17 (m, 1H), 2.01-1.92 (m, 2H); $^{13}\text{C NMR}$ (75.5 MHz, CDCl_3) δ 176.08, 156.11, 143.77, 143.60, 141.34, 127.78, 127.11, 125.05, 120.04, 82.41, 69.87, 67.16, 53.07, 47.14, 30.78, 14.97. ESI-MS $[\text{M}+\text{Na}]^+$ calcd. for $\text{C}_{21}\text{H}_{19}\text{NNaO}_4$ 372.12, found 372.13.

Appendix 6. Evaluation of the Smac binding site of Survivin for the design of potential inhibitors of Survivin.

The work described in this appendix relates to my original dissertation project involving the study of Survivin and our work towards identifying ligands of the Smac binding site of Survivin for the purpose of antagonizing Survivin's inhibition of apoptosis.

Introduction

Apoptosis

Apoptosis (programmed cell death) is a tightly regulated cellular process that is essential for proper organogenesis. In addition, induction of apoptosis is believed to be the primary mechanism of action of most chemotherapeutic agents and radiation therapy. Apoptosis is mediated by the family of cysteine proteases known as caspases. While normally present as inactive zymogens in the cell, caspases can be cleaved and activated in response to various apoptotic stimuli such as chemotherapeutic agents and radiation therapy. The initiation of the caspase cascade ultimately leads to the destruction of cellular machinery and the phenotypic hallmarks of apoptosis, namely cell shrinkage, DNA fragmentation and membrane blebbing²¹⁰.

Caspases are divided into two classes: the initiator caspases-8, -9 and -10 and the effector caspases-3, -6 and -7. Typically, the initiator caspases are cleaved first and subsequently cleave the effector caspases. Activated effector caspases then proceed to break down cellular proteins leading to cell death²¹¹.

There are two major pathways that lead to the activation of caspases (reviewed by Debatin 2004 and Nachmias *et al.* 2004)^{211,212}. The extrinsic (death receptor) pathway operates in response to stimulation of the tumor necrosis factor (TNF) family of membrane-bound death receptors²¹¹. Various ligands such as Fas and TRAIL can stimulate the receptors. This in turn causes the formation of the death-inducing signaling complex (DISC) and the dimerization and activation of caspase-8^{212,213}. Caspase-8 then continues on to activate downstream effector caspases.

The second major pathway is the intrinsic (mitochondrial) pathway. In response to apoptotic stimuli, cellular proteins such as the Bcl-2 pro-apoptotic proteins Bax, Bid and Bim are cleaved and translocate to the mitochondrial outer membrane where they oligomerize and form pore-like structures²¹². The resulting permeabilization of the outer mitochondrial membrane releases cytochrome c, along with other pro-apoptotic proteins such as the second mitochondria-derived activator of caspases/direct IAP binding protein with low pI (Smac/DIABLO), HtrA2/Omi, apoptosis-inducing factor (AIF), and endonuclease G. The release of cytochrome c triggers the formation of an oligomeric complex known as the apoptosome which includes cytochrome c, Apaf-1, dATP and pro-caspase-9²¹². The apoptosome leads to the cleavage and activation of caspase-9 which then activates effector caspases.

Intervention with apoptosis leads to continued cell growth and proliferation. Cells that should have been eliminated as a result of normal developmental processes or due to cellular damage such as DNA damage or viral infection are therefore allowed to continue growing and dividing. The family of proteins known as the inhibitors of apoptosis proteins (IAPs) has been shown to play major roles in inhibiting caspase activity and mediating the cell cycle.

IAPs are defined by having one or more *N*-terminal baculovirus IAP-repeat (BIR) domains. Each BIR domain is approximately 70 amino acids long and consists of a characteristic zinc fold with a zinc atom tetrahedrally coordinated by one histidine and three cysteine residues^{211,214-216}. In addition to the BIR domains, some IAPs have a C-terminal RING finger and also a caspase recruitment domain (CARD). To date, eight human IAPs have been identified and are subdivided into classes based on the homology of their BIR domains and the presence or absence of a RING finger and CARD. Homologous IAPs have also been identified in several other species including insects, yeast and mice^{211,213,217}.

Although IAPs have been shown to have several functions, much attention has been paid to their inhibitory effects on caspases. Many of the caspases, including X chromosome-linked IAP (XIAP), cIAP-1, cIAP-2, Livin and Survivin, have been shown to bind to and inhibit caspases-3, -7, and -9^{211,213}. To help regulate IAPs, cells express endogenous inhibitors, namely Smac/DIABLO, HtrA2/Omi and XAF-1 (XIAP associated

factor-1)²¹¹. However, overexpression of IAPs can overwhelm the endogenous IAP inhibitors and lead to inhibition of apoptosis.

Due to their important roles in mediating apoptosis, deregulation of IAPs can have catastrophic consequences. Indeed, overexpression of IAPs, such as XIAP and Survivin, has been demonstrated in numerous human cancers^{211,218}. The rampant expression of IAPs leads to cell preservation even in the presence of transforming mutations and cytotoxic agents (i.e. chemotherapeutics). In the case of transforming mutations in cancers, inhibition of apoptosis by IAPs can result in the accumulation of additional mutations, malignant phenotypes and possibly secondary metastases²¹¹. Thus, targeting IAPs can have a dual benefit of sensitizing primary tumors to current anti-cancer treatments while helping prevent the formation of secondary metastases.

Survivin

Survivin (SVV), a 16.5 kDa (142 amino acids) protein, is the smallest member of the IAP family, consisting of only a single BIR domain and no RING finger or CARD (Figure 1)²¹⁹. Instead, SVV has a unique C-terminal α -helix about 65 Å in length that protrudes out into solution^{220,221}. The BIR domain of SVV bears structural homology to the second BIR domain of XIAP; however, its Smac-binding site is more closely related to the third BIR domain of XIAP^{221,222}. In solution, SVV forms a homodimer through its BIR domain and has been shown to interact with numerous proteins including heat shock protein 90 (Hsp90), Hepatitis B x-interacting protein (HBXIP), polymerized tubulin, caspases and Smac/DIABLO (Figure 1 and 2)^{217,220-228}. SVV has also been shown to associate with Aurora B kinase at mitotic structures²²⁹. Hsp90 was shown to be important for preventing the proteasomal degradation of SVV, while HBXIP was demonstrated to be a necessary cofactor protein for binding to pro-caspase-9. In addition, SVV activity is regulated by phosphorylation of threonine 34 and 117 by the p34^{cdc2}-cyclin-B1 complex and Aurora B kinase, respectively^{226,230}.

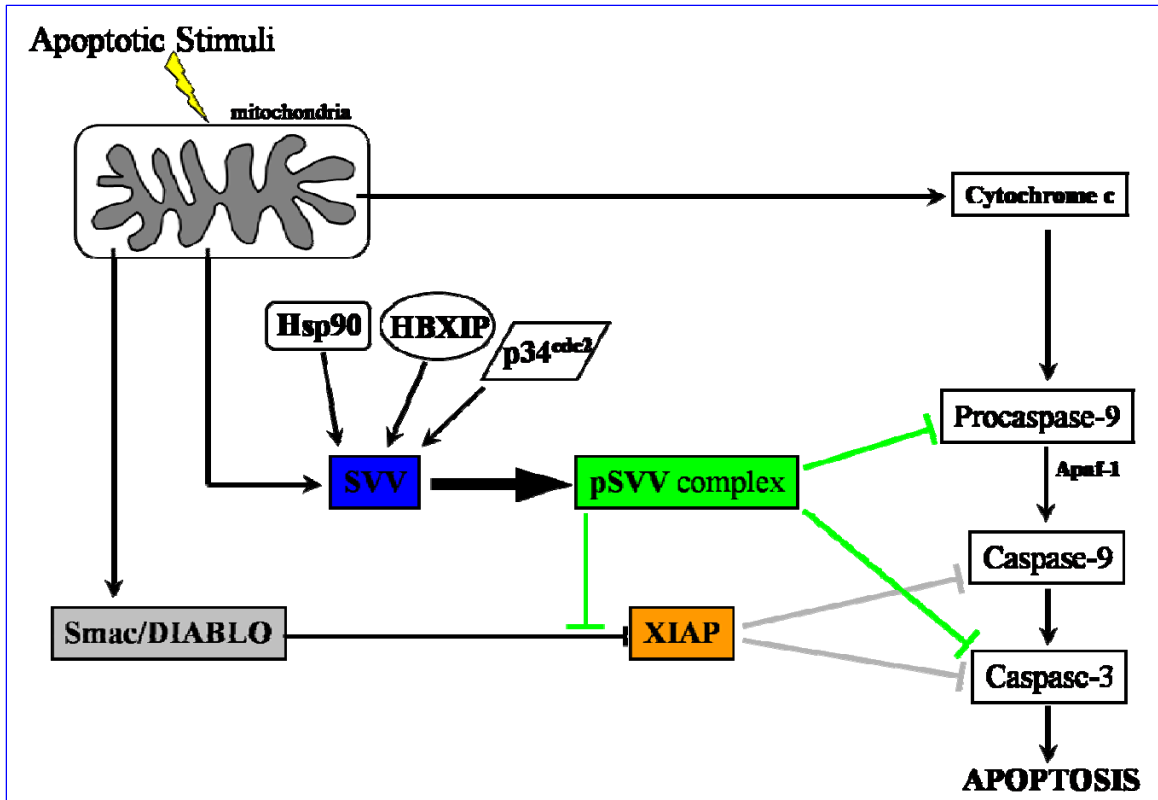


Figure 1. Diagram of SVV's reported roles in inhibiting apoptosis.

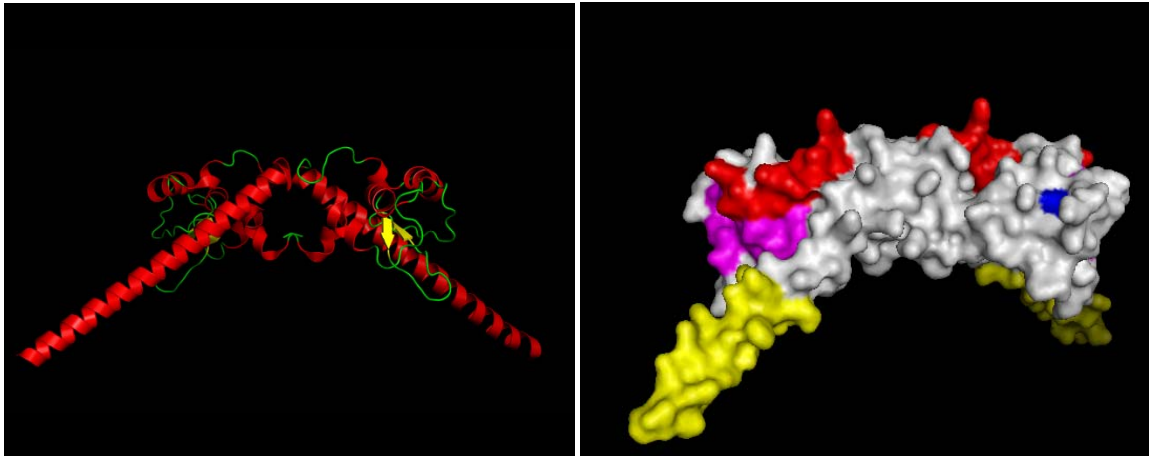


Figure 2. Crystal structure of human SVV homodimer (PDB code: 1E31). Left: SVV is represented as a cartoon and colored by secondary structure (red, α -helix; yellow, β -sheet; green, loop) as determined by PyMol. Right: SVV is shown as a surface map with known binding and phosphorylation sites indicated by color (red, Hsp90; yellow, tubulin; magenta, Smac; blue, phospho-threonine 34).

The expression of SVV is highly regulated in normal tissues. Typically, SVV is found only in spermatogonia, fetal and hematopoietic tissues, and is virtually undetectable in adult differentiated tissues^{219,231-234}. In normal proliferating cells, SVV is nearly undetectable in the G1-phase, but becomes upregulated 6- and 40-fold in S-phase and

G2/M-phase, respectively²²⁴. Immediately following cytokinesis, SVV is rapidly degraded by the ubiquitin-proteasome pathway ($t_{1/2} \sim 30$ minutes)²³⁵.

In contrast to normal tissues where SVV expression is strictly regulated, cancer cells often show constitutive expression of SVV²³⁶. Furthermore, SVV upregulation is believed to be an early event in malignant transformation and has been shown to impart resistance to chemotherapy and radiation treatment^{233,237,238}. The subcellular localization and functions of SVV also appear to differ between normal and cancerous cells. In dividing cells, SVV is found in the nucleus and cytoplasm^{237,239}. During cell division, SVV has been shown to associate with microtubules and bind mature caspase-9, possibly inhibiting a default apoptosis mechanism associated with the cell cycle^{221,224,226,229,238,240}. In cancerous tissues, however, SVV localizes to the intermitochondrial membrane space where it appears to play a role in inhibiting the mitochondrial apoptosis pathway during apoptotic stimuli²³⁷. Recently, SVV was demonstrated to bind the pro-apoptotic protein Smac/Diablo in the mitochondria and delay its release during apoptotic stimuli²⁴¹. Additional reports have also shown that SVV has the potential to inhibit mature caspase-3 and -7 and pro-caspase-9, although these reports do not distinguish between cytosolic, nuclear and mitochondrial SVV (Figure 1)^{225,227,233}. SVV has also been shown to act in a synergistic manner with XIAP to enhance XIAP stability and caspase inhibitory potential²⁴². For a more thorough summary of SVV's postulated cellular roles, readers are referred to the recent review by D.C. Altieri²⁴³. Thus, SVV's selective overexpression in cancer and its contribution to chemotherapy and radiation therapy resistance makes it an attractive target for the design of novel anti-cancer agents.

Based on the structural similarities of SVV's BIR domain to that of XIAP BIR3, we sought to identify peptide ligands of the SVV-Smac binding site to determine if such ligands could antagonize SVV's inhibition of caspase activity. In the process, we developed a homogeneous fluorescence polarization assay as well as a caspase functional assay to evaluate our compounds. We adapted our caspase functional assay for 96-well plate format and screened the National Cancer Institute's Structural Diversity (1990 compounds), Mechanistic (879 compounds) and Challenge (89 compounds) sets of compounds but were unsuccessful at identifying a potential inhibitor of SVV. Furthermore, the peptide ligands identified in our FP assay which are believed to bind to the putative Smac binding site of SVV failed to rescue caspase activity in our caspase functional assay.

In addition, we generated a mutant form of SVV containing the D71R substitution, which has been reported to be incapable of binding Smac/DIABLO²²⁸. We demonstrated that recombinant SVV D71R is incapable of binding to our Smac-derived peptide tracers used in our FP assay. Despite this lack of binding to Smac-like peptides, we found that whole cell extracts from HEK 293 cells stably transfected SVV D71R are capable of inhibiting caspase activity to the same degree as extracts transfected with wild type SVV. Thus, we postulate that SVV's inhibition of caspase activity is not due to direct binding of caspases through its putative Smac-binding site.

Results

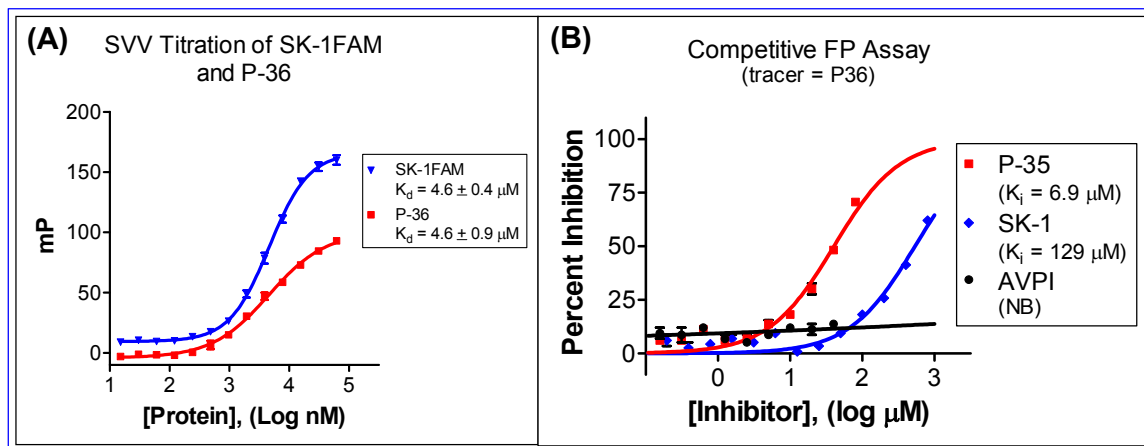
Development of a fluorescence polarization competitive binding assay for SVV

In the search for ligands of the Smac binding site, we thought that a high throughput binding assay such as a FP assay would be useful for screening libraries of compounds. Our lab has developed such an assay for XIAP using Smac-based peptides. Since both Smac and its *Drosophila* homolog Hid have been shown to bind to SVV at the same site, we decided to test our fluorescently-labeled Smac peptides²²² in addition to a Hid-based peptide (AVPFY; referred to as SK-1fam). Both PSmac-36 and SK-1fam bound to SVV with $K_d \sim 5 \mu\text{M}$ (Table 1; Figure 3A). We then developed competitive FP binding assays using 10 nM of either tracer and 15 μM SVV protein. When SK-1FAM was used as the tracer we found that the unlabeled SK-1 did not demonstrate dose-dependent inhibition (data not shown). In contrast, when we used P-36 as the tracer, the unlabeled P-35 peptide showed dose-dependent inhibition with a calculated K_i value of 6.9 μM (Figure 3B). This value was in good agreement with the K_d value of 4.6 μM determined for P-36, and indicated that the fluorescent tag was not altering the binding mode of the tracer. We chose to use P-36 as the tracer for our subsequent competitive FP assays. Interestingly, neither a nine amino acid peptide based on the N-terminus of mature Smac (a.k.a. Smac-9mer) nor the shorter AVPI tetrapeptide showed binding to SVV. In addition, SK-1 had a calculated K_i value of 129 μM (Figure 3B), which is in stark contrast to the reported K_d of 7 μM ²²² based on NMR studies or the K_d of the labeled peptide SK-1FAM. This could be due to a different binding mode for P-35 and SK-1. It may also be the result of a disfavorable binding interaction with the free C-terminus of the unlabeled peptide compared to the labeled peptide which has an additional β -Ala-Lys(5-FAM) and an amide capped C-terminus.

Table 1. Peptide sequences.

Name	Sequence*
P-35	Abu-RPFK-NH ₂
P-36	Abu-RPFK(5-FAM)-NH ₂
SK-1	AVPFY-OH
SK-1FAM	AVPFY-βA-K(5-FAM)-NH ₂
Smac-9mer	AVPIAQKSE-OH
AVPI	AVPI-OH

*All peptides have free N-termini.

**Figure 3.** FP binding results for labeled and unlabeled peptides.

Nevertheless, P-36 was chosen to be the tracer for subsequent FP assays. We then screened a small library of peptides derived from Smac peptide and the Hid peptide AVPFY (Appendix 8) that was reported to bind to the Smac binding site²²². All of the peptides were screened at 200 μM . P-35 (80 μM) was used as a positive control. As shown in Figure 4, P-35 showed approximately 70% inhibition of binding while the next most potent peptide from the set gave less than 60% inhibition at even at 200 μM . Again, this could be due to the fact that the natural peptides (SK1-SK-12) each have an exposed C-terminus that might be affecting their binding. However, peptides with amino-functionalized C-termini (SK-15 - SK-33) intended to exploit the binding pocket in SVV that is utilized by the tyrosine of AVPFY also showed very weak inhibition.

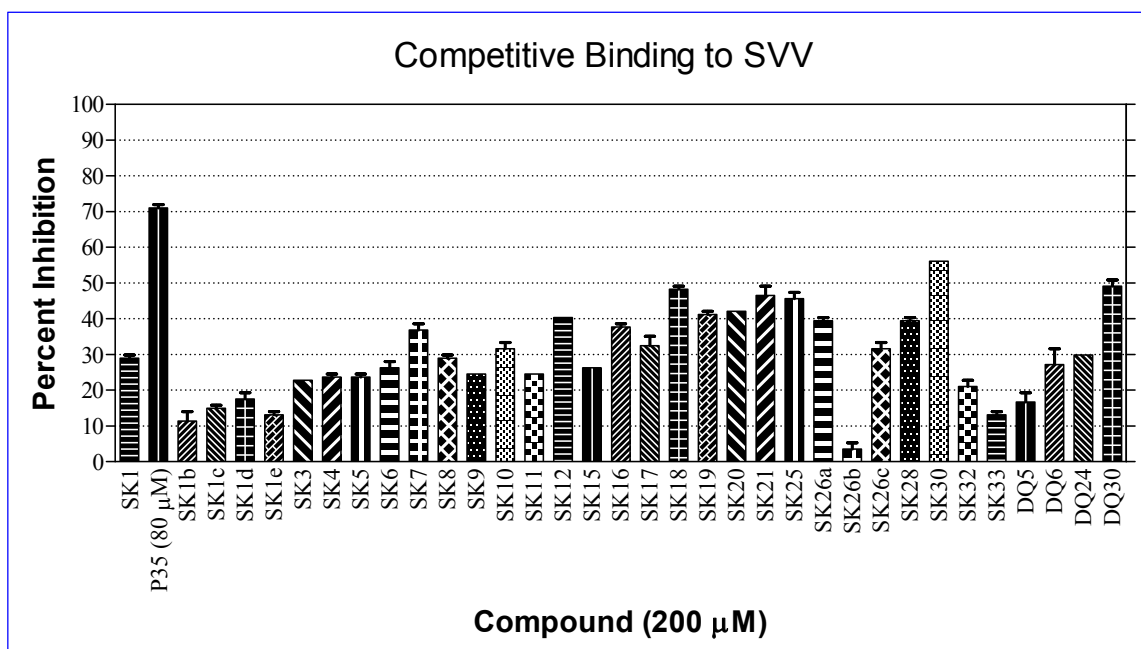


Figure 4 Screening of Smac and Hid-derived peptides. The FP assay was conducted with 10 nM P-36 and 15 μM recombinant SVV. Compounds were screened in duplicate.

Development of a caspase functional assay with whole cell extracts

Due to the lack of inhibitor potency of our Smac and Hid-derived peptides, we questioned whether our P-36 tracer was truly binding at the putative Smac binding site in SVV. Thus, we also developed a caspase functional assay as a second test of our compounds. Such an assay would assess a compound's ability to inhibit SVV's function instead of only measuring its binding affinity. The drawback is that the assay is more complicated and less amenable to high throughput screening.

Our initial attempts to establish a caspase functional assay using recombinant SVV protein or protein expressed and purified from HEK 293 cells were unsuccessful. Instead we switched to using whole cell extracts from HEK 293 transfected with SVV. Experiments using transiently transfected cell extracts gave variable results; however, reproducible results were finally obtained using cell extracts from stably transfected cells. Cell extracts collected from these cells transfected with SVV and treated with exogenous dATP and cytochrome c (to activate caspases) showed a drastic reduction in caspase-3 activity compared to extracts from cells stably transfected with the pcDNA3.1 vector control (Figure 5A).

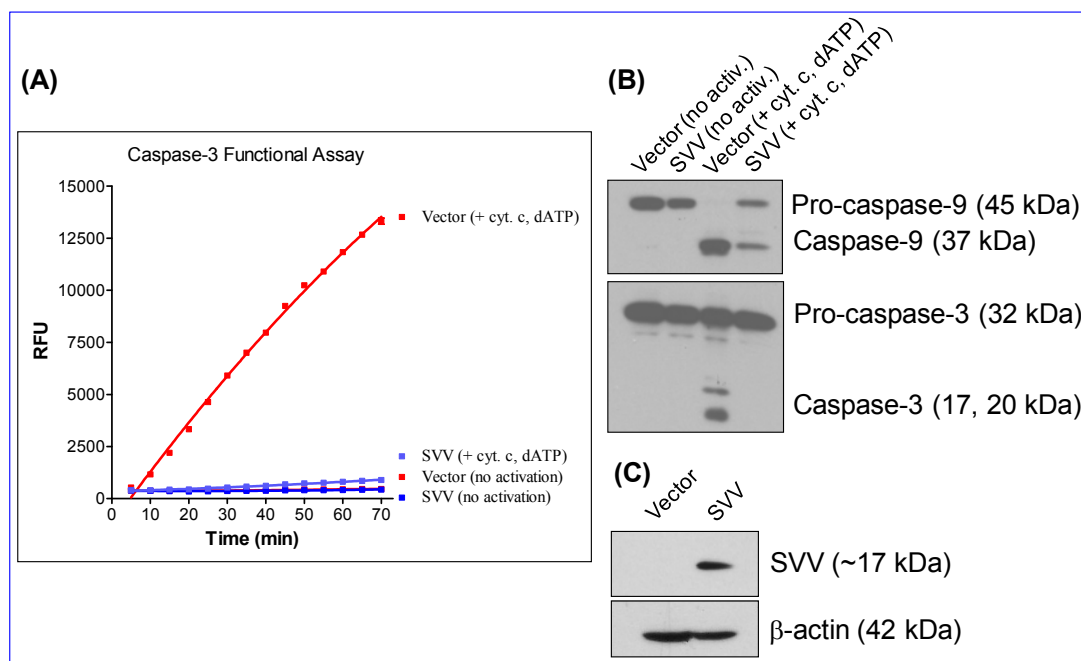


Figure 5. Inhibition of caspase activity by SVV in cell extracts. A) Caspase-3 functional assay. Whole cell extracts (35 μ g) from HEK 293 cells stably transfected with SVV or vector control were treated with dATP (1.25 mM) and cytochrome c (0.12 mg/mL) to activate caspase function. Negative controls for no caspase activation were prepared by adding buffer instead of dATP and cytochrome c. Reactions were activated for 60 minutes at 30°C and then activated extract was diluted in assay buffer and mixed with DEVD-AFC substrate. Cleavage of the AFC fluorophore was monitored by measuring AFC fluorescence using excitation and emission wavelengths of 400 and 505 nm, respectively. B) Western blot of cell extracts (35 μ g). All reactions were incubated at 30°C for 60 minutes. C) Western blot of cell extracts (35 μ g) stably transfected with vector control or SVV.

In addition, western blot analysis of activated cell extracts showed a significant reduction in activated caspase-9 and a complete inhibition of caspase-3 activation (Figure 5B). These results were reproducible and consistent. In order to screen compound libraries, I adapted this assay for use in a 96 well plate which allowed the screening of up to 300 compounds per day.

Screening of compound libraries using the caspase functional assay

Since PSmac-35 was the most potent inhibitor identified from the FP assay, I tested this compound along with SK-1 in the caspase functional assay. Neither compound was able to restore caspase activity in the cell extracts containing SVV (Figure 6) even at 200-500 μ M concentrations. In addition, 2 μ M of SH-164, a potent inhibitor of XIAP (K_d ~ 50 nM), was unable to rescue caspase activity. The only increase in activity was seen

in the vector control in which P35 and SH-164 are likely inhibiting background levels of XIAP and giving rise to additional caspase activity.

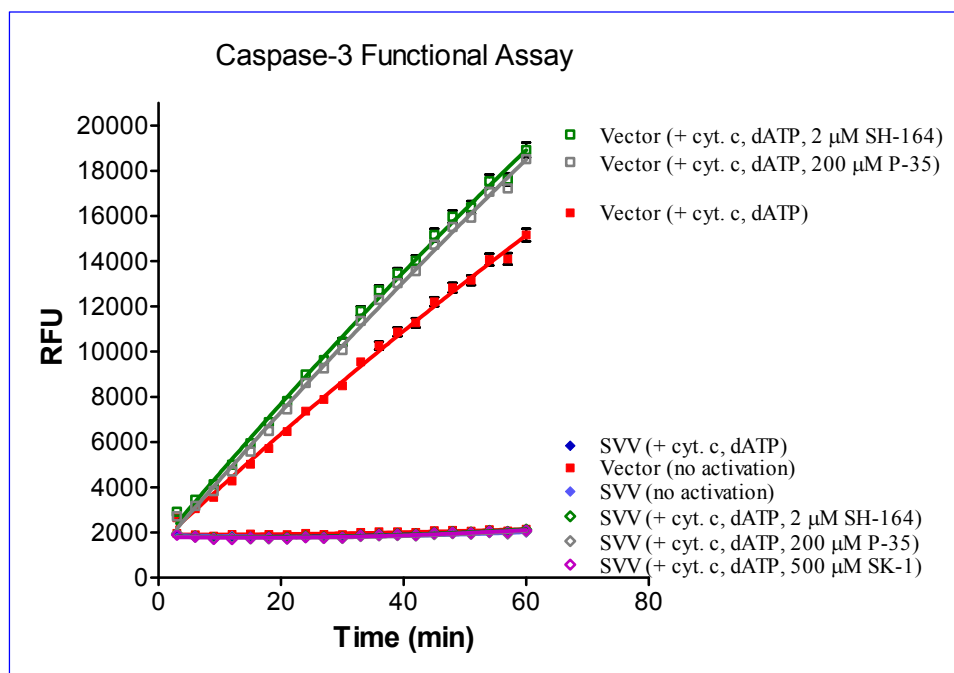


Figure 6. Caspase-3 functional assay. Whole cell extracts (35 μ g) from HEK 293 cells stably transfected with SVV or vector control were treated with P-35, SK-1, SH-164 or DMSO and then treated with dATP and cytochrome c to activate caspase function. Negative controls for no caspase activation were prepared by adding buffer instead of dATP and cytochrome c. Reactions were activated for 60 minutes at 30°C and then activated extract was diluted in assay buffer and mixed with DEVD-AFC substrate. Cleavage of the AFC fluorophore was monitored by measuring AFC fluorescence using excitation and emission wavelengths of 400 and 505 nm, respectively.

The fact that these compounds, which we believed bound SVV at the Smac binding site, were unable to inhibit SVV led us to suspect that the Smac binding site was not relevant for SVV's inhibition of caspase activity. We next turned our attention to screening small libraries of compounds from the National Cancer Institute. In all, I screened the Structural Diversity (1990 compounds), Mechanistic (879 compounds) and Challenge (89 compounds) sets of compounds. All of the compounds were screened at 100 μ M. However, we were unable to identify any compounds that showed significant rescue of caspase activity. This could be because the level of SVV in the cell extracts is too high, and the compounds are not able to inhibit all of the SVV. It may also be due to the fact that our screening set was fairly small. However, a common hit rate for high throughput screening experiments is ~ 1%, in which case we would have expected 1-3 compounds to show some noticeable activity. Furthermore, by using the functional assay instead of

the FP competitive binding assay to do the screening, we should have been able to identify compounds that inhibit SVV both directly (prevent binding to caspases) and indirectly (disrupt binding of critical cofactor proteins).

Functional analysis of the SVV D71R mutant

Since the compounds that are believed to bind the Smac binding site of SVV were unable to inhibit SVV in the caspase functional assay, we asked the question of whether this binding site is critical for SVV function. To address this question, we performed site-directed mutagenesis to make the SVV D71R mutant. Asp 71 (Glu 314 in XIAP) is located at the end of the Smac binding pocket and is believed to make electrostatic interactions with the N-terminus of mature Smac protein and, by extension, the N-terminus of our peptides. This mutant protein has been reported to abolish binding to Smac protein²²⁸. Vector constructs of the mutant protein were made for expression in *E. coli* and for transfection.

The mutant SVV D71R protein was expressed and purified from *E. coli* under the same conditions as SVV and tested for binding to the PSmac-36 and SK-1FAM tracers. As shown in Figure 7, SVV D71R is unable to bind either tracer.

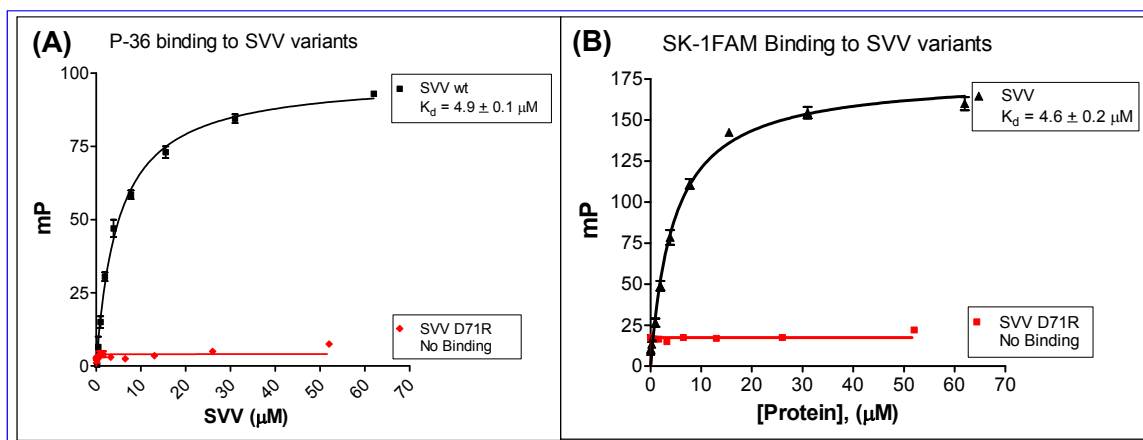


Figure 7. SVV D71R does not bind PSmac-36 or SK-1fam.

To verify that the SVV D71R protein was properly folded and able to dimerize the same as wild type SVV, I performed gel filtration and protein crosslinking experiments (Figure 8). Both the wild type and mutant proteins eluted as dimers and were crosslinked as dimers with dithiobis(succinimidylpropionate) (i.e. DSP) indicating that the proteins were both folded and behaving in a similar manner.

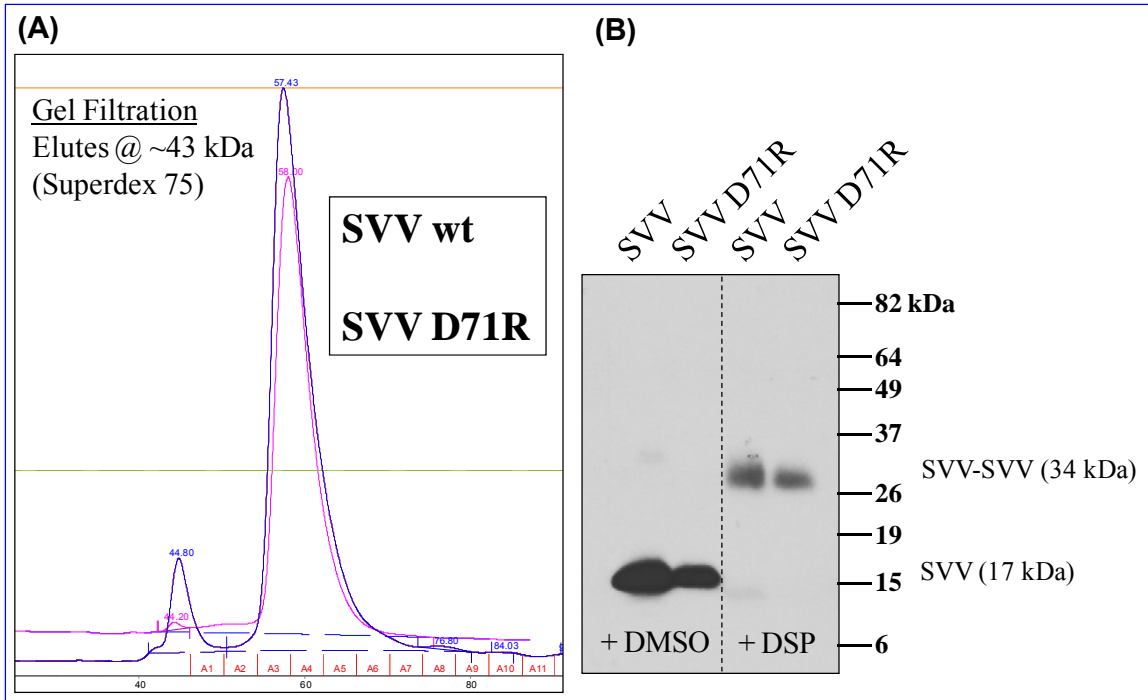


Figure 8. Purified SVV and SVV D71R are folded and dimerize the same. A) Gel filtration experiment. 1 mg of SVV (blue) and SVV D71R (pink) elute with the same retention time. B) DSP crosslinking experiment. Proteins were incubated in PBS buffer at room temperature with DMSO or DSP and then separated by SDS-PAGE and analyzed by western blot with anti-SVV antibody.

I also created a HEK 293 cell line stably transfected with SVV D71R-myc-His₆. Preliminary results from the caspase functional assay indicate that SVV D71R is active and able to inhibit caspase activation to the same extent as wild type SVV (Figure 9).

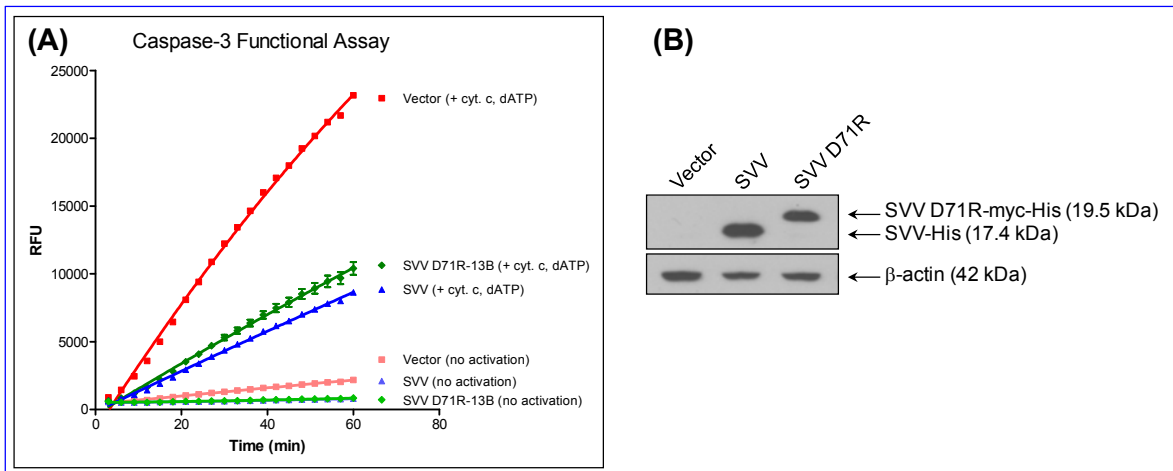


Figure 9. SVV and SVV D71R have equal inhibitory potential. A) Functional assay with cell extracts (35 μ g) from HEK 293 cells stably transfected with vector control, SVV or SVV D71R. B) Western blot for SVV expression in whole extracts.

As is seen in Figure 9, SVV and the mutant protein did not give full suppression of caspase activity in this particular experiment. This is the only batch of cell lysate that has not given nearly complete inhibition. Thus, this was probably due to a poor preparation of cell lysate. As a note, DTT was accidentally omitted from the lysis buffer during the preparation of the cell lysate and could be the cause for the reduced inhibition of SVV. Experiments are in progress to confirm these results.

Discussion

SVV is an attractive target for the design of novel anticancer agents due to its extremely low expression levels in normal tissue. Sequence alignments along with X-ray and NMR structures of SVV have illustrated the similarities between the BIR domain of SVV and the BIR2 and BIR3 domains of XIAP²¹⁹⁻²²². Studies have shown that SVV is able to inhibit caspase activation and that its overexpression in cancer contributes to drug resistance^{233,237,238,242}. Furthermore, SVV has been shown to bind to Hid peptide, the *Drosophila* homolog of vertebrate Smac, which among other roles is believed to be an endogenous inhibitor of IAPs such as XIAP²²². We therefore developed a FP-based SVV binding assay using a Smac-derived peptide and demonstrated that it binds to SVV with low micromolar affinity. We hoped to use this assay as a starting point and to improve the binding affinity of our tracer and the sensitivity of our assay. Thus, we used our FP assay to screen a small collection of peptides based on the Hid AVPFY sequence, but were unsuccessful in identifying peptides with more potent binding affinities.

Instead we worked to develop a caspase-3 functional assay to identify inhibitors of SVV. We first tried adding recombinant SVV to whole cell extracts, but this form of SVV was unable to inhibit the activation of caspases by exogenous dATP and cytochrome c. SVV purified from transfected HEK 293 cells was also incapable of inhibiting caspase activity when added back to cell extracts. Finally, we were able to demonstrate inhibition of caspase activation using cell extracts from HEK 293 cells transfected with SVV. Under these conditions, we were able to reproducibly demonstrate complete inhibition of caspase activation. We used this functional assay to screen approximately 3000 compounds from the NCI Structural Diversity, Mechanistic, and Challenge sets of compounds. However, we were still unsuccessful in identifying an inhibitor. Furthermore, the Smac and Hid based peptides P-35 and SK-1 and also the potent XIAP inhibitor SH-164 were all ineffective at antagonizing SVV inhibition of caspase activity.

These combined results from our FP and functional assays, led us to wonder if the putative Smac binding site in SVV was functionally relevant for SVV's inhibition of caspase activity. We therefore used site-directed mutagenesis to create a SVV D71R mutant that abolishes binding to Smac through the loss of the ion pairing between the N-terminus of Smac and the carboxylic acid of D71²²⁸. We demonstrated that this protein behaves in an identical manner compared to wild type SVV forming a dimer in solution and eluting with the same retention time during gel filtration. As expected, the mutant SVV D71R did not bind to our Smac and Hid-derived tracers used in our FP assay. However, when we performed our caspase functional assay with cell extracts from cells transfected with SVV D71R, we found that the protein was still capable of inhibiting caspase activation to a degree similar to wild type SVV handled under the same conditions. Thus, we hypothesize that the putative Smac binding site of SVV is not relevant for the ability of SVV to inhibit caspase activation. Support of this hypothesis comes from the fact that SVV is significantly smaller than other IAPs such as XIAP and that numerous binding cofactors have been identified for SVV including HBXIP, HSP90 and XIAP^{223,225,242}. Thus, it is likely that the role of SVV in the inhibition of apoptosis is through the formation of a protein-protein complex and does not necessarily rely on the Smac binding site of SVV.

Conclusions

In summary, Survivin is an attractive target for anti-cancer therapy. While virtually undetectable in most adult non-proliferating cells, Survivin is upregulated and constitutively expressed in many of the most common human cancers. Antisense methods and inhibitors of SVV protein expression have validated SVV as a potential target for anti-cancer therapies. Nevertheless, no direct binding small molecule inhibitors of SVV have been identified to date.

I have established an FP competitive binding assay based on peptide ligands that we believe bind at the putative Smac binding site. In addition I have developed a caspase functional assay using whole cell extracts from cells stably transfected with SVV and the SVV D71R. Our results show that ligands that bind at the Smac binding site are unable to antagonize SVV's inhibition of caspases in our functional assay. Furthermore, SVV D71R which is believed to be incapable of binding Smac directly is still able to inhibit caspase activity to the same degree as the wild type SVV. These data suggest that,

unlike XIAP, the Smac binding site of SVV may not be a relevant binding site and that SVV likely inhibits caspase activation through another mechanism.

Experimental Methods

Plasmids

Full length SVV plasmid was a kind gift from Dr. York Tomita (Georgetown University). Survivin was cloned into pGEX-4T1 vector. SVV D71R was generated by site directed mutagenesis using the following primers:

(forward) 5'-GGCTGGGAGCCAGATCGCGACCCCATAGAGG-3' and

(reverse) 5'-CCTCTATGGGGTCGCGATCTGGCTCCCAGCC-3'.

For transfection experiments, SVV and SVV D71R were cloned into pcDNA3.1-His and pcDNA3.1-myc-His, respectively.

Protein Purification

BL21 DE3 *Escherichia coli* cells were transformed with pGEX-4T1 SVV or SVV D71R constructs. Cells were cultured in LB media with 50 µg/mL ampicillin until the OD₆₀₀ was approximately 0.6 and then protein expression was induced with 50 µM IPTG and 100 µM ZnOAc₂ at 20°C overnight. Cells were resuspended in cold lysis buffer (PBS, 1 mM DTT, 50 µM ZnOAc₂, 1 mM PMSF, Roche Complete protease inhibitor cocktail), treated with lysozyme (0.2 µg) and lysed by sonication. The proteins were purified by affinity chromatography using GST-Sepharose Fast Flow resin (GE Healthcare). The proteins were then cleaved from resin with thrombin (20 units) in cleavage buffer (50 mM Tris-HCl, 1 mM DTT, 50 µM ZnOAc₂, pH 8.0) at 4°C overnight. The supernatant was treated with fresh GST-Sepharose Fast Flow resin for an additional 1 hour. The proteins were then further purified by anion exchange using an Amersham Biosciences P-920 FPLC equipped with a 6 mL Resource Q column equilibrated with Buffer A (50 mM Tris-HCl, pH 8.0, 50 µM ZnOAc₂, 1 mM DTT). Proteins were eluted using a gradient of Buffer B (50 mM Tris-HCl, pH 8.0, 50 µM ZnOAc₂, 1 mM DTT, 1 M NaCl). Proteins eluted at approximately 22-23% Buffer B. Proteins supplemented with 10% glycerol, aliquotted and stored at -80°C.

Peptide Synthesis

Peptides were synthesized by automated solid phase peptide synthesis as described in Chapter 2. Wang resin or 2-chlorotrityl resin was used for all peptides except the

fluorescein-labeled peptides. Peptides with modified C-termini were prepared on 2-chlorotrityl resin and cleaved with 2% TFA/DCM, concentrated in vacuo and precipitated with cold ether. The free carboxy terminus was coupled to the indicated amine under standard peptide coupling conditions with HBTU, HOBT and DIEA. The [8,5] β -turn mimetic used in peptide SK-32 was synthesized previously²⁴⁴. DQ-5 – DQ-24 were synthesized previously by Dr. Dongguang Qin in our lab. All peptides were deprotected with 95% TFA/H₂O for 1 hour and then concentrated, precipitated with cold ether and purified by semi-preparative RP-HPLC as previously described.

FP assays

FP experiments were performed as described in Chapter 2. P-36 was used at a concentration of 10 nM. For competitive experiments, 15 μ M SVV was used.

Transfection Experiments

Human embryonic kidney 293 cells were cultured in Dubelco's Modified Eagle Medium, supplemented with 10 % fetal bovine serum and 50 units penicillin and streptomycin at 37°C in a humidified atmosphere with 5% CO₂. When cells were approximately 90% confluent, pcDNA3.1-SVV constructs were transfected with Lipofectamine 2000 in Opti-MEM media according to the manufacturer's protocol. Stably transfected cells were selected with 400 μ g/mL G-418 and single clones were isolated by limiting dilution and then expanded and maintained in culture media supplemented with 200 μ g/mL G-418.

Caspase-9 functional assay

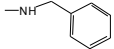
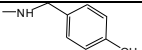
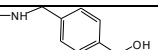
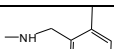
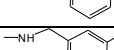
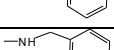
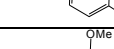
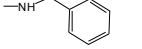
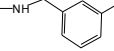
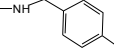
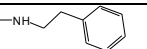

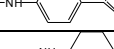
HEK 293 cells stably transfected with SVV, SVV D71R or pcDNA3.1 vector control were harvested and the cells were suspended in lysis buffer (50 mM KCl, 5 mM EGTA, 2 mM MgCl₂, 0.2% CHAPS, 50 mM HEPES, 1 mM DTT, 200 mM PMSF, Roche Complete protease inhibitor cocktail, pH 7.6) at a concentration of approximately 150 x 10⁶ cells/mL and lysed by flash freezing in liquid nitrogen. The cell extract was thawed on ice, centrifuged and the supernatant was collected and the protein concentration was calculated using the Bradford protein assay method²⁴⁵. Cell extracts were normalized using additional lysis buffer. Caspase activation reactions were prepared on ice by diluting 35 μ g total protein in assay buffer (25 mM HEPES, 1 mM EDTA, 10% sucrose, 0.1% CHAPS, pH 7.4), with inhibitor or DMSO (2 μ L), cytochrome c (2.5 μ L, 1.5 mg/mL prepared in assay buffer) and dATP (2.5 μ L, 10 mM prepared in assay buffer) in a final volume of 20 μ L. The reactions were incubated at 30°C for 60 minutes. Caspase-3

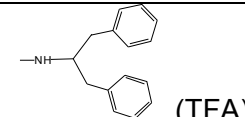
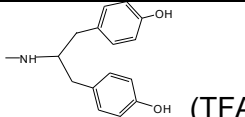
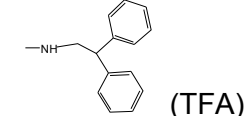
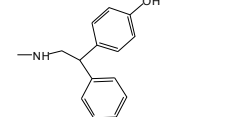
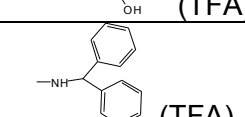
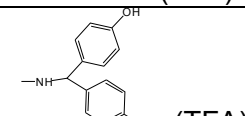
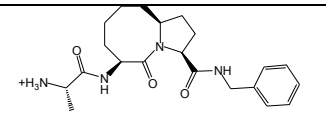
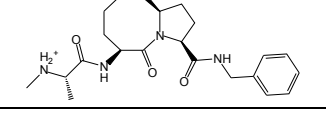
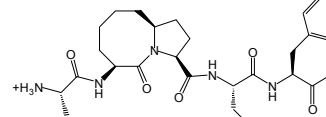
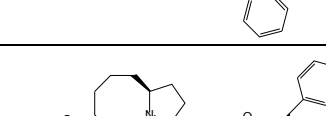
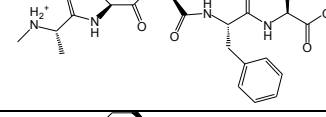
functional assays were then prepared by dispensing activated cell extract (4 μ L) into 96-well, black, round-bottom plates (Fisher Scientific) and diluting with assay buffer (91 μ L) and Ac-DEVD-AFC (5 μ L, 500 μ M in DMSO). Reactions were incubated at 37°C in a Tecan Ultra microplate reader and relative fluorescence units (RFU) were measured at 3 minute intervals by using excitation and emission wavelengths of 400 and 505 nm, respectively. Positive controls (equivalent to 100% inhibition) utilized cell extract prepared with buffer instead of cytochrome-c and dATP.

Immunoblotting

Cell extracts (35 μ g) were mixed with 1 volume of 2X SDS loading dye, heated at 90°C for 5 minutes and then analyzed by SDS PAGE. The proteins were transferred to 0.2 μ m PVDF membranes at 100 V for 2 hours at 4°C and the membranes were blocked with 5% milk, probed with primary antibodies against SVV (Cell Signaling Technology), β -actin (Sigma), caspase-9 (Stressgen), caspase-3 (Stressgen) at 4°C overnight, and then treated with secondary antibodies conjugated to horseradish peroxidase and visualized by chemiluminescent detection.

Appendix 7. Peptide library for SVV.

	Compound
SK-1	AVPF-Y (TFA)
SK-1b	ALPL-F (TFA)
SK-1c	ALPL-Y (TFA)
SK-1d	ALPL-W (TFA)
SK-1e	ALPL-FW (TFA)
SK-2	AVPF-F (TFA)
SK-3	AVPF-I (TFA)
SK-4	AVPF-L (TFA)
SK-5	AVPF-V (TFA)
SK-6	AVPF-W (TFA)
SK-7	AVPF-YY (TFA)
SK-8	AVPF-YF (TFA)
SK-9	AVPF-YI (TFA)
SK-10	AVPF-YL (TFA)
SK-11	AVPF-YV (TFA)
SK-12	AVPF-YW (TFA)
	AVPF-“R”
SK-13	 (TFA)
SK-14	 (TFA)
SK-15	 (TFA)
SK-16	 (TFA)
SK-17	 (TFA)
SK-18	 (TFA)
SK-19	 (TFA)
SK-20	 (TFA)
SK-21	 (TFA)
SK-22	 (TFA)
SK-23	 (TFA)
SK-24	 (TFA)
SK-25	 (TFA)

SK-26	 (TFA)
SK-27	 (TFA)
SK-28	 (TFA)
SK-29	 (TFA)
SK-30	 (TFA)
SK-31	 (TFA)
DQ-5	 (Cl)
DQ-6	 (Cl)
SK-32	 (Cl)
DQ-30	 (Cl)
DQ-24	 (Cl x 2)

References

- (1) Sharma, R. P. *Drosoph Inf Serv* **1973**, *50*, 134.
- (2) Nusse, R.; Varmus, H. E. *Cell* **1982**, *31*, 99.
- (3) Rijsewijk, F.; Schuermann, M.; Wagenaar, E.; Parren, P.; Weigel, D.; Nusse, R. *Cell* **1987**, *50*, 649.
- (4) Clevers, H. *Cell* **2006**, *127*, 469.
- (5) Hartmann, C. *Trends Cell Biol* **2006**, *16*, 151.
- (6) Logan, C. Y.; Nusse, R. *Annu Rev Cell Dev Biol* **2004**, *20*, 781.
- (7) Okamura, R. M.; Sigvardsson, M.; Galceran, J.; Verbeek, S.; Clevers, H.; Grosschedl, R. *Immunity* **1998**, *8*, 11.
- (8) Reya, T.; Clevers, H. *Nature* **2005**, *434*, 843.
- (9) Chien, A. J.; Conrad, W. H.; Moon, R. T. *J Invest Dermatol* **2009**, *129*, 1614.
- (10) Seifert, J. R.; Mlodzik, M. *Nat Rev Genet* **2007**, *8*, 126.
- (11) Veeman, M. T.; Axelrod, J. D.; Moon, R. T. *Dev Cell* **2003**, *5*, 367.
- (12) Kühl, M.; Sheldahl, L. C.; Park, M.; Miller, J. R.; Moon, R. T. *Trends Genet* **2000**, *16*, 279.
- (13) Komekado, H.; Yamamoto, H.; Chiba, T.; Kikuchi, A. *Genes Cells* **2007**, *12*, 521.
- (14) Willert, K.; Brown, J. D.; Danenberg, E.; Duncan, A. W.; Weissman, I. L.; Reya, T.; Yates, J. R., 3rd; Nusse, R. *Nature* **2003**, *423*, 448.
- (15) MacDonald, B. T.; Tamai, K.; He, X. *Dev Cell* **2009**, *17*, 9.
- (16) Takada, R.; Satomi, Y.; Kurata, T.; Ueno, N.; Norioka, S.; Kondoh, H.; Takao, T.; Takada, S. *Dev Cell* **2006**, *11*, 791.
- (17) Hausmann, G.; Banziger, C.; Basler, K. *Nat Rev Mol Cell Biol* **2007**, *8*, 331.
- (18) Hendrickx, M.; Leyns, L. *Dev Growth Differ* **2008**, *50*, 229.
- (19) Parma, P.; Radi, O.; Vidal, V.; Chaboissier, M. C.; Dellambra, E.; Valentini, S.; Guerra, L.; Schedl, A.; Camerino, G. *Nat Genet* **2006**, *38*, 1304.
- (20) Kamata, T.; Katsube, K.; Michikawa, M.; Yamada, M.; Takada, S.; Mizusawa, H. *Biochim Biophys Acta* **2004**, *1676*, 51.
- (21) Kazanskaya, O.; Glinka, A.; del Barco Barrantes, I.; Stannek, P.; Niehrs, C.; Wu, W. *Dev Cell* **2004**, *7*, 525.
- (22) Nam, J. S.; Turcotte, T. J.; Smith, P. F.; Choi, S.; Yoon, J. K. *J Biol Chem* **2006**, *281*, 13247.
- (23) Bhanot, P.; Brink, M.; Samos, C. H.; Hsieh, J. C.; Wang, Y.; Macke, J. P.; Andrew, D.; Nathans, J.; Nusse, R. *Nature* **1996**, *382*, 225.
- (24) Tamai, K.; Semenov, M.; Kato, Y.; Spokony, R.; Liu, C. M.; Katsuyama, Y.; Hess, F.; Saint-Jeannet, J. P.; He, X. *Nature* **2000**, *407*, 530.
- (25) Binnerts, M. E.; Kim, K. A.; Bright, J. M.; Patel, S. M.; Tran, K.; Zhou, M.; Leung, J. M.; Liu, Y.; Lomas, W. E., 3rd; Dixon, M.; Hazell, S. A.; Wagle, M.; Nie, W. S.; Tomasevic, N.; Williams, J.; Zhan, X.; Levy, M. D.; Funk, W. D.; Abo, A. *Proc Natl Acad Sci U S A* **2007**, *104*, 14700.
- (26) Hsieh, J. C.; Rattner, A.; Smallwood, P. M.; Nathans, J. *Proc Natl Acad Sci U S A* **1999**, *96*, 3546.

- (27) Kaykas, A.; Yang-Snyder, J.; Heroux, M.; Shah, K. V.; Bouvier, M.; Moon, R. T. *Nat Cell Biol* **2004**, *6*, 52.
- (28) He, X.; Semenov, M.; Tamai, K.; Zeng, X. *Development* **2004**, *131*, 1663.
- (29) Glinka, A.; Wu, W.; Delius, H.; Monaghan, A. P.; Blumenstock, C.; Niehrs, C. *Nature* **1998**, *391*, 357.
- (30) Bafico, A.; Liu, G.; Yaniv, A.; Gazit, A.; Aaronson, S. A. *Nat Cell Biol* **2001**, *3*, 683.
- (31) Mao, B.; Wu, W.; Li, Y.; Hoppe, D.; Stannek, P.; Glinka, A.; Niehrs, C. *Nature* **2001**, *411*, 321.
- (32) Semenov, M. V.; Tamai, K.; Brott, B. K.; Kuhl, M.; Sokol, S.; He, X. *Curr Biol* **2001**, *11*, 951.
- (33) Mao, B.; Wu, W.; Davidson, G.; Marhold, J.; Li, M.; Mechler, B. M.; Delius, H.; Hoppe, D.; Stannek, P.; Walter, C.; Glinka, A.; Niehrs, C. *Nature* **2002**, *417*, 664.
- (34) Wirths, O.; Waha, A.; Weggen, S.; Schirmacher, P.; Kuhne, T.; Goodyer, C. G.; Albrecht, S.; Von Schweinitz, D.; Pietsch, T. *Lab Invest* **2003**, *83*, 429.
- (35) Hoang, B.; Moos, M., Jr.; Vukicevic, S.; Luyten, F. P. *J Biol Chem* **1996**, *271*, 26131.
- (36) Bafico, A.; Gazit, A.; Pramila, T.; Finch, P. W.; Yaniv, A.; Aaronson, S. A. *J Biol Chem* **1999**, *274*, 16180.
- (37) Hsieh, J. C.; Kodjabachian, L.; Rebbert, M. L.; Rattner, A.; Smallwood, P. M.; Samos, C. H.; Nusse, R.; Dawid, I. B.; Nathans, J. *Nature* **1999**, *398*, 431.
- (38) Itasaki, N.; Jones, C. M.; Mercurio, S.; Rowe, A.; Domingos, P. M.; Smith, J. C.; Krumlauf, R. *Development* **2003**, *130*, 4295.
- (39) Li, X.; Zhang, Y.; Kang, H.; Liu, W.; Liu, P.; Zhang, J.; Harris, S. E.; Wu, D. *J Biol Chem* **2005**, *280*, 19883.
- (40) Semenov, M.; Tamai, K.; He, X. *J Biol Chem* **2005**, *280*, 26770.
- (41) Nagafuchi, A.; Takeichi, M. *EMBO J* **1988**, *7*, 3679.
- (42) Ozawa, M.; Baribault, H.; Kemler, R. *EMBO J* **1989**, *8*, 1711.
- (43) McCrea, P. D.; Turck, C. W.; Gumbiner, B. *Science* **1991**, *254*, 1359.
- (44) McCrea, P. D.; Gumbiner, B. M. *J Biol Chem* **1991**, *266*, 4514.
- (45) Huber, A. H.; Nelson, W. J.; Weis, W. I. *Cell* **1997**, *90*, 871.
- (46) Shitashige, M.; Hirohashi, S.; Yamada, T. *Cancer Sci* **2008**, *99*, 631.
- (47) Kimelman, D.; Xu, W. *Oncogene* **2006**, *25*, 7482.
- (48) Huang, H.; He, X. *Curr Opin Cell Biol* **2008**, *20*, 119.
- (49) Major, M. B.; Camp, N. D.; Berndt, J. D.; Yi, X.; Goldenberg, S. J.; Hubbert, C.; Biechele, T. L.; Gingras, A. C.; Zheng, N.; Maccoss, M. J.; Angers, S.; Moon, R. T. *Science* **2007**, *316*, 1043.
- (50) Liu, C. M.; Li, Y. M.; Semenov, M.; Han, C.; Baeg, G. H.; Tan, Y.; Zhang, Z. H.; Lin, X. H.; He, X. *Cell* **2002**, *108*, 837.
- (51) Amit, S.; Hatzubai, A.; Birman, Y.; Andersen, J. S.; Ben-Shushan, E.; Mann, M.; Ben-Neriah, Y.; Alkalay, I. *Genes Dev* **2002**, *16*, 1066.
- (52) Kitagawa, M.; Hatakeyama, S.; Shirane, M.; Matsumoto, M.; Ishida, N.; Hattori, K.; Nakamichi, I.; Kikuchi, A.; Nakayama, K.; Nakayama, K. *Embo J.* **1999**, *18*, 2401.
- (53) Aberle, H.; Bauer, A.; Stappert, J.; Kispert, A.; Kemler, R. *Embo J.* **1997**, *16*, 3797.
- (54) Zeng, X.; Tamai, K.; Doble, B.; Li, S.; Huang, H.; Habas, R.; Okamura, H.; Woodgett, J.; He, X. *Nature* **2005**, *438*, 873.
- (55) Davidson, G.; Wu, W.; Shen, J.; Bilic, J.; Fenger, U.; Stannek, P.; Glinka, A.; Niehrs, C. *Nature* **2005**, *438*, 867.
- (56) Wallingford, J. B.; Habas, R. *Development* **2005**, *132*, 4421.

- (57) Itoh, K.; Antipova, A.; Ratcliffe, M. J.; Sokol, S. *Mol Cell Biol* **2000**, *20*, 2228.
- (58) Wong, H. C.; Bourdelas, A.; Krauss, A.; Lee, H. J.; Shao, Y.; Wu, D.; Mlodzik, M.; Shi, D. L.; Zheng, J. *Mol Cell* **2003**, *12*, 1251.
- (59) Kriehoff, E.; Behrens, J.; Mayr, B. *J Cell Sci* **2006**, *119*, 1453.
- (60) Parker, D. S.; Ni, Y. Y.; Chang, J. L.; Li, J.; Cadigan, K. M. *Mol Cell Biol* **2008**, *28*, 1815.
- (61) Kramps, T.; Peter, O.; Brunner, E.; Nellen, D.; Froesch, B.; Chatterjee, S.; Murone, M.; Zullig, S.; Basler, K. *Cell* **2002**, *109*, 47.
- (62) Mosimann, C.; Hausmann, G.; Basler, K. *Nat Rev Mol Cell Biol* **2009**, *10*, 276.
- (63) He, T. C.; Sparks, A. B.; Rago, C.; Hermeking, H.; Zawel, L.; da Costa, L. T.; Morin, P. J.; Vogelstein, B.; Kinzler, K. W. *Science* **1998**, *281*, 1509.
- (64) Tetsu, O.; McCormick, F. *Nature* **1999**, *398*, 422.
- (65) Kim, P. J.; Plescia, J.; Clevers, H.; Fearon, E. R.; Altieri, D. C. *Lancet* **2003**, *362*, 205.
- (66) Jho, E. H.; Zhang, T.; Domon, C.; Joo, C. K.; Freund, J. N.; Costantini, F. *Mol Cell Biol* **2002**, *22*, 1172.
- (67) Yamada, T.; Takaoka, A. S.; Naishiro, Y.; Hayashi, R.; Maruyama, K.; Maesawa, C.; Ochiai, A.; Hirohashi, S. *Cancer Research* **2000**, *60*, 4761.
- (68) Zhang, X.; Gaspard, J. P.; Chung, D. C. *Cancer Res* **2001**, *61*, 6050.
- (69) Brabletz, T.; Jung, A.; Dag, S.; Hlubek, F.; Kirchner, T. *Am J Pathol* **1999**, *155*, 1033.
- (70) Arce, L.; Yokoyama, N. N.; Waterman, M. L. *Oncogene* **2006**, *25*, 7492.
- (71) Giese, K.; Cox, J.; Grosschedl, R. *Cell* **1992**, *69*, 185.
- (72) Love, J. J.; Li, X.; Case, D. A.; Giese, K.; Grosschedl, R.; Wright, P. E. *Nature* **1995**, *376*, 791.
- (73) Cavallo, R. A.; Cox, R. T.; Moline, M. M.; Roose, J.; Polevoy, G. A.; Clevers, H.; Peifer, M.; Bejsovec, A. *Nature* **1998**, *395*, 604.
- (74) Roose, J.; Molenaar, M.; Peterson, J.; Hurenkamp, J.; Brantjes, H.; Moerer, P.; van de Wetering, M.; Destree, O.; Clevers, H. *Nature* **1998**, *395*, 608.
- (75) Behrens, J.; von Kries, J. P.; Kuhl, M.; Bruhn, L.; Wedlich, D.; Grosschedl, R.; Birchmeier, W. *Nature* **1996**, *382*, 638.
- (76) Molenaar, M.; van de Wetering, M.; Oosterwegel, M.; Peterson-Maduro, J.; Godsave, S.; Korinek, V.; Roose, J.; Destree, O.; Clevers, H. *Cell* **1996**, *86*, 391.
- (77) van de Wetering, M.; Cavallo, R.; Dooijes, D.; van Beest, M.; van Es, J.; Loureiro, J.; Ypma, A.; Hursh, D.; Jones, T.; Bejsovec, A.; Peifer, M.; Mortin, M.; Clevers, H. *Cell* **1997**, *88*, 789.
- (78) Courey, A. J.; Jia, S. *Genes Dev* **2001**, *15*, 2786.
- (79) Graham, T. A.; Weaver, C.; Mao, F.; Kimelman, D.; Xu, W. Q. *Cell* **2000**, *103*, 885.
- (80) Sampietro, J.; Dahlberg, C. L.; Cho, U. S.; Hinds, T. R.; Kimelman, D.; Xu, W. Q. *Molecular Cell* **2006**, *24*, 293.
- (81) Thompson, B. J. *Current Biology* **2004**, *14*, 458.
- (82) Townsley, F. M.; Thompson, B.; Bienz, M. *Journal of Biological Chemistry* **2004**, *279*, 5177.
- (83) Adachi, S.; Jigami, T.; Yasui, T.; Nakano, T.; Ohwada, S.; Omori, Y.; Sugano, S.; Ohkawara, B.; Shibuya, H.; Nakamura, T.; Akiyama, T. *Cancer Res* **2004**, *64*, 8496.
- (84) de la Roche, M.; Worm, J.; Bienz, M. *BMC Cancer* **2008**, *8*.
- (85) Sustmann, C.; Flach, H.; Ebert, H.; Eastman, Q.; Grosschedl, R. *Mol. Cell. Biol.* **2008**, *28*, 3526.

- (86) Moon, R. T.; Kohn, A. D.; De Ferrari, G. V.; Kaykas, A. *Nature Reviews Genetics* **2004**, *5*, 689.
- (87) Giles, R. H.; van Es, J. H.; Clevers, H. *Biochim Biophys Acta* **2003**, *1653*, 1.
- (88) Huang, C. L.; Liu, D.; Ishikawa, S.; Nakashima, T.; Nakashima, N.; Yokomise, H.; Kadota, K.; Ueno, M. *Eur J Cancer* **2008**, *44*, 2680.
- (89) Balemans, W.; Ebeling, M.; Patel, N.; Van Hul, E.; Olson, P.; Dioszegi, M.; Lacza, C.; Wuyts, W.; Van Den Ende, J.; Willems, P.; Paes-Alves, A. F.; Hill, S.; Bueno, M.; Ramos, F. J.; Tacconi, P.; Dikkers, F. G.; Stratakis, C.; Lindpaintner, K.; Vickery, B.; Foerzler, D.; Van Hul, W. *Hum Mol Genet* **2001**, *10*, 537.
- (90) Brunkow, M. E.; Gardner, J. C.; Van Ness, J.; Paepfer, B. W.; Kovacevich, B. R.; Proll, S.; Skonier, J. E.; Zhao, L.; Sabo, P. J.; Fu, Y.; Alisch, R. S.; Gillett, L.; Colbert, T.; Tacconi, P.; Galas, D.; Hamersma, H.; Beighton, P.; Mulligan, J. *Am J Hum Genet* **2001**, *68*, 577.
- (91) Niemann, S.; Zhao, C.; Pascu, F.; Stahl, U.; Aulepp, U.; Niswander, L.; Weber, J. L.; Muller, U. *Am J Hum Genet* **2004**, *74*, 558.
- (92) Babij, P.; Zhao, W.; Small, C.; Kharode, Y.; Yaworsky, P. J.; Bouxsein, M. L.; Reddy, P. S.; Bodine, P. V.; Robinson, J. A.; Bhat, B.; Marzolf, J.; Moran, R. A.; Bex, F. *J Bone Miner Res* **2003**, *18*, 960.
- (93) Boyden, L. M.; Mao, J.; Belsky, J.; Mitzner, L.; Farhi, A.; Mitnick, M. A.; Wu, D.; Insogna, K.; Lifton, R. P. *N Engl J Med* **2002**, *346*, 1513.
- (94) Bjorklund, P.; Akerstrom, G.; Westin, G. *PLoS Med* **2007**, *4*, e328.
- (95) Uematsu, K.; He, B. A.; You, L.; Xu, Z. D.; McCormick, F.; Jablons, D. M. *Oncogene* **2003**, *22*, 7218.
- (96) You, L.; He, B.; Uematsu, K.; Xu, Z.; Mazieres, J.; Lee, A.; McCormick, F.; Jablons, D. M. *Cancer Res* **2004**, *64*, 3474.
- (97) Kinzler, K. W.; Vogelstein, B. *Cell* **1996**, *87*, 159.
- (98) Bienz, M.; Clevers, H. *Cell* **2000**, *103*, 311.
- (99) Nishisho, I.; Nakamura, Y.; Miyoshi, Y.; Miki, Y.; Ando, H.; Horii, A.; Koyama, K.; Utsunomiya, J.; Baba, S.; Hedge, P. *Science* **1991**, *253*, 665.
- (100) Morin, P. J.; Sparks, A. B.; Korinek, V.; Barker, N.; Clevers, H.; Vogelstein, B.; Kinzler, K. W. *Science* **1997**, *275*, 1787.
- (101) Rubinfeld, B.; Albert, I.; Porfiri, E.; Fiol, C.; Munemitsu, S.; Polakis, P. *Science* **1996**, *272*, 1023.
- (102) Nakatsuru, S.; Yanagisawa, A.; Ichii, S.; Tahara, E.; Kato, Y.; Nakamura, Y.; Horii, A. *Hum Mol Genet* **1992**, *1*, 559.
- (103) Polakis, P. *Genes Dev.* **2000**, *14*, 1837.
- (104) Liu, W.; Dong, X.; Mai, M.; Seelan, R. S.; Taniguchi, K.; Krishnadath, K. K.; Halling, K. C.; Cunningham, J. M.; Boardman, L. A.; Qian, C.; Christensen, E.; Schmidt, S. S.; Roche, P. C.; Smith, D. I.; Thibodeau, S. N. *Nat Genet* **2000**, *26*, 146.
- (105) Lammi, L.; Arte, S.; Somer, M.; Jarvinen, H.; Lahermo, P.; Thesleff, I.; Pirinen, S.; Nieminen, P. *Am J Hum Genet* **2004**, *74*, 1043.
- (106) Satoh, S.; Daigo, Y.; Furukawa, Y.; Kato, T.; Miwa, N.; Nishiwaki, T.; Kawasoe, T.; Ishiguro, H.; Fujita, M.; Tokino, T.; Sasaki, Y.; Imaoka, S.; Murata, M.; Shimano, T.; Yamaoka, Y.; Nakamura, Y. *Nat Genet* **2000**, *24*, 245.
- (107) Rivera, M. N.; Kim, W. J.; Wells, J.; Driscoll, D. R.; Brannigan, B. W.; Han, M.; Kim, J. C.; Feinberg, A. P.; Gerald, W. L.; Vargas, S. O.; Chin, L.; Iafrate, A. J.; Bell, D. W.; Haber, D. A. *Science* **2007**, *315*, 642.
- (108) Ying, Y.; Tao, Q. *Epigenetics* **2009**, *4*, 307.
- (109) Veeck, J.; Niederacher, D.; An, H.; Klopocki, E.; Wiesmann, F.; Betz, B.; Galm, O.; Camara, O.; Durst, M.; Kristiansen, G.; Huszka, C.; Knuchel, R.; Dahl, E. *Oncogene* **2006**, *25*, 3479.

- (110) Suzuki, H.; Toyota, M.; Carraway, H.; Gabrielson, E.; Ohmura, T.; Fujikane, T.; Nishikawa, N.; Sogabe, Y.; Nojima, M.; Sonoda, T.; Mori, M.; Hirata, K.; Imai, K.; Shinomura, Y.; Baylin, S. B.; Tokino, T. *Br J Cancer* **2008**, *98*, 1147.
- (111) Suzuki, H.; Tokino, T.; Shinomura, Y.; Imai, K.; Toyota, M. *Pharmacogenomics* **2008**, *9*, 1917.
- (112) Aguilera, O.; Fraga, M. F.; Ballestar, E.; Paz, M. F.; Herranz, M.; Espada, J.; Garcia, J. M.; Munoz, A.; Esteller, M.; Gonzalez-Sancho, J. M. *Oncogene* **2006**, *25*, 4116.
- (113) Sato, H.; Suzuki, H.; Toyota, M.; Nojima, M.; Maruyama, R.; Sasaki, S.; Takagi, H.; Sogabe, Y.; Sasaki, Y.; Idogawa, M.; Sonoda, T.; Mori, M.; Imai, K.; Tokino, T.; Shinomura, Y. *Carcinogenesis* **2007**, *28*, 2459.
- (114) Kawakami, K.; Hirata, H.; Yamamura, S.; Kikuno, N.; Saini, S.; Majid, S.; Tanaka, Y.; Kawamoto, K.; Enokida, H.; Nakagawa, M.; Dahiya, R. *Cancer Res* **2009**, *69*, 8603.
- (115) Ai, L.; Tao, Q.; Zhong, S.; Fields, C. R.; Kim, W. J.; Lee, M. W.; Cui, Y.; Brown, K. D.; Robertson, K. D. *Carcinogenesis* **2006**, *27*, 1341.
- (116) Urakami, S.; Shiina, H.; Enokida, H.; Kawakami, T.; Tokizane, T.; Ogishima, T.; Tanaka, Y.; Li, L. C.; Ribeiro-Filho, L. A.; Terashima, M.; Kikuno, N.; Adachi, H.; Yoneda, T.; Kishi, H.; Shigeno, K.; Konety, B. R.; Igawa, M.; Dahiya, R. *Clin Cancer Res* **2006**, *12*, 383.
- (117) Mikami, I.; You, L.; He, B.; Xu, Z. D.; Batra, S.; Lee, A. Y.; Mazieres, J.; Reguart, N.; Uematsu, K.; Koizumi, K.; Jablons, D. M. *Bmc Cancer* **2005**, *5*.
- (118) You, L.; He, B.; Xu, Z. D.; Uematsu, K.; Mazieres, J.; Mikami, I.; Reguart, N.; Moody, T. W.; Kitajewski, J.; McCormick, F.; Jablons, D. M. *Oncogene* **2004**, *23*, 6170.
- (119) Green, D. W.; Roh, H.; Pippin, J. A.; Drebin, J. A. *Journal of Surgical Research* **2001**, *101*, 16.
- (120) Naishiro, Y.; Yamada, T.; Takaoka, A. S.; Hayashi, R.; Hasegawa, F.; Imai, K.; Hirohashi, S. *Cancer Research* **2001**, *61*, 2751.
- (121) Kwong, K. Y.; Zou, Y.; Day, C. P.; Hung, M. C. *Oncogene* **2002**, *21*, 8340.
- (122) Thun, M. J.; Namboodiri, M. M.; Heath, C. W., Jr. *N Engl J Med* **1991**, *325*, 1593.
- (123) Giardiello, F. M.; Hamilton, S. R.; Krush, A. J.; Piantadosi, S.; Hylind, L. M.; Celano, P.; Booker, S. V.; Robinson, C. R.; Offerhaus, G. J. A. *N. Engl. J. Med.* **1993**, *328*, 1313.
- (124) Janssens, N.; Janicot, M.; Perera, T. *Investigational New Drugs* **2006**, *24*, 263.
- (125) Takahashi-Yanaga, F.; Sasaguri, T. *Journal of Pharmacological Sciences* **2007**, *104*, 293.
- (126) Goluboff, E. T. *Expert Opin Investig Drugs* **2001**, *10*, 1875.
- (127) Li, H.; Liu, L.; David, M. L.; Whitehead, C. M.; Chen, M.; Fetter, J. R.; Sperl, G. J.; Pamukcu, R.; Thompson, W. J. *Biochem Pharmacol* **2002**, *64*, 1325.
- (128) Dihlmann, S.; Siermann, A.; Doeberitz, M. V. *Oncogene* **2001**, *20*, 645.
- (129) Bos, C. L.; Kodach, L. L.; van den Brink, G. R.; Diks, S. H.; van Santen, M. M.; Richel, D. J.; Peppelenbosch, M. P.; Hardwick, J. C. *Oncogene* **2006**, *25*, 6447.
- (130) Lepourcelet, M.; Chen, Y. N. P.; France, D. S.; Wang, H. S.; Crews, P.; Petersen, F.; Bruseo, C.; Wood, A. W.; Shivdasani, R. A. *Cancer Cell* **2004**, *5*, 91.
- (131) Trosset, J. Y.; Dalvit, C.; Knapp, S.; Fasolini, M.; Veronesi, M.; Mantegani, S.; Gianellini, L. M.; Catana, C.; Sundstrom, M.; Stouten, P. F.; Moll, J. K. *Proteins* **2006**, *64*, 60.
- (132) Lu, W.; Tinsley, H. N.; Keeton, A.; Qu, Z.; Piazza, G. A.; Li, Y. *Eur J Pharmacol* **2009**, *602*, 8.

- (133) Minke, K. S.; Staib, P.; Puetter, A.; Gehrke, I.; Gandhirajan, R. K.; Schlosser, A.; Schmitt, E. K.; Hallek, M.; Kreuzer, K. A. *Eur. J. Haematol.* **2009**, *82*, 165.
- (134) Takemaru, K. I.; Ohmitsu, M.; Li, F. Q. *Handb Exp Pharmacol* **2008**, 261.
- (135) Emami, K. H.; Nguyen, C.; Ma, H.; Kim, D. H.; Jeong, K. W.; Eguchi, M.; Moon, R. T.; Teo, J. L.; Kim, H. Y.; Moon, S. H.; Ha, J. R.; Kahn, M. *Proc Natl Acad Sci U S A* **2004**, *101*, 12682.
- (136) Fujii, N.; You, L.; Xu, Z. D.; Uematsu, K.; Shan, J. F.; He, B.; Mikami, I.; Edmondson, L. R.; Neale, G.; Zheng, J.; Guy, R. K.; Jablons, D. M. *Cancer Research* **2007**, *67*, 573.
- (137) You, L.; Xu, Z. D.; Punchihewa, C.; Jablons, D. M.; Fujii, N. *Molecular Cancer Therapeutics* **2008**, *7*, 1633.
- (138) Zhang, Y.; Appleton, B. A.; Wiesmann, C.; Lau, T.; Costa, M.; Hannoush, R. N.; Sidhu, S. S. *Nat Chem Biol* **2009**, *5*, 217.
- (139) Fujii, N.; Haresco, J. J.; Novak, K. A. P.; Stokoe, D.; Kuntz, I. D.; Guy, R. K. *Journal of the American Chemical Society* **2003**, *125*, 12074.
- (140) Grandy, D.; Shan, J. F.; Zhang, X. X.; Rao, S.; Akunuru, S.; Li, H. Y.; Zhang, Y. H.; Alpatov, I.; Zhang, X. A.; Lang, R. A.; Shi, D. L.; Zheng, J. J. *Journal of Biological Chemistry* **2009**, *284*, 16256.
- (141) Chen, B. Z.; Dodge, M. E.; Tang, W.; Lu, J. M.; Ma, Z. Q.; Fan, C. W.; Wei, S. G.; Hao, W. N.; Kilgore, J.; Williams, N. S.; Roth, M. G.; Amatruda, J. F.; Chen, C.; Lum, L. *Nature Chemical Biology* **2009**, *5*, 100.
- (142) Lee, E.; Salic, A.; Kruger, R.; Heinrich, R.; Kirschner, M. W. *PLoS Biol* **2003**, *1*, E10.
- (143) Karamouzis, M. V.; Konstantinopoulos, P. A.; Papavassiliou, A. G. *Cell Res* **2007**, *17*, 324.
- (144) Itoyama, T.; Nanjungud, G.; Chen, W.; Dyomin, V. G.; Teruya-Feldstein, J.; Jhanwar, S. C.; Zelenetz, A. D.; Chaganti, R. S. *Genes Chromosomes Cancer* **2002**, *35*, 318.
- (145) Willis, T. G.; Zalcborg, I. R.; Coignet, L. J.; Wlodarska, I.; Stul, M.; Jadayel, D. M.; Bastard, C.; Treleaven, J. G.; Catovsky, D.; Silva, M. L.; Dyer, M. J. *Blood* **1998**, *91*, 1873.
- (146) Hoffmans, R.; Basler, K. *Development* **2004**, *131*, 4393.
- (147) Hoffmans, R.; Städeli, R.; Basler, K. *Current Biology* **2005**, *15*, 1207.
- (148) Brembeck, F. H.; Schwarz-Romond, T.; Bakkers, J.; Wilhelm, S.; Hammerschmidt, M.; Birchmeier, W. *Genes Dev.* **2004**, *18*, 2225.
- (149) Fiedler, M.; Sanchez-Barrena, M. J.; Nekrasov, M.; Mieszczanek, J.; Rybin, V.; Muller, J.; Evans, P.; Bienz, M. *Mol Cell* **2008**, *30*, 507.
- (150) Sakamoto, I.; Ohwada, S.; Toya, H.; Togo, N.; Kashiwabara, K.; Oyama, T.; Nakajima, T.; Ito, H.; Adachi, S.; Jigami, T.; Akiyama, T. *Cancer Sci* **2007**, *98*, 83.
- (151) Toya, H.; Oyama, T.; Ohwada, S.; Togo, N.; Sakamoto, I.; Horiguchi, J.; Koibuchi, Y.; Adachi, S.; Jigami, T.; Nakajima, T.; Akiyama, T. *Cancer Sci* **2007**, *98*, 484.
- (152) Phan, J.; Li, Z.; Kasprzak, A.; Li, B.; Sebti, S.; Guida, W.; Schonbrunn, E.; Chen, J. *J Biol Chem* **2010**, *285*, 2174.
- (153) Bernal, F.; Tyler, A. F.; Korsmeyer, S. J.; Walensky, L. D.; Verdine, G. L. *J Am Chem Soc* **2007**, *129*, 2456.
- (154) Burke, T. J.; Loniello, K. R.; Beebe, J. A.; Ervin, K. M. *Comb Chem High Throughput Screen* **2003**, *6*, 183.
- (155) Leopoldo, M.; Lacivita, E.; Berardi, F.; Perrone, R. *Drug Discov Today* **2009**, *14*, 706.
- (156) Fägerstam, L. G.; Frostell-Karlsson, Å.; Karlsson, R.; Persson, B.; Rönnerberg, I. *Journal of Chromatography* **1992**, *597*, 397.

- (157) Zhang, J. H.; Chung, T. D. Y.; Oldenburg, K. R. *Journal of Biomolecular Screening* **1999**, *4*, 67.
- (158) Kaiser, E.; Colescot, R. I.; Bossing, C. D.; Cook, P. I. *Anal. Biochem.* **1970**, *34*, 595.
- (159) Nikolovska-Coleska, Z.; Wang, R. X.; Fang, X. L.; Pan, H. G.; Tomita, Y.; Li, P.; Roller, P. P.; Krajewski, K.; Saito, N. G.; Stuckey, J. A.; Wang, S. M. *Anal. Biochem.* **2004**, *332*, 261.
- (160) Mayr, L. M.; Bojanic, D. *Curr Opin Pharmacol* **2009**, *9*, 580.
- (161) Descalzo, A. B.; Xu, H. J.; Shen, Z.; Rurack, K. *Ann N Y Acad Sci* **2008**, *1130*, 164.
- (162) Descalzo, A. B.; Xu, H. J.; Xue, Z. L.; Hoffmann, K.; Shen, Z.; Weller, M. G.; You, X. Z.; Rurack, K. *Org Lett* **2008**, *10*, 1581.
- (163) Fonseca, S. B.; Pereira, M. P.; Kelley, S. O. *Adv Drug Deliv Rev* **2009**, *61*, 953.
- (164) Futaki, S.; Suzuki, T.; Ohashi, W.; Yagami, T.; Tanaka, S.; Ueda, K.; Sugiura, Y. *J Biol Chem* **2001**, *276*, 5836.
- (165) Pujals, S.; Sabido, E.; Tarrago, T.; Giralt, E. *Biochem Soc Trans* **2007**, *35*, 794.
- (166) Hook, D. F.; Gessier, F.; Noti, C.; Kast, P.; Seebach, D. *Chembiochem* **2004**, *5*, 691.
- (167) Davies, J. S. *J Pept Sci* **2003**, *9*, 471.
- (168) Haridas, V. *Eur. J. Org. Chem.* **2009**, 5112.
- (169) Henchey, L. K.; Jochim, A. L.; Arora, P. S. *Curr Opin Chem Biol* **2008**, *12*, 692.
- (170) Schafmeister, C. E.; Po, J.; Verdine, G. L. *Journal of the American Chemical Society* **2000**, *122*, 5891.
- (171) Bernal, F.; Tyler, A. F.; Korsmeyer, S. J.; Walensky, L. D.; Verdine, G. L. *Journal of the American Chemical Society* **2007**, *129*, 2456.
- (172) Chapman, R. N.; Dimartino, G.; Arora, P. S. *Journal of the American Chemical Society* **2004**, *126*, 12252.
- (173) Wang, D.; Chen, K.; Dimartino, G.; Arora, P. S. *Org Biomol Chem* **2006**, *4*, 4074.
- (174) Wang, D.; Liao, W.; Arora, P. S. *Angew Chem Int Ed Engl* **2005**, *44*, 6525.
- (175) Le Chevalier Isaad, A.; Papini, A. M.; Chorev, M.; Rovero, P. *J Pept Sci* **2009**, *15*, 451.
- (176) Cantel, S.; Halperin, J. A.; Chorev, M.; Scrima, M.; D'Ursi, A. M.; Levy, J. J.; DiMarchi, R. D.; Le Chevalier, A.; Rovero, P.; Papini, A. M. *Adv Exp Med Biol* **2009**, *611*, 175.
- (177) Jagasia, R.; Holub, J. M.; Bollinger, M.; Kirshenbaum, K.; Finn, M. G. *J Org Chem* **2009**, *74*, 2964.
- (178) Kolb, H. C.; Sharpless, K. B. *Drug Discov. Today* **2003**, *8*, 1128.
- (179) Kolligs, F. T.; Hu, G.; Dang, C. V.; Fearon, E. R. *Mol Cell Biol* **1999**, *19*, 5696.
- (180) Brannon, M.; Gomperts, M.; Sumoy, L.; Moon, R. T.; Kimelman, D. *Genes Dev* **1997**, *11*, 2359.
- (181) Fischer, P. M.; Zhelev, N. Z.; Wang, S.; Melville, J. E.; Fahraeus, R.; Lane, D. P. *J Pept Res* **2000**, *55*, 163.
- (182) Walensky, L. D.; Pitter, K.; Morash, J.; Oh, K. J.; Barbuto, S.; Fisher, J.; Smith, E.; Verdine, G. L.; Korsmeyer, S. J. *Mol Cell* **2006**, *24*, 199.
- (183) Bird, G. H.; Bernal, F.; Pitter, K.; Walensky, L. D. *Methods Enzymol* **2008**, *446*, 369.

- (184) Henchey, L. K.; Kushal, S.; Dubey, R.; Chapman, R. N.; Olenyuk, B. Z.; Arora, P. S. *J Am Chem Soc* **2010**, *132*, 941.
- (185) Moellering, R. E.; Cornejo, M.; Davis, T. N.; Del Bianco, C.; Aster, J. C.; Blacklow, S. C.; Kung, A. L.; Gilliland, D. G.; Verdine, G. L.; Bradner, J. E. *Nature* **2009**, *462*, 182.
- (186) Walensky, L. D.; Kung, A. L.; Escher, I.; Malia, T. J.; Barbuto, S.; Wright, R. D.; Wagner, G.; Verdine, G. L.; Korsmeyer, S. J. *Science* **2004**, *305*, 1466.
- (187) Williams, R. M.; Im, M. N. *Journal of the American Chemical Society* **1991**, *113*, 9276.
- (188) Cantel, S.; Isaad Ale, C.; Scrima, M.; Levy, J. J.; DiMarchi, R. D.; Rovero, P.; Halperin, J. A.; D'Ursi, A. M.; Papini, A. M.; Chorev, M. *J Org Chem* **2008**, *73*, 5663.
- (189) Jagasia, R.; Holub, J. M.; Bollinger, M.; Kirshenbaum, K.; Finn, M. G. *J. Org. Chem.* **2009**, *74*, 2964.
- (190) Nishi, K.; Komine, Y.; Sakai, N.; Maruyama, T.; Otagiri, M. *FEBS Lett.* **2005**, *579*, 3596.
- (191) Kumaran, S.; Roy, R. P. *J. Pept. Res.* **1999**, *53*, 284.
- (192) Luo, P.; Baldwin, R. L. *Biochemistry* **1997**, *36*, 8413.
- (193) Shepherd, N. E.; Hoang, H. N.; Abbenante, G.; Fairlie, D. P. *J Am Chem Soc* **2005**, *127*, 2974.
- (194) Wang, D.; Chen, K.; Kulp Iii, J. L.; Arora, P. S. *J Am Chem Soc* **2006**, *128*, 9248.
- (195) Belokon, Y. N.; Bessalova, N. B.; Churkina, T. D.; Cisarova, I.; Ezernitskaya, M. G.; Harutyunyan, S. R.; Hrdina, R.; Kagan, H. B.; Kocovsky, P.; Kochetkov, K. A.; Larionov, O. V.; Lyssenko, K. A.; North, M.; Polasek, M.; Peregudov, A. S.; Prisyazhnyuk, V. V.; Vyskocil, S. *J Am Chem Soc* **2003**, *125*, 12860.
- (196) Belokon, Y. N.; Tararov, V. I.; Maleev, V. I.; Savel'eva, T. F.; Ryzhov, M. G. *Tetrahedron-Asymmetry* **1998**, *9*, 4249.
- (197) Suzuki, T.; Futaki, S.; Niwa, M.; Tanaka, S.; Ueda, K.; Sugiura, Y. *J Biol Chem* **2002**, *277*, 2437.
- (198) Cardozo, A. K.; Buchillier, V.; Mathieu, M.; Chen, J.; Ortis, F.; Ladriere, L.; Allaman-Pillet, N.; Poirot, O.; Kellenberger, S.; Beckmann, J. S.; Eizirik, D. L.; Bonny, C.; Maurer, F. *Biochim Biophys Acta* **2007**, *1768*, 2222.
- (199) Huisgen, R.; Szeimies, G.; Mobius, L. *Chem. Ber.-Recl.* **1967**, *100*, 2494.
- (200) Gans, P. J.; Lyu, P. C.; Manning, M. C.; Woody, R. W.; Kallenbach, N. R. *Biopolymers* **1991**, *31*, 1605.
- (201) Pace, C. N.; Scholtz, J. M. *Biophys. J.* **1998**, *75*, 422.
- (202) Turner, J. J.; Wilschut, N.; Overkleeft, H. S.; Klaffke, W.; van der Marel, G. A.; van Boom, J. H. *Tetrahedron Letters* **1999**, *40*, 7039.
- (203) Katayama, H.; Hojo, H.; Ohira, T.; Nakahara, Y. *Tetrahedron Letters* **2008**, *49*, 5492.
- (204) Kawamoto, S. A.; Thompson, A. D.; Coleska, A.; Nikolovska-Coleska, Z.; Yi, H.; Wang, S. *Biochemistry* **2009**, *48*, 9534.
- (205) Hoffmans, R.; Basler, K. *Mechanisms of Development* **2007**, *124*, 59.
- (206) Städeli, R.; Basler, K. *Mechanisms of Development* **2005**, *122*, 1171.
- (207) Huber, A. H.; Weis, W. I. *Cell* **2001**, *105*, 391.
- (208) Oltersdorf, T.; Elmore, S. W.; Shoemaker, A. R.; Armstrong, R. C.; Augeri, D. J.; Belli, B. A.; Bruncko, M.; Deckwerth, T. L.; Dinges, J.; Hajduk, P. J.; Joseph, M. K.; Kitada, S.; Korsmeyer, S. J.; Kunzer, A. R.; Letai, A.; Li, C.; Mitten, M. J.; Nettlesheim, D. G.; Ng, S.; Nimmer, P. M.; O'Connor, J. M.; Oleksijew, A.; Petros, A. M.; Reed, J. C.; Shen, W.; Tahir, S. K.; Thompson, C. B.; Tomaselli, K. J.; Wang, B. L.; Wendt, M. D.; Zhang, H. C.; Fesik, S. W.; Rosenberg, S. H. *Nature* **2005**, *435*, 677.

- (209) Shuker, S. B.; Hajduk, P. J.; Meadows, R. P.; Fesik, S. W. *Science* **1996**, 274, 1531.
- (210) Hengartner, M. O. *Nature* **2000**, 407, 770.
- (211) Nachmias, B., Ashhab, Y. and Ben-Yehuda, D. *Semin. Cancer. Biol.* **2004**, 14, 231.
- (212) Debatin, K.-M. *Cancer Immunol. Immunother.* **2004**, 53, 153.
- (213) Schimmer, A. D. *Cancer Res.* **2004**, 64, 7183.
- (214) Birnbaum, M. J., Clem, R.J. and Miller, L.K. *J. Virol.* **1994**, 68, 2521.
- (215) Crook, N. E., Clem, R.J. and Miller, L.K. *J. Virol.* **1993**, 67, 2168.
- (216) Vaux, D. L. a. S., *J. Nat. Rev. Mol. Cell Biol.* **2005**, 6, 287.
- (217) Muchmore, S. W., Chen, J., Jakob, C., Zakula, D., Matayoshi, E.D., Wu, W., Zhang, H., Li, F., Ng, S.-C. and Altieri, D.C. *Mol. Cell* **2000**, 6, 173.
- (218) McEleny, K. R., Watson, R.W.G., Coffey, R.N.T., O'Neill, A.J. and Fitzpatrick, J.M. *Prostate* **2002**, 51, 133.
- (219) Ambrosini, G., Adida, C. and Altieri, D.C. *Nature Med.* **1997**, 3, 917.
- (220) Chantalat, L., Skoufias, D.A., Kleman, J.-P., Jung, B., Dideberg, O. and Margolis, R.L. *Mol. Cell* **2000**, 6, 183.
- (221) Verdecia, M. A., Huang, H.-k., Dutil, E., Kaiser, D.A., Hunter, T. and Noel, J.P. *Nat. Struct. Biol.* **2000**, 7, 602.
- (222) Sun, C., Nettesheim, D., Liu, Z. and Olejniczak, E.T. *Biochemistry* **2005**, 44, 11.
- (223) Fortugno, P., Beltrami, E., Plescia, J., Fontana, J., Pradhan, D., Marchisio, P.C., Sessa, W.C. and Altieri, D.C. *Proc. Natl. Acad. Sci. U.S.A.* **2003**, 100, 13791.
- (224) Li, F., Ambrosini, G., Chu, E.Y., Plescia, J., Tognin, S., Marchisio, P.C. and Altieri, D.C. *Nature* **1998**, 396, 580.
- (225) Marusawa, H., Matsuzawa, S.-i., Welsh, K., Zou, H., Armstrong, R., Tamm, I. and Reed, J.C. *EMBO J.* **2003**, 22, 2729.
- (226) O'Connor, D. S., Grossman, D., Plescia, J., Li, F., Zhang, H., Villa, A., Tognin, S., Marchisio, P.C. and Altieri, D.C. *Proc. Natl. Acad. Sci. USA* **2000**, 97, 13103.
- (227) Shin, S., Sung, B.-J., Cho, Y.-S., Kim, H.-J., Ha, N.-C., Hwang, J.-I., Chung, C.-W., Jung, Y.-K. and Oh, B.-H. *Biochemistry* **2001**, 40, 1117.
- (228) Song, Z., Yao, X. and Wu, M. *J. Biol. Chem.* **2003**, 278, 23130.
- (229) Tarnawski, A., Pai, R., Chiou, S.-K. and Chu, E.C. *Biochem. Biophys. Res. Commun.* **2005**, 334, 207.
- (230) Delacour-Larose, M. T., My-Nhung Hoang ; Dimitrov, Stefan; Molla, Annie *Cell Cycle* **2007**, 6, 1878.
- (231) Krieg, A., Mahotka, C., Krieg, T., Grabsch, H., Müller, W., Takeno, S., Suschek, C.V., Heydthausen, M., Gabbert, H.E. and Gerharz, C.D. *Br. J. Cancer* **2002**, 86, 737.
- (232) Gurbuxani, S., Xu, Y., Keerthivasan, G., Wickrema, A. and Crispino, J.D. *Proc. Natl. Acad. Sci. U.S.A.* **2005**, 102, 11480.
- (233) Tamm, I., Wang, Y., Sausville, E., Scudiero, D.A., Vigna, N., Oltersdorf, T. and Reed, J.C. *Cancer Res.* **1998**, 58, 5315.
- (234) Spaulding, B., Pan, D., Ghadersohi, A., Nielsen, G., Jensen, S., Gellert, F., Ling, X., Zhang, M., Black, A. and Li, F. *Histopathology* **2006**, 49, 622.
- (235) Zhao, J., Tenev, T., Martins, L.M., Downward, J. and Lemoine, N.R. *J. Cell Sci.* **2000**, 113, 4363.
- (236) Altieri, D. C. *Oncogene* **2003**, 22, 8581.
- (237) Dohi, T., Beltrami, E., Wall, N.R., Plescia, J. and Altieri, D.C. *J. Clin. Invest.* **2004**, 114, 1117.

- (238) Grossman, D., McNiff, J.M., Li, F. and Altieri, D.C. *J. Invest. Dermatol.* **1999**, 113, 1076.
- (239) Rodriguez, J. A., Span, S.W., Ferreira, C.G.M., Kruyt, F.A.E. and Giaccone, G. *Exp. Cell Res.* **2002**, 275, 44.
- (240) Li, F., Ackermann, E.J., Bennett, C.F., Rothermel, A.L., Plescia, J., Tognin, S., Villa, A., Marchisio, P.C. and Altieri, D.C. *Nature Cell Biol.* **1999**, 1, 461.
- (241) Ceballos-Cancino, G. E., M.; Maldonado, V.; Melendez-Zajgla, J. *Oncogene* **2007**, 26, 7569.
- (242) Dohi, T., Okada, K., Xia, F., Wilford, C.E., Samuel, T., Welsh, K., Marusawa, H., Zou, H., Armstrong, R., Matsuzawa, S.-i., Salvesen, G.S., Reed, J.C. and Altieri, D.C. *J. Biol. Chem.* **2004**, 279, 34087.
- (243) Altieri, D. C. *Curr. Opin. in Cell Biol.* **2006**, 18, 609.
- (244) Duggan, H. M. E.; Hitchcock, P. B.; Young, D. W. *Organic & Biomolecular Chemistry* **2005**, 3, 2287.
- (245) Bradford, M. M. *Anal. Biochem.* **1976**, 72, 248.